frontiers | Research Topics

Case reports in cancer imaging and image-directed interventions 2022

Edited by
Marco Ravanelli and Antonio Bottari

Published in
Frontiers in Oncology

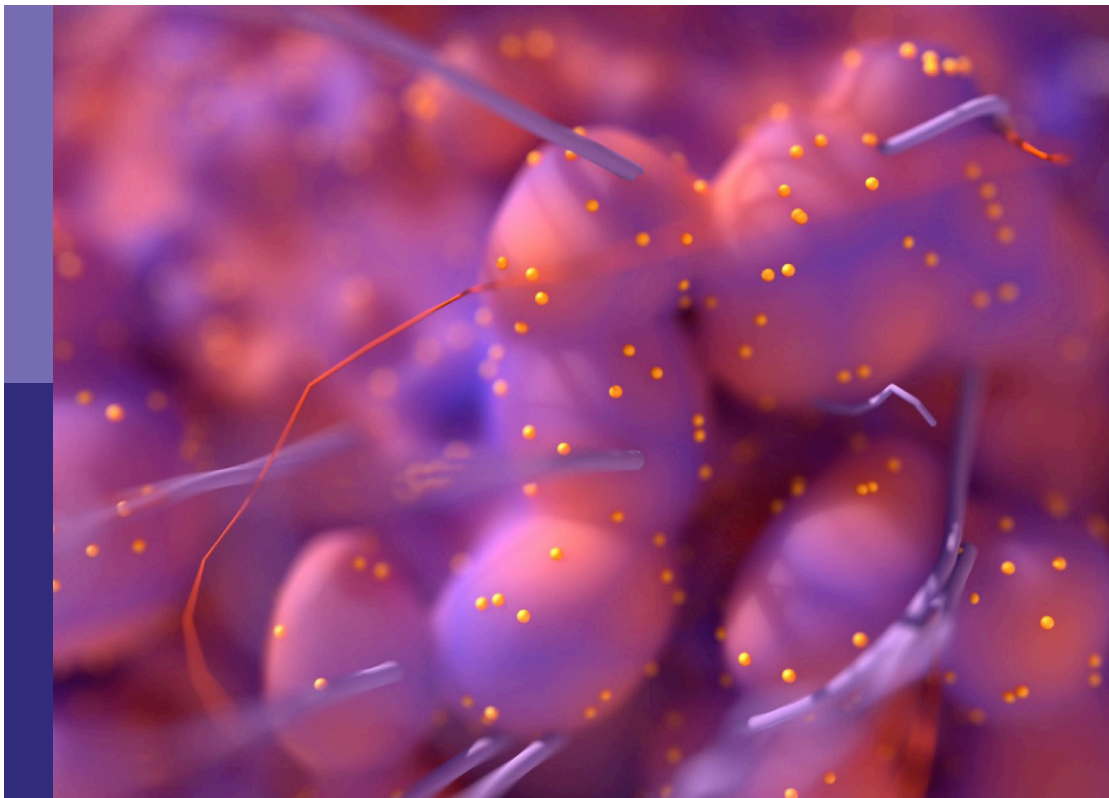

ISSN 1664-8714
ISBN 978-2-8325-4063-3
DOI 10.3389/978-2-8325-4063-3

About Frontiers

Frontiers is more than just an open access publisher of scholarly articles: it is a pioneering approach to the world of academia, radically improving the way scholarly research is managed. The grand vision of Frontiers is a world where all people have an equal opportunity to seek, share and generate knowledge. Frontiers provides immediate and permanent online open access to all its publications, but this alone is not enough to realize our grand goals.

Frontiers journal series

The Frontiers journal series is a multi-tier and interdisciplinary set of open-access, online journals, promising a paradigm shift from the current review, selection and dissemination processes in academic publishing. All Frontiers journals are driven by researchers for researchers; therefore, they constitute a service to the scholarly community. At the same time, the *Frontiers journal series* operates on a revolutionary invention, the tiered publishing system, initially addressing specific communities of scholars, and gradually climbing up to broader public understanding, thus serving the interests of the lay society, too.

Dedication to quality

Each Frontiers article is a landmark of the highest quality, thanks to genuinely collaborative interactions between authors and review editors, who include some of the world's best academicians. Research must be certified by peers before entering a stream of knowledge that may eventually reach the public - and shape society; therefore, Frontiers only applies the most rigorous and unbiased reviews. Frontiers revolutionizes research publishing by freely delivering the most outstanding research, evaluated with no bias from both the academic and social point of view. By applying the most advanced information technologies, Frontiers is catapulting scholarly publishing into a new generation.

What are Frontiers Research Topics?

Frontiers Research Topics are very popular trademarks of the *Frontiers journals series*: they are collections of at least ten articles, all centered on a particular subject. With their unique mix of varied contributions from Original Research to Review Articles, Frontiers Research Topics unify the most influential researchers, the latest key findings and historical advances in a hot research area.

Find out more on how to host your own Frontiers Research Topic or contribute to one as an author by contacting the Frontiers editorial office: frontiersin.org/about/contact

Case reports in cancer imaging and image-directed interventions : 2022

Topic editors

Marco Ravanelli — University of Brescia, Italy

Antonio Bottari — Università degli Studi di Messina, Italy

Citation

Ravanelli, M., Bottari, A., eds. (2023). *Case reports in cancer imaging and image-directed interventions : 2022*. Lausanne: Frontiers Media SA.

doi: 10.3389/978-2-8325-4063-3

Table of contents

frontiers | Frontiers in Oncology

TYPE Editorial
PUBLISHED 21 November 2023
DOI 10.3389/fonc.2023.1310454

OPEN ACCESS

EDITED AND REVIEWED BY
Zaver Bhujwalla,
Johns Hopkins University, United States

*CORRESPONDENCE
Antonio Bottari
bottaria@unime.it

RECEIVED 09 October 2023
ACCEPTED 10 November 2023
PUBLISHED 21 November 2023

CITATION
Bottari A (2023) Editorial: Case reports in cancer imaging and image-directed interventions : 2022.
Front. Oncol. 13:1310454.
doi: 10.3389/fonc.2023.1310454

Editorial: Case reports in cancer imaging and image-directed interventions : 2022

Antonio Bottari*

Dipartimento di Scienze Biomediche, Odontoiatriche, Morfologiche e Funzionali per Immagini, Università degli Studi di Messina, Messina, Italy

KEYWORDS

interventional radiology (IR), interventional oncology (IO), cancer imaging, image-guided biopsies, image-guided radiotherapy

Editorial on the Research Topic
Case reports in cancer imaging and image-directed interventions : 2022

Today, imaging is an indispensable tool for cancer detection and characterization.

Both morphological and functional imaging, independently but, above all, in an integrated manner, allow early diagnosis of numerous neoplastic pathologies.

In recent years, technology has enabled notable growth in diagnostic imaging thanks, for example, to the possibility of acquiring very thin slices, new MRI sequences, or increasingly elaborate and high-performance postprocessing, which is extremely useful in some pathologies or in certain anatomical districts (1, 2).

Nowadays, besides the diagnostic role, there is the possibility of using imaging as a guide to treat some of these pathologies in a less invasive way.

Interventional radiology and, specifically, interventional oncology have by now a consolidated role in the therapeutic process of many neoplasms, assuming the role of the fourth pillar of anti-tumor therapy alongside surgery, radiotherapy, and medical oncology (3-7).

In this Frontiers Research Topic, the authors were expected to provide case reports that highlight unique cases of patients that present with an unexpected diagnosis, treatment outcome, or clinical course (8).

Several contributions focused on the diagnosis of rare tumors or rare manifestations of more common tumors (Li et al.; Wang et al.; Hu et al.; Fischerova et al.).

Li et al. presented a case of osteofibrous dysplasia-like adamantinoma, a rare bone tumor (0.4% of all primary bone tumors) recently proposed in the new WHO classification of bone tumors of 2020 and classified as an intermediate locally aggressive tumor. Imaging can demonstrate the lesion and could provide support for differential diagnosis, although a multidisciplinary evaluation is required to reach the diagnosis.

Another very rare tumor that could involve bone was reported by (Wang et al.).

Proliferating trichilemmal tumors originate from the outer root sheath of hair follicles generally located in the head and neck region. Other localizations are uncommon in this condition.[18] F-FDG-PET could be very useful in identifying both the tumor and any metastatic lymph nodes.

Starting from the presentation of a case, Hu et al. provide a comprehensive literature review of primary intracranial Ewing sarcomas/primitive neuroectodermal tumors, an extremely rare condition with poor prognosis. Unfortunately, only in few cases, they manifest themselves with relatively specific features at imaging; therefore, final diagnosis mainly depends on pathology and immunohistochemistry.

Fischerova et al. reported a rare case of retroperitoneal nodal endometroid carcinoma diagnosed through US-guided biopsy without any macroscopic relevance in the abdomen and pelvis. Immunohistochemical and genetic analysis helped to detect an unknown Lynch syndrome, a congenital condition that could lead to carcinogenesis.

Another aspect of the present Research Topic has been reported by Zhang et al., Li et al., and (Zhang et al.). All of them focused their articles on the usefulness of the uncommon application of specific imaging techniques in certain clinical conditions.

Zhang et al. proposed the use of multimodality US in the detection and characterization of metastasis of rare subtype of renal cell carcinoma (fumarate hydratase-deficient RCC). Application of grayscale, color Doppler, power Doppler, and contrast-enhanced US allow to detect metastasis; characterization could be feasible by ultrasonographic findings accompanied by US-guided biopsy.

In their article, Li et al. enhanced the strength of ^{68}Ga-conjugated fibroblast-activation protein inhibitor (FAPI) PET/CT versus ^{18}F-FDG in the identification process of intra-abdominal breast cancer metastasis thanks to a better tumor-to-background ratio and lack of interference by non-specific gastrointestinal physiological uptake.

Zhang et al. described contrast-enhanced ultrasound (CEUS) findings of intraperitoneal nodal large B-cell lymphoma. Usually, CT and PET/CT are employed for diagnosis and staging, but in recent years, many studies have focused on alternative imaging methods. CEUS can demonstrate the changes of vascularity of lymph nodes and, at the same time, allow to perform US-guided biopsy to confirm diagnosis.

This Research Topic is completed by two Case Reports involving hepatic diseases.

Shao et al. described a unique imaging pattern of a metastatic neuroendocrine neoplasm characterized by a steatosis area surrounding the hepatic localization. In this article, US findings were reported, and the support of CEUS in differential diagnosis was enhanced.

Congenital portosystemic shunts in children were the focus of (Zhang et al.). The prevalence of these vascular anomalies is 1 in 30000-50000 neonates and may present with various symptoms.

Imaging is essential in diagnosis with US as the first modality of choice in early identification, allowing the prompt management of potentially life-threatening manifestations. Moreover, imaging has a strong role in treatment thanks to the efficacy of endovascular techniques in occluding the shunts.

In conclusion, the contributions presented in this Research Topic have enriched our knowledge of cancer imaging, shedding light on rare neoplastic conditions, their imaging findings, and the implications for the choice of appropriate treatment, often performed under imaging guidance.

All of these studies provide suggestions for further investigation in this field.

Author contributions

AB: Writing – original draft, Writing – review & editing.

Conflict of interest

The author declares that the research was conducted in the absence of any commercial or financial relationships that could be construed as a potential conflict of interest.

Publisher's note

frontiers | Frontiers in Oncology

TYPE Case Report
PUBLISHED 13 October 2022
DOI 10.3389/fonc.2022.1035800

OPEN ACCESS

EDITED BY
Andrea Ciarmiello,
Sant'Andrea University Hospital, Italy

REVIEWED BY
Chunhong Li,
Suining Central Hospital, China
Junya Fukai,
Wakayama Medical University, Japan

*CORRESPONDENCE
Jiong Cai
jiong_cai@163.com
Pan Wang
1298178828@qq.com
Dandan Li
807442003@qq.com

SPECIALTY SECTION
This article was submitted to Cancer Imaging and Image-directed Interventions, a section of the journal Frontiers in Oncology

RECEIVED 03 September 2022
ACCEPTED 23 September 2022
PUBLISHED 13 October 2022

CITATION
Hu X, Huang Q, Wang J, Li D, Wang P and Cai J (2022) Case report: Primary intracranial EWs/PNET in adults: Clinical experience and literature review.
Front. Oncol. 12:1035800.
doi: 10.3389/fonc.2022.1035800

Case report: Primary intracranial EWs/PNET in adults: Clinical experience and literature review

Xianwen Hu[1], Qi Huang[1], Ju Wang[1], Dandan Li[2*], Pan Wang[1*] and Jiong Cai[1*]

[1]Department of Nuclear Medicine, Affiliated Hospital of Zunyi Medical University, Zunyi, China, [2]Department of Obstetrics, Zunyi Hospital of Traditional Chinese Medicine, Zunyi, China

Introduction: Adult primary intracranial Ewing sarcomas (EWs)/primitive neuroectodermal tumors (PNETs) are extremely rare, with only 30 patients published before us. The imaging features and treatment strategies of primary intracranial EWs/PNETs are unclear due to its rarity. The aim of this study was to investigate the clinical features, imaging findings, treatment, survival analysis, and prognosis of adult EWs/PNETs, and a systematic review was conducted based on the patient we treated and published literature.

Case description: A 19-year-old male patient suffered from head pain due to an accidental fall on a motorcycle that occurred more than 10 days before going to the hospital, and underwent computed tomography (CT) examination; it was found that the left temporo-occipital fossa was occupied. Magnetic resonance imaging (MRI) was recommended to understand the nature of the lesion, and the result showed that it has a high probability of being a meningioma. He underwent surgical removal of the mass under general anesthesia, and surprisingly, postoperative pathology revealed EWs/PNET. The disease has a high degree of malignancy, and the patient developed multiple metastases throughout the body 5 years after surgery.

Conclusion: Primary intracranial EWs/PNETs in adult patients are rare, of which imaging findings should be considered as one of the differential diagnoses of meningioma, hemangiopericytoma, and malignant triton tumor. Larger solid-cystic masses with septum-like enhancement may be relatively specific imaging findings of intracranial EWs/PNETs. The prognosis of primary adult intracranial EWs/PNETs is poor. Radical tumor resection combined with radiotherapy and chemotherapy is currently the main and possibly the most effective treatment method.

KEYWORDS

Ewing sarcomas, primitive neuroectodermal tumors, EWs/PNET, intracranial, magnetic resonance imaging, PET/CT

Introduction

Ewing sarcomas (EWs) and primitive neuroectodermal tumors (PNETs) share the same genetic and histological features; thus, they are collectively referred to as EWs/PNETs, which originate in the neuroectoderm and are mainly composed of primitive neuroectodermal cells (1). EWs/PNETs are highly malignant small round cell tumors with multi-directional differentiation potential, and can be divided into two types according to their origin in bone or soft tissue: intraosseous and extraosseous (2). About 85%–90% of the patients with EWs/PNET show the typical chromosomal translocation t(11;22)(q24;12), which leads to the fusion of the gene EWSR1 and the ETS family gene FLI1 (1, 3). The clinical manifestations of intracranial EWs/PNETs usually include headache, vomiting, dizziness, and other symptoms of intracranial hypertension, and some patients may manifest as eye movement disorders, decreased vision, and unsteady gait (4). Laboratory tests for intracranial EWs/PNETs are usually non-positive, of which imaging studies are often misdiagnosed as meningiomas due to their rarity and mostly dural origin, and the diagnosis of the disease is mainly based on pathology and immunohistochemistry. The prognosis of intracranial EWs/PNETs is poor, associated with age more than 14 years at diagnosis, initial tumor volume more than 200 ml, being male, development of metastases, etc. (2, 5, 6). The primary intracranial EWs/PNETs are extremely rare, the incidence of which is lower in adults than in children, and the published literature is only found in case or case series. Herein, we report a 19-year-old male patient with pathologically confirmed EWs/PNET originating in the left temporo-occipital fossa, who was discovered incidentally on imaging after an accidental fall. Moreover, we reviewed the published literature on adults (≥18 years of age) with intracranial EWs, summarized the radiological and clinical features of this rare tumor, and discussed its imaging differential diagnosis in detail.

Case description

A 19-year-old male patient suffered from head pain due to an accidental fall on a motorcycle that occurred more than 10 days before going to the hospital, and underwent computed tomography (CT) examination; a mass was found in the left temporo-occipital fossa. He was admitted to our hospital for further diagnosis and treatment. His parents were healthy and no family members had a history of similar diseases. Magnetic resonance imaging (MRI) was recommended to understand the nature of the lesion, and the result showed that it has a high probability of being a meningioma (as shown in Figure 1). No obvious positive signs were found in physical examination, and all laboratory indexes were within the normal reference value range. Based on the established diagnosis of a left temporo-occipital fossa space-occupying lesion, the patient underwent surgical resection of the tumor under general anesthesia. During the operation, the left temporoparietal horseshoe-shaped skin flap was taken, and the scalp was incised in full thickness to expose the skull and then a bone flap with a size of about 6 cm × 6 cm was removed. After the bone flap was taken out, it was found that the dura of about 2 cm × 2 cm was invaded by the tumor and broke through, and the inner plate of the covering skull was not invaded by the tumor. The dura was cut along the edge of the tumor invading the dura, and the tumor was removed together. The tumor tissue was gray, with clear demarcation from the surrounding brain tissue, abundant blood supply, soft texture, and a size of about 4.0 cm × 5.0 cm × 4.0 cm. Postoperatively, the resected tumor tissue was sent for pathological examination, and the results showed that there were diffusely distributed round cells in the tumor (as shown in Figure 2). Immunohistochemical staining showed that tumor cells positively expressed CD99, Vimentin, Bcl-2, ki-67 (about 40%), weakly expressed CD56, SMA, and negatively expressed CD34, CgA, CK, Desmin, EMA, S100, etc. Ewing's sarcoma breakpoint region 1 (EWSR1) gene rearrangement was identified by fluorescence *in situ* hybridization in a foreign hospital. Based on these findings, the patient was diagnosed with intracranial extraosseous EWs/PNET. He did not undergo further radiotherapy and chemotherapy after the operation. At the 5th year after the operation, the patient was re-admitted to the hospital because of multiple bone pains throughout the body. ^{18}F-FDG PET/CT was recommended to evaluate the patient's systemic condition, and the results revealed multiple high radioactive uptake foci throughout the body (as shown in Figure 3). Biopsy of the lesion at the iliac bone revealed the same disease as he had previously suffered. He then received a vincristine–cyclophosphamide–doxorubicin chemotherapy regimen and palliative radiation targeting the lesions of the humerus, ilium, and acetabulum. Unfortunately, he passed away 3 months after starting maintenance therapy with chemoradiotherapy.

Literature review

Primary intracranial EWs/PNET case reports and case series published in PubMed, Embase, and Web of Science databases as of 1 June 2022 were searched, with language restrictions limited to English. The following keywords were used: Ewing's sarcoma, EWs, primitive neuroectodermal tumors, PNET, intracranial, and dura mater. The first author, publication year and country, as well as the patient's age, gender, main clinical symptoms, CT and MRI imaging findings, treatment methods, and follow-up results were recorded for each case (as shown in Table 1).

Through a systematic search, 30 adult primary intracranial EWs/PNETs were published prior to our present case (1, 4, 7–28). A total of 31 patients including our patient, consisted of 17 male and 14 female patients with a median age of 37 years, with

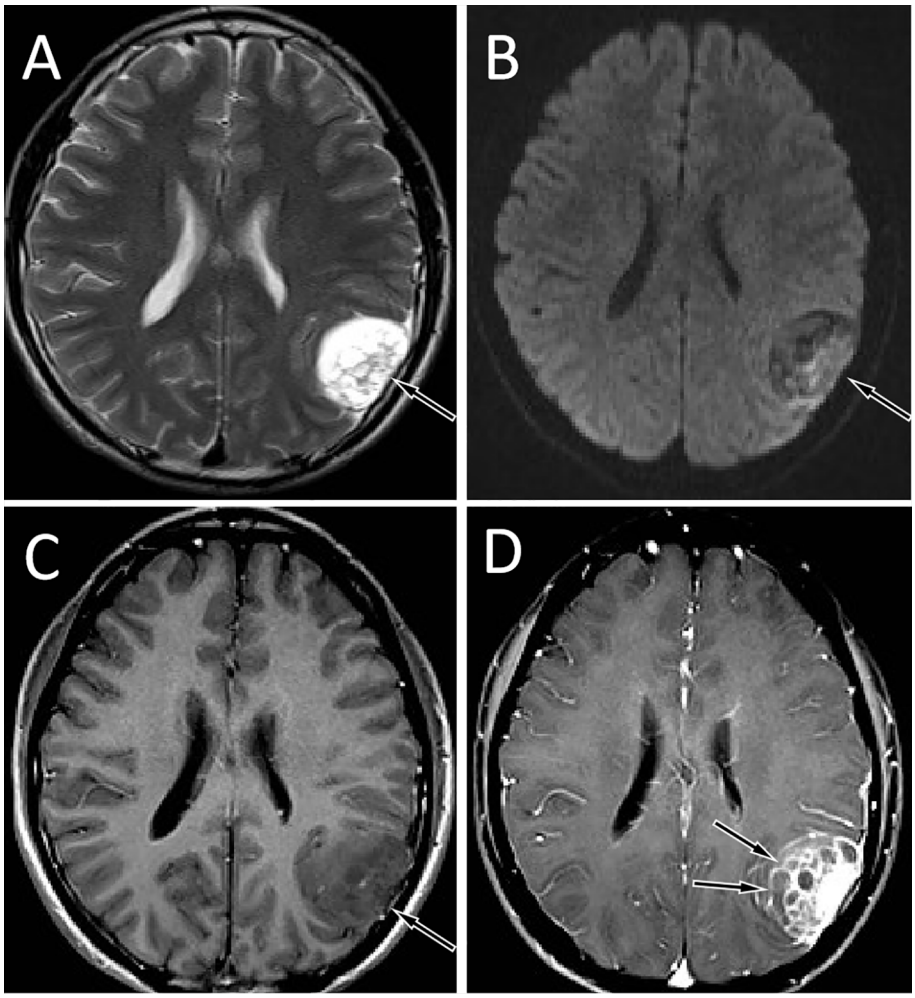

FIGURE 1
Brain MRI showed that the tumor was located in the left temporo-occipital fossa. T2WI sequence showed that the lesion was high signal (**A**, arrow). Diffusion-weighted imaging showed that the movement of water molecules was not restricted and showed heterogeneous low signal (**B**, arrow). The T1WI sequence showed that the lesion was slightly low signal (**C**, arrow), and the solid component of the tumor was significantly enhanced on contrast-enhanced T1WI, with multiple unenhanced cysts around it, and septum-like enhancement was seen in between (**D,** arrows).

the top three cases published from China (23%), USA (19%), and Italy (13%), and the detailed distribution of patients is shown in Figures 4A, B. Most patients came to the hospital for medical assistance due to short-term headache, dizziness, vomiting, and visual disturbances. Rare clinical symptoms include epilepsy, fever, memory loss, skull invasion in some patients, and local signs of scalp soft tissue swelling. The main foci originated from frontal fossa (7/31), temporal fossa (5/31), followed by posterior fossa, parietal fossa, pontine cerebellar triangle, frontotemporal fossa, frontoparietal fossa, parietal fossa junction, cavernous sinus, etc. Most of the tumor foci were solid-cystic; only four cases were solid with small diameters, ranging from 1.4 to 3.5 cm. The solid component of the tumor showed isodense or slightly high density on CT, slightly low or isointense on T1WI, and hypointense-to-hyperintense on T2WI. On contrast-enhanced CT or T1WI, most of the solid components of the tumor were significantly enhanced, and septum-like enhancement was seen in the cystic components; only one patient showed ring enhancement. Solid tumors all showed obvious uniform enhancement. Of all adults with primary intracranial EWs/PNETs, seven had cranial involvement at diagnosis, and three had meningeal or spinal metastases (as shown in Figure 4C). Most of the patients received surgical resection of the tumor combined with radiotherapy and chemotherapy. Overall, intracranial EWs/PNET has a poor prognosis, with a median survival of 38 months and a 5-year survival rate of only 18%. There was no significant difference in overall survival between male and female patients, and cranial

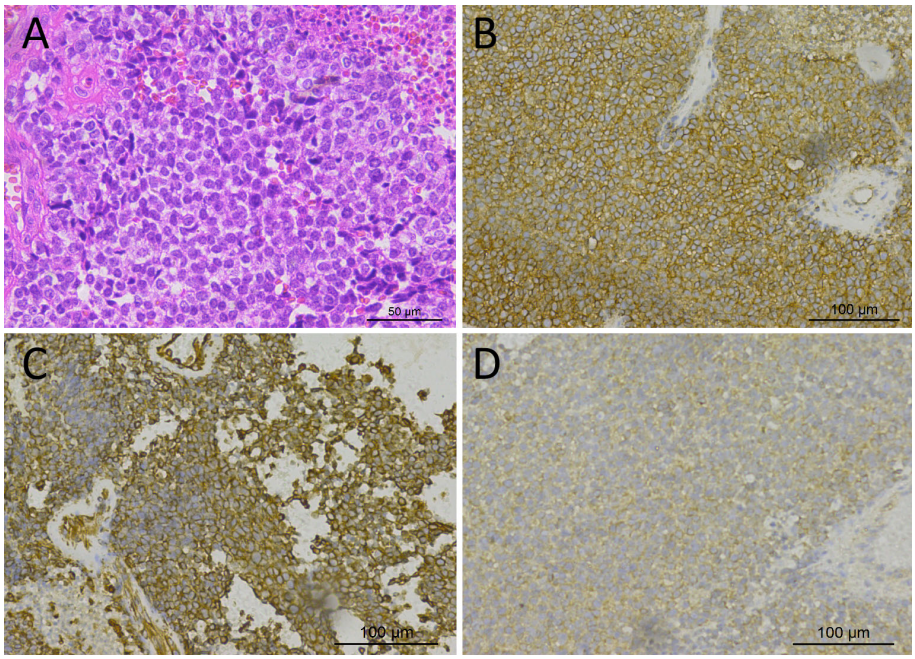

FIGURE 2
Hematoxylin–eosin staining showed that the tumor tissue was composed of small round cells with relatively uniform morphology, and the nuclei were deeply stained **(A)**. Immunohistochemical staining showed that tumor cells positively expressed CD99 **(B)**, Vimentin **(C)**, and Bcl-2 **(D)**.

invasion or distant metastasis at the first visit was a prognostic factor (as shown in Figure 5).

Discussion

Intracranial EWs/PNETs are rare and account for only 0.03% of all intracranial tumors (29), which is more common in children and adolescents, and previous studies have shown that the median age at diagnosis of intracranial EWs/PNET is 15 years, and there are slightly more male than female patients (30). The case reported here is an intracranial EWs/PNET in the left temporo-occipital fossa of a 19-year-old male patient who was found incidentally after a trauma and had no previous clinical symptoms. In addition, we reviewed all cases of primary intracranial EWs/PNET in adults (≥18 years of age); 30 patients had been reported before our case. The oldest reported patient with primary intracranial EWs/PNET was 69 years old, and the median age at diagnosis of adult patients was 37 years. Our current study shows that the supratentorial fossa including the temporal fossa and frontal fossa are the most common sites for intracranial EWs/PNET, and the most common clinical manifestations include headache, dizziness, vomiting, and visual disturbances, without specificity.

Imaging tests including CT and MRI play a significant role in the diagnosis of central nervous system diseases, especially MRI. On imaging, primary intracranial EWs/PNET is mostly a mass that grows with the dura mater as a wide base, which can grow across the cranial fossa and midline of the brain. Large cystic necrotic areas can be seen in most tumors, and hemorrhage can be seen in some patients, but few calcifications appear. The adjacent skull may be compressed and thinned or invaded to cause bone destruction. Our study showed that intracranial EWs/PNETs were mostly solid-cystic masses, in which the solid components were mostly isodense or slightly hypodense on CT, and only a few small masses showed uniform density. On the T1WI sequence of MRI, the solid component of the tumor was slightly hypointense or isointense, and T2WI was hypo-to-hyperintense, while the cystic part was hypointense on T1WI sequence and hyperintense on T2WI. On contrast-enhanced CT or T1WI, the solid part of the tumor in most patients was significantly enhanced, and the adjacent dura mater was significantly enhanced; only a patient showed primary ring-enhancing cystic lesions in all published cases (13). Notably, on contrast-enhanced scans, septum-like enhancement was seen in cystic regions of tumors in our patient and most of the published literature, which we believe is different from other tumors. Intracranial EWs/PNET including our patient and the published cases were misdiagnosed as meningioma or

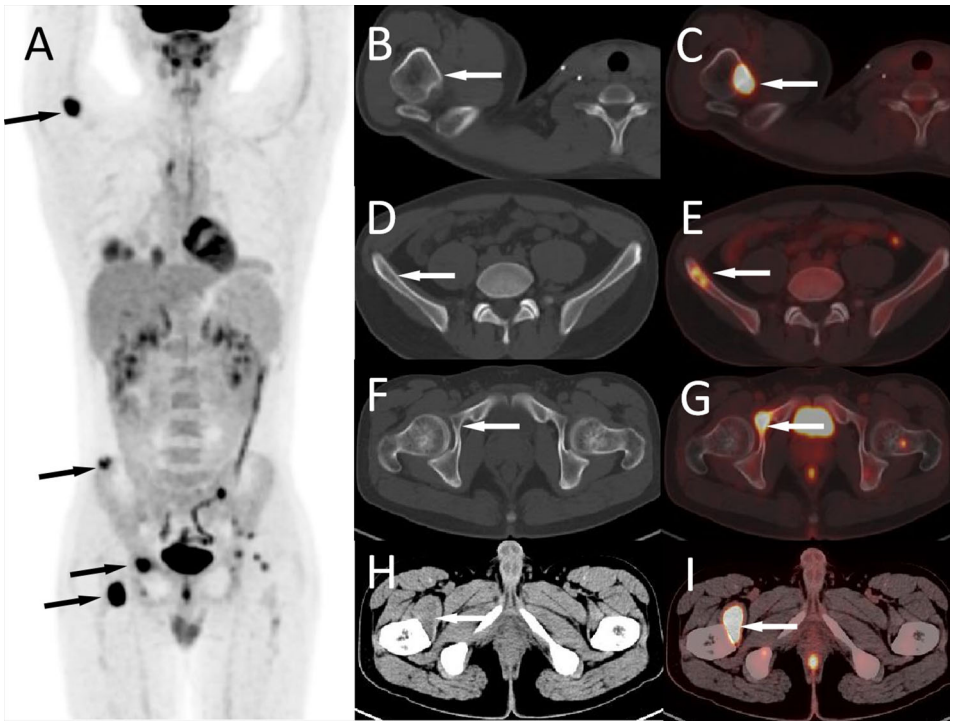

FIGURE 3
The patient's ^{18}F-FDG PET/CT at 5 years after operation; the maximum intensity projection figure showed multiple FDG concentration foci throughout the body (**A**, arrows). Axial figures showed that the right humerus (**B**, CT; **C**, PET/CT fusion), ilium (**D**, CT; **E**, PET/CT fusion), and acetabulum (**F**, CT; **G**, PET/CT fusion) can be seen with iso-density or slightly hypodense bone destruction areas with high radioactive uptake (arrows). Moreover, a hypodense mass with FDG accumulation was seen in the right iliopsoas muscle (**H**, CT; **I**, PET/CT fusion, arrows).

hemangiopericytoma (HPC) preoperatively; thus, these two tumors are the most important imaging differential diagnoses for intracranial EWs/PNET. Meningiomas are common adult central nervous system tumors, mostly benign. Meningiomas on CT are mostly isodense or high-density spherical or hemispherical masses, with a higher probability of calcification, but with less low-density cystic necrosis, and even if present, the volume of cystic necrosis is small (31). On MRI, the signal of meningiomas is relatively uniform, and the T1WI and T2WI sequences are iso-to-hyperintense, and hyperintensity is more common on DWI, while our patient was hypointense on DWI, which is different from it. Angiography can clearly show the internal and external carotid arteries supplying blood to the meningioma. Typical signs include the tumor body compressing adjacent blood vessels, but the tumor body and its interface are still smooth, showing a "holding ball" change (32). HPC is a malignant tumor with abundant blood vessels, which often leads to low-density necrotic foci due to insufficient local blood supply to the tumor, and the morphology of the tumor is irregular, most of which is lobulated (33), while the shape of EWs/PNET is more regular. On contrast-enhanced scans, HPC was more enhanced and intratumoral vascular flow void signals were more common, and angiography showed multiple tortuous and thickened vascular shadows in the mass (34), which is different from EWs/PNET. Moreover, malignant triton tumor (MTT), namely, malignant schwannoma with rhabdomyoma differentiation, another rare intracranial tumor, is often misdiagnosed as meningioma in previous literature reports; thus, it should also be considered as one of the differential diagnoses of EWs/PNET. MTT is usually equal and slightly hyperdense on CT, and a small volume of cystic necrosis is often seen. Tumors on MRI are mostly low signal on T1WI and high signal on T2WI, and arc or linear low-signal shadows appear in the high-signal tumor tissue, which is relatively specific for the diagnosis of MTT (35).

The diagnosis of EWs/PNET mainly depends on pathology and immunohistochemistry. Under the microscope, the tumors are composed of small round cells or elliptic cells, with hyperchromatic nuclei, and mildly basophilic cytoplasm and Homer–Wright chrysanthemum or Flexner–Weinsteiner chrysanthemum structures can be seen in some tumors (2, 29). Immunohistochemistry showed that almost all tumor cells of intracranial EWs/PNET patients consistently and diffusely expressed CD99, but there was no specificity (36). In addition, tumor cells

TABLE 1 Clinical and imaging features of the cases of primary intracranial EWs/PNETs.

Author, year, country	Gender/ age	Main symptoms and signs	Onset of symptoms (months)	Location	Morphological	CT[a]	MRI		CECT/MRI Degree/ septum-like	MD (cm)	Metastases at diagnosis	Treatment	Recurrence	Metastasis	Follow-up/ (months)
							T1WI	T2WI							
Batur/2021/ Turkey (7)	44/M	Headache	4	Left posterior fossa	Solid-cystic	–	Slightly high	Isointense	Obvious/Y	–	N	Surgery	N	N	Alive/36
Deshpande/ 2021/India (8)	33/M	Headache, nausea, vomiting	–	Left temporal fossa	Solid-cystic	–	–	–	Obvious /Y	–	N	Surgery, focal RT (55.8 Gy/31#), COG protocol (IE/ VAC, 48 weeks)	N	N	Alive/18
Deshpande/ 2021/India (8)	33/F	Left eye movement impairment	–	Left frontal fossa	–	–	–	–	–	–	N	Surgery, focal RT (54 Gy/30#), vincristine + cisplatin (2 weeks), discontinued in view of intolerance	Y	Vertebral	Alive/17
Jiang/2020/ China (4)	55/F	Memory decline	1	Left frontal fossa	Solid-cystic	Slightly higher density	Hypointense-to-isointense	Hypointense-to-hyperintense	Obvious/Y	6.5	N	Surgery, focal RT (55 Gy/30#)	N	N	Alive/18
Howell/2020/ USA (9)	37/M	Dizziness, headache, nausea, vomiting	1	Multifocal (pineal region, third and fourth ventricles)	Solid-cystic	–	–	–	–	–	Y (Spinal cord)	4 weeks vincristine, 36 Gy	N	N	Alive/7
Huang/2020/ Australia (10)	19/M	Headache, vomiting	0.5	Left frontal fossa	Solid-cystic	High density	Hypointense-to-isointense	Hypointense-to-hyperintense	Obvious/Y	7.1	N	Surgery, VIDE+VAI, focal RT	N	N	Alive/12
Chen/2019/ China (11)	23/M	Swelling over the scalp, headache	2	Left temporoparietal fossa	Solid-cystic	–	Hypointense-to-isointense	Hypointense-to-hyperintense	Obvious/Y	–	Bone involvement	Surgery, 55 Gy	N	Spinal cord	Died/6
Chen/2019/ China (11)	18/M	Headache, swelling over the scalp	7	Left temporal fossa	Solid-cystic	–	Hypointense-to-isointense	Hypointense-to-hyperintense	Obvious/Y	–	Bone involvement	Surgery, 50 Gy	Y	N	Died/23
Chen/2019/ China (11)	43/M	Epilepsy	1	Right parietal fossa	Solid-cystic	–	Hypointense-to-isointense	Hypointense-to-hyperintense	Obvious/Y	–	N	Surgery, VAC+ actinomycin D, 50 Gy	Y	N	Died/48
Chen/2019/ China (11)	22/F	Swelling over the scalp	1	Right temporal fossa	Solid-cystic	–	Hypointense-to-isointense	Hypointense-to-hyperintense	Obvious/Y	–	Bone involvement	Surgery, VAC, 55 Gy	Y	Skull	Died/38

(Continued)

10.3389/fonc.2022.1035800

TABLE 1 Continued

Author, year, country	Gender/ age	Main symptoms and signs	Onset of symptoms (months)	Location	Morphological	CT[a]	MRI		CECT/MRI Degree/ septum-like	MD (cm)	Metastases at diagnosis	Treatment	Recurrence	Metastasis	Follow-up/ (months)
							T1WI	T2WI							
Ke/2017/ China (12)	43/M	Epilepsy	–	Right parietal fossa	–	–	Hypointense-to-isointense	Hypointense-to-hyperintense	Obvious/Y	–	N	Surgery, VDAC	Y	N	Died/48
AndenHeuvel/ 2015/USA (13)	61/M	Left hemiparesis	2	Right frontal and temporal fossa	Solid-cystic	–	–	–	Ring reinforcement	6.2	N	Surgery	N	N	–
Salunke/2014/ India (14)	52/M	Fever, headache	1	Posterior fossa	Solid-cystic	–	–	–	Obvious/Y	6.0	Bone involvement	Surgery, VAC + ifosfamide, focal RT 50 Gy	Y	N	Died/6.5
Cole/2014 /USA (15)	51/F	Visual disturbances	–	Posterior fossa	Solid-cystic	–	–	–	Obvious/Y	3.53	N	Surgery, VCD (alternated with EI every 3 weeks) for 14 cycles. After the 4th cycle, doxorubicin was displaced into dactinomycin	N	N	Alive/24
Huguenard/ 2021/USA (16)	34/M	Headache, back pain	3	Right frontal fossa	Solid-cystic	High density	Hypointense-to-isointense	Hypointense-to-hyperintense	Obvious/Y	3.7	Pia mater, meninges	Surgery, VC + cisplatin, FOCAL RT	Y	Spinal cord	Died/6
Mellai/2010/ Italy (17)	56/F	Headache, confusion	–	Right temporal fossa	Solid-cystic	–	–	–	Obvious/Y	–	N	Surgery	N	N	Alive/18
Attabib/2006/ Canada (18)	48/F	Headache, left ptosis	6	Left cavernous fossa	–	–	–	–	Obvious/N	4.0	N	Surgery, VCD (alternated with EI every 3 weeks), 54 Gy	N	N	Alive/14
D'Antonio/ 2004/Italy (19)	50/F	Headaches, vomiting	–	Right parieto-temporal fossa	–	–	–	–	Obvious/Y	6.0	N	Surgery	N	N	Alive/12
Simmons/ 2001/UK (20)	67/F	Headache, facial paralysis	18	Right CA	–	–	–	–	–	–	Bone involvement	Palliative radiation	Y	Meninges	Died/13
Kalamarides/ 2001/France (21)	34/F	Vertigo, tinnitus	12	Left CA	Solid	–	–	Hyperintense	Obvious/N	1.8	N	Surgery, craniospinal radiotherapy (35 Gy with an overdosage to 55 Gy over the tumor bed)	Y	N	Alive/12
Kalamarides/ 2001/France (21)	41/F	Dizziness, left deafness	12	Left CA	Solid	–	–	Hyperintense	Obvious /N	1.4	N	Surgery, craniospinal radiotherapy (35 Gy with an overdosage to 55 Gy over the tumor bed)	N	N	Alive/12
Tanboon/ 2012/Canada (22)	22/F	Headache, vomiting, blurred vision	3	Right frontal fossa	Solid-cystic	–	–	–	Obvious/Y	4.0	Bone involvement	Surgery	Y	Multiple bones,	Died/13

(Continued)

10.3389/fonc.2022.1035800

TABLE 1 Continued

Author, year, country	Gender/ age	Main symptoms and signs	Onset of symptoms (months)	Location	Morphological	CT[a]	MRI		CECT/MRI Degree/ septum-like	MD (cm)	Metastases at diagnosis	Treatment	Recurrence	Metastasis	Follow-up/ (months)
							T1WI	T2WI							
														cervical LNs	
Antonelli/ 2011/Italy (23)	37/M	Headache, coma	0.5	Right frontotemporal fossa	Solid-cystic	Isodensity	–	–	Obvious/Y	–	N	Surgery, RT 6 weeks	Y	N	Alive/17
Mobley/2006/ USA (24)	21/M	Headache, double vision	2	Right occipital fossa	Predominantly solid	Isodensity	–	–	Obvious/Y	3.5	N	Surgery, Dactinomycin, VAC, 54 Gy	Y	Cervical and thoracic spine	Alive/17
Idrees M/ 2005/ USA (25)	46/M	Headache, nausea, and vomiting	0.5	Cavernous sinus and sella	Solid	Isodensity	Isointense	Hyperintense	Obvious/N	2.3	N	Vincristine, 5,400 cGy	–	–	–
Ishii/2001/ Japan (26)	19/F	Headache	–	Right frontal fossa	–	–	–	–	–	–	N	Surgery, VAC, palliative radiation	Y	–	Died/36
Papotti/1998/ Italy (27)	30/F	Headache, dizziness	–	Right frontal fossa	Solid-cystic	–	–	–	–	7.0	N	Surgery, VAC, 50 Gy	Y	Thoracic spine	Died/120
Haveman/ 2020/ Netherlands (28)	53.76/M	–	–	Temporal fossa	–	–	–	–	–	–	LNs, CNS	Surgery, 6xVIDE, 7xVAC, RT	–	–	Died/15
Haveman/ 2020/ Netherlands (28)	30.36/F	–	–	Frontal fossa	–	–	–	–	–	–	Bone involvement	Surgery, 6x VIDE, 8x VAI, RT	–	–	Died/38
Haveman/ 2020/ Netherlands (28)	69.34/M	–	–	Parieto-occipital	–	–	–	–	–	–	N	Surgery, 6x VIDE, 7x VAC, RT	–	–	Died/15
Current case	19/M	Accidental discovery	N	Left temporal fossa	Solid-cystic	Isodensity	Slight hypointense	Hyperintense	Obvious/Y	5.0	N	Surgery, VAC, palliative radiation	N	Multiple bones and muscles	Died/66

[a]refers to the solid component density of the tumor. M, male; F, female; Y, yes; N, not; CT, computed tomography; CNS, central nervous system; MRI, magnetic resonance imaging; CE, contrast enhancement; CA, cerebellopontine angle; R, radiotherapy; LNs, lymph nodes; VAC, vincristine, doxorubicin, cyclophosphamide; VCE, vincristine, cyclophosphamide, epirubicin; VIDE + C, vincristine, ifosfamide, doxorubicin, etoposide plus cyclophosphamide; VIDE, vincristine, ifosfamide, doxorubicin, etoposide; VTI, vincristine, temozolomide, irinotecan; VAI, vincristine, actinomycin D; RT, radiotherapy.

10.3389/fonc.2022.1035800

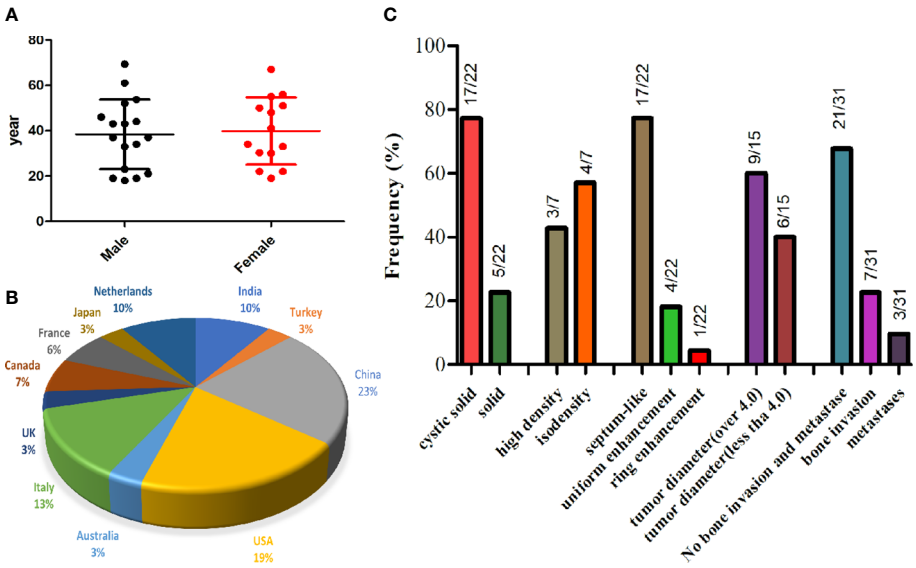

FIGURE 4
The gender and age distribution **(A)** and country proportion **(B)** of 31 adult patients with primary intracranial EWs/PNET, and imaging features of primary intracranial EWs/PNET **(C)**.

expressed Vimentin, NSE, Syn, and membrane protein FLI-1 to varying degrees, and molecular detection to find EWSR1 gene rearrangement is the current gold standard for diagnosing EWs/PNETs (2, 12).

Due to its rarity, the standard treatment regimen for intracranial EWs/PNET has not been established, and surgery for the purpose of total tumor resection is currently the main treatment method. In our review of the published literature, most patients were treated with a combination of radiotherapy and chemotherapy including vincristine, cyclophosphamide, doxorubicin, ifosfamide, etoposide, doxorubicin, and radiomycin D and other drugs after surgical resection (30). Our study including 31 adults with intracranial EWs/PNET showed that the prognosis was poor, and the longest follow-up was 10 years in a patient who eventually metastasized to the thoracic spine, progressed, and died (27). Among these patients, their median survival was only 38 months, and the 5-year survival rate was less than 20%.

In conclusion, adult patients with primary intracranial EWs/PNET are rare, whose imaging findings should be considered as one of the differential diagnoses of meningioma, HPC, and MTT. There are large cystic lesions in the tumor, and septum-like enhancement on contrast-enhanced scan may be a relatively specific feature of EWs/PNET, whereas the rarity of the disease limits the clinical application of our findings, and more cases and long-term follow-up studies are needed in the future to fully understand EWs/PNET in the adult population.

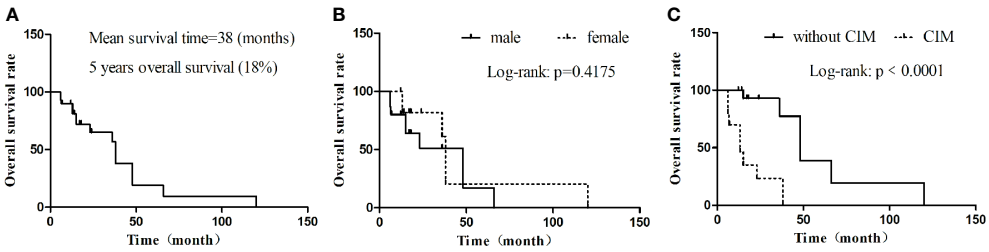

FIGURE 5
Kaplan–Meier OS. **(A)** OS in all cases; **(B)** OS by gender; **(C)** OS by whether there are cranial invasion or distant metastasis. CIM, cranial invasion or distant metastasis; MST, median survival time; OS, overall survival.

Data availability statement

The original contributions presented in the study are included in the article/Supplementary Material. Further inquiries can be directed to the corresponding authors.

Ethics statement

Written informed consent was obtained from the individual (s), and minor(s)' legal guardian/next of kin, for the publication of any potentially identifiable images or data included in this article.

Author contributions

JC and PW: funding acquisition; DL: investigation; QH and JW: methodology; XH: writing—original draft; XH, PW, and JC: writing—review and editing. All authors contributed to the article and approved the submitted version.

Funding

This study was funded by the National Natural Science Foundation of the People's Republic of China, NSFC (grant numbers: 81571712), Zunyi Medical College Research Start Fund 2018ZYFY03, and QianKeHe platform talents [2017] (Grant No. 5733-035).

Conflict of interest

The authors declare that the research was conducted in the absence of any commercial or financial relationships that could be construed as a potential conflict of interest.

Publisher's note

All claims expressed in this article are solely those of the authors and do not necessarily represent those of their affiliated organizations, or those of the publisher, the editors and the reviewers. Any product that may be evaluated in this article, or claim that may be made by its manufacturer, is not guaranteed or endorsed by the publisher.

References

1. de Alava E. Ewing Sarcoma, an update on molecular pathology with therapeutic implications. *Surg Pathol Clin* (2017) 10:575–85. doi: 10.1016/j.path.2017.04.001

2. Applebaum MA, Worch J, Matthay KK, Goldsby R, Neuhaus J, West DC, et al. Clinical features and outcomes in patients with extraskeletal Ewing sarcoma. *Cancer* (2011) 117(13):3027–32. doi: 10.1002/cncr.25840

3. Grünewald T, Cidre-Aranaz F, Surdez D, Tomazou EM, de Álava E, Kovar H, et al. Ewing Sarcoma. *Nat Rev Dis Primers* (2018) 4:5. doi: 10.1038/s41572-018-0003-x

4. Jiang Y, Zhao L, Wang Y, Liu X, Wu X, Li Y. Primary intracranial Ewing Sarcoma/Peripheral primitive neuroectodermal tumor mimicking meningioma: A case report and literature review. *Front Oncol* (2020) 10:528073. doi: 10.3389/fonc.2020.528073

5. Bacci G, Longhi A, Ferrari S, Mercuri M, Versari M, Bertoni F. Prognostic factors in non-metastatic ewing's sarcoma tumor of bone: an analysis of 579 patients treated at a single institution with adjuvant or neoadjuvant chemotherapy between 1972 and 1998. *Acta Oncol* (2006) 45:469–75. doi: 10.1080/02841860500519760

6. Ladenstein R, Pötschger U, Le Deley MC, Whelan J, Paulussen M, Oberlin O, et al. Primary disseminated multifocal Ewing sarcoma: results of the Euro-EWING 99 trial. *J Clin Oncol* (2010) 28:3284–91. doi: 10.1200/JCO.2009.22.9864

7. Ishii N, Hiraga H, Sawamura Y, Shinohe Y, Nagashima K. Alternative EWS-FLI1 fusion gene and MIC2 expression in peripheral and central primitive neuroectodermal tumors. *Neuropathology* (2001) 21(1):40–4. doi: 10.1046/j.1440-1789.2001.00367.x

8. Deshpande G, Epari S, Gupta C, Shetty O, Gurav M, Chinnaswamy G, et al. Primary intracranial Ewing sarcoma/ peripheral primitive neuroectodermal tumor, an entity of unacquaintance: a series of 8 cases. *Childs Nerv Syst* (2021) 37:839–49. doi: 10.1007/s00381-020-04850-w

9. Howell SG, Lyon KA, Garrett DJr, Huang JH, Fonkem E. Optimum treatment for primary intracranial Ewing sarcoma. *Proc (Bayl Univ Med Cent)* (2020) 33:430–2. doi: 10.1080/08998280.2020.1755199

10. Huang J, Ghent F, Levingston R, Scholsem M. Intracranial Ewing sarcoma - a case report. *Surg Neurol Int* (2020) 11:134. doi: 10.25259/SNI_178_2020

11. Chen J, Jiang Q, Zhang Y, Yu Y, Zheng Y, Chen J, et al. Clinical features and long-term outcome of primary intracranial Ewing Sarcoma/Peripheral primitive neuroectodermal tumors: 14 cases from a single institution. *World Neurosurg* (2019) 122:e1606–1606e1614. doi: 10.1016/j.wneu.2018.11.151

12. Ch K, Duan Q, Yang H, Zhu F, Yan M, Xu SP, et al. Meningeal Ewing Sarcoma/Peripheral PNET: Clinicopathological, immunohistochemical and FISH study of four cases. *Neuropathology* (2017) 37:35–44. doi: 10.1111/neup.12325

13. VandenHeuvel KA, Al-Rohil RN, Stevenson ME, Qian J, Gross NL, McNall-Knapp R, et al. Primary intracranial ewing's sarcoma with unusual features. *Int J Clin Exp Pathol* (2015) 8:260–74.

14. Salunke P, Sharma M, Gupta K. Ewing Sarcoma of the occipital bone in an? elderly patient. *World Neurosurg* (2014) 81:e10–2. doi: 10.1016/j.wneu.2010.12.050

15. Cole M, Parajuli S, Laske D, Goldstein L, Morrison T, Mukherjee A, et al. Peripheral primitive neuroectodermal tumor of the dura in a 51-year-old woman following intensive treatment for breast cancer. *Am J Case Rep* (2014) 15:294–9. doi: 10.12659/AJCR.890656

16. Huguenard AL, Li YD, Sharifai N, Perkins SM, Dahiya S, Chicoine MR. Multifocal primary central nervous system Ewing sarcoma presenting with intracranial hemorrhage and leptomeningeal dissemination: illustrative case. *J Neurosurg Case Lessons* (2021) 1:CASE2042. doi: 10.3171/CASE2042

17. Mellai M, Caldera V, Comino A, Fortunato M, Bernucci C, Schiffer D. PNET/ESFT of the cranial vault: a case report. *Clin Neuropathol* (2010) 29:372–7. doi: 10.5414/npp29372

18. Attabib NA, West M, Rhodes RH. Peripheral primitive neuroectodermal tumor of the cavernous sinus: case report. *Neurosurgery* (2006) 58:E992. doi: 10.1227/01.NEU.0000210215.73374.EE

19. D'Antonio A, Caleo A, Garcia JF, Marsilia GM, De Dominicis G, Boscaino A. Primary peripheral PNET/Ewing's sarcoma of the dura with FISH analysis. *Histopathology* (2004) 45:651–4. doi: 10.1111/j.1365-2559.2004.01961.x

20. Simmons MA, Luff DA, Banerjee SS, Ramsden RT. Peripheral primitive neuroectodermal tumour (pPNET) of the cerebellopontine angle presenting in adult life. *J Laryngol Otol* (2001) 115:848–52. doi: 10.1258/0022215011909161

21. Kalamarides M, Dewolf E, Couvelard A, Shahidi A, Bouccara D, Cyna-Gorse F, et al. Extraaxial primitive neuroectodermal tumor mimicking a vestibular schwannoma: diagnostic and therapeutic difficulties. *Rep two cases J Neurosurg* (2001) 94:612–6. doi: 10.3171/jns.2001.94.4.0612

22. Tanboon J, Sitthinamsuwan B, Paruang T, Marrano P, Thorner PS. Primary intracranial Ewing sarcoma with an unusually aggressive course: a case report and review of the literature. *Neuropathology* (2012) 32:293–300. doi: 10.1111/j.1440-1789.2011.01258.x

23. Antonelli M, Caltabiano R, Chiappetta C, Oliva MA, Giangaspero F, Lanzafame S. Primary peripheral PNET/Ewing's sarcoma arising in the meninges, confirmed by the presence of the rare translocation t (21,22) (q22;q12). *Neuropathology* (2011) 31:549–55. doi: 10.1111/j.1440-1789.2010.01196.x

24. Mobley BC, Roulston D, Shah GV, Bijwaard KE, McKeever PE. Peripheral primitive neuroectodermal tumor/Ewing's sarcoma of the craniospinal vault: case reports and review. *Hum Pathol* (2006) 37:845–53. doi: 10.1016/j.humpath.2006.02.011

25. Idrees M, Gandhi C, Betchen S, Strauchen J, King W, Wolfe D. Intracranial peripheral primitive neuroectodermal tumors of the cavernous sinus: a diagnostic peculiarity. *Arch Pathol Lab Med* (2005) 129:e11–5. doi: 10.5858/2005-129-e11-IPPNTO

26. Ishii N, Hiraga H, Sawamura Y, Shinohe Y, Nagashima K. Alternative EWS-FLI1 fusion gene and MIC2 expression in peripheral and central primitive neuroectodermal tumors. *Neuropathology* (2001) 21:40–4. doi: 10.1046/j.1440-1789.2001.00367.x

27. Papotti M, Abbona G, Pagani A, Monga G, Bussolati G. Primitive neuroectodermal tumor of the meninges: An histological, immunohistochemical, ultrastructural, and cytogenetic study. *Endocr Pathol* (1998) 9:275–80. doi: 10.1007/BF02739968

28. Haveman LM, Ranft A, Berg H, Klco-Brosius S, Ladenstein R, Paulussen M, et al. Primary and metastatic intracranial Ewing sarcoma at diagnosis: Retrospective international study and systematic review. *Cancers (Basel)* (2020) 12(6):1675. doi: 10.3390/cancers12061675

29. Yim J, Lee WS, Kim SK, Kang HJ, Bae J, Park SH. Intracranial Ewing sarcoma with whole genome study. *Childs Nerv Syst* (2019) 35:547–52. doi: 10.1007/s00381-018-3997-1

30. Cherif El Asri A, Benzagmout M, Chakour K, Chaoui MF, Laaguili J, Chahdi H, et al. Primary intracranial pPNET/Ewing sarcoma: Diagnosis, management, and prognostic factors dilemma-a systematic review of the literature. *World Neurosurg* (2018) 115:346–56. doi: 10.1016/j.wneu.2018.04.164

31. Shijo M, Honda H, Koyama S, Ishitsuka K, Maeda K, Kuroda J, et al. Dura mater graft-associated Creutzfeldt-Jakob disease with 30-year incubation period. *Neuropathology* (2017) 37:275–81. doi: 10.1111/neup.12359

32. Dabus G, Linfante I, McDermott MW. Angiography and embolization of meningiomas. *Handb Clin Neurol* (2020) 169:193–202. doi: 10.1016/B978-0-12-804280-9.00013-5

33. Wang X, Zhang X, Zhou Q, Zhou X, Chen L, Huang G, et al. Hemangiopericytoma arose from the site of meningioma resection. *J Craniofac Surg* (2017) 28:e329–329e330. doi: 10.1097/SCS.0000000000003576

34. Sibtain NA, Butt S, Connor SE. Imaging features of central nervous system haemangiopericytomas. *Eur Radiol* (2007) 17:1685–93. doi: 10.1007/s00330-006-0471-3

35. Hu X, He X, Wang P, Zou Y, Li D, Cai J, et al. Intracranial malignant triton tumor in children: A case report. *Iran J Radiol* (2021) 18(1):e106103. doi: 10.1097/MD.0000000000016797

36. Pappo AS, Dirksen U. Rhabdomyosarcoma, Ewing sarcoma, and other round cell sarcomas. *J Clin Oncol* (2018) 36:168–79. doi: 10.1200/JCO.2017.74.7402

frontiers | Frontiers in Oncology

TYPE Case Report
PUBLISHED 18 October 2022
DOI 10.3389/fonc.2022.896477

OPEN ACCESS

EDITED BY
Francesca Sanguedolce,
University of Foggia, Italy

REVIEWED BY
Aleksandr Shulyak,
National Academy of Medical Sciences of Ukraine, Ukraine
Weidong Gan,
Nanjing Drum Tower Hospital, China

*CORRESPONDENCE
Diming Cai
doccai@163.com

SPECIALTY SECTION
This article was submitted to Cancer Imaging and Image-directed Interventions, a section of the journal Frontiers in Oncology

RECEIVED 15 March 2022
ACCEPTED 28 September 2022
PUBLISHED 18 October 2022

CITATION
Zhang X, Zhang Y, Li Y, Shen P, Liu Z, Zeng H, Zhang M, Chen N, Yao J, Huang R and Cai D (2022) Case report: Ultrasonographic findings of retroperitoneum and abdominal wall metastases of renal cell carcinoma with FH gene deletion.
Front. Oncol. 12:896477.
doi: 10.3389/fonc.2022.896477

Case report: Ultrasonographic findings of retroperitoneum and abdominal wall metastases of renal cell carcinoma with FH gene deletion

Xuhui Zhang[1], Yue Zhang[1], Yongzhong Li[1], Pengfei Shen[2], Zhenghua Liu[2], Hao Zeng[2], Mengni Zhang[3], Ni Chen[3], Jin Yao[4], Rui Huang[5] and Diming Cai[1]*

[1]Department of Ultrasound Medicine, West China Hospital, Sichuan University, Chengdu, China, [2]Department of Urology, West China Hospital, Sichuan University, Chengdu, China, [3]Department of Pathology, West China Hospital, Sichuan University, Chengdu, China, [4]Department of Radiology, West China Hospital, Sichuan University, Chengdu, China, [5]Department of Nuclear Medicine, West China Hospital, Sichuan University, Chengdu, China

Renal cell carcinoma with FH gene deletion is a rare subtype of renal cell carcinoma. There had been few reports about ultrasonographic imaging of metastasis of renal cell carcinoma with FH gene deletion. This case reported one of the features of metastasis of renal cell carcinoma with FH gene deletion of a male patient 7 months after undergoing radical nephrectomy. He was diagnosed with a renal malignant tumor before the operation and confirmed to be primary FH gene-deficient renal cell carcinoma after undergoing radical nephrectomy in another hospital. Reexamination 7 months after the operation indicated that multiple metastases all over the body were found; therefore, he came to our hospital for further diagnosis and therapy. The tumors have metastasized in the lungs, bones, and lymph nodes adjacent to the left reproductive vessels and external iliac vessels, retroperitoneum, and abdominal wall so far as confirmed by PET/CT or MRI. Ultrasonographic findings of masses in the retroperitoneum and abdominal wall are fully discussed, which have been confirmed by biopsy and diagnosed as renal cell carcinoma with FH gene deletion by pathology.

KEYWORDS

case report, ultrasound, fumarate hydratase-deficient renal cell carcinoma, metastasis, imaging

Introduction

Renal cell carcinoma with FH gene deletion is a rare subtype of renal cell carcinoma (RCC). These tumors are usually metastatic at presentation and typically solitary and unilateral, unlike other familial RCC syndromes that are characterized by bilateral multifocal tumors (1). Many patients who presented with local or distant metastasis succumbed to the disease <5 years from the initial diagnosis (2). There had been few reports about ultrasonographic imaging of metastasis of renal cell carcinoma with FH gene deletion. This case reported one of the features of metastasis of renal cell carcinoma with FH gene deletion of a male patient 7 months after undergoing radical nephrectomy.

Case description

A 36-year-old man presented with a left lumbar mass of 1-month duration without obvious inducement 7 months after undergoing radical nephrectomy. The present study was performed in accordance with the Declaration of Helsinki and was approved by the Ethics Committee of our hospital. In another hospital, the tumor in the left kidney was diagnosed as renal malignancy preoperatively, which was proved to be primary FH gene-deficient renal cell carcinoma after radical nephrectomy. Seven months after the operation, the patient came to our hospital because of multiple metastases in a large number of organs diagnosed by MRI, which were hard, mobilized poorly, and progressively enlarged. The tumor in the abdominal wall near the left waist was resected in our hospital, and targeted therapy and immunotherapy were performed postoperatively. The patient's parents are alive, his brothers or sisters are in good health, and there is no family or genetic history.

Physical examination showed that the shape of the abdomen was normal and that there was no tenderness or rebound pain. During palpation of the waist of the left kidney area, a hard and poorly mobilized lump that was as big as an egg was found.

Clinical biochemical test (normal values are given in parentheses) showed that creatinine (68–108) was 151 μmol/L, estimated glomerular filtration rate (56–122) was 50.46 ml/min/1.73 m^2, cystatin-C (0.51–1.09) was 1.64 mg/L, uric acid (240–490) was 572 μmol/L, triglyceride (0.29–1.83) was 4.42 mmol/L, anion gap (12.0–20.0) was 22.2 mmol/L, and calcium (2.11–2.52) was 2.54 mmol/L.

The features of ultrasound

The tumors in the retroperitoneum of the left renal region and the abdominal wall near the left waist were probed by ultrasonography. Ultrasonographic images (Aixplorer US system; SuperSonic Imagine, Aix-en-Provence, France) showed a septal cystic mass of about 8.9 × 4.6 × 5.3 cm with an ill–defined margin, relatively regular shape, and heterogeneous echo in the retroperitoneum of the left renal region by grayscale using a low-frequency transducer (SL 6-1 multifrequency convex transducer) (Figure 1A). The septum featured an uneven thickness, with 0.6 cm as the thickest. There were punctiform and linear color Doppler signals in the mass. The ultrasound images also showed a hypoechoic mass of about 2.4 × 1.9 × 3.0 cm with a relatively circumscribed margin, regular shape, and heterogeneous echo in the abdominal wall near the left waist, and patchy anechoic areas could be seen inside the mass by grayscale using a high-frequency probe (SL 10-2 multifrequency linear probe). There were punctiform and linear blood flow signals in the mass in both color Doppler (Figure 1B) and power Doppler. Contrast-enhanced ultrasound showed that the septum of the cystic mass in the retroperitoneum displayed rapid hyperenhancement in the arterial phase, equal enhancement in the venous phase, and equal enhancement in the delayed phase after intravenous injection of ultrasound contrast agent SonoVue (Bracco SpA, Milan, Italy). The part of the cyst was not enhanced in three phases. Contrast-enhanced ultrasound also showed that the mass in the abdominal wall displayed rapid hyperenhancement in the arterial phase (Figure 2), slightly low enhancement in the venous phase, and low enhancement in the delayed phase, and anechoic areas showed non-enhancement in three phases. Ultrasonography suggested that there was a septal cystic mass in the retroperitoneum of the left renal region, and combined with the features of contrast-enhanced ultrasound, it was considered Bosniak grade IV, which could be ascribed to tumor recurrence possibly; the mass in the abdominal wall near the left waist was considered tumor metastasis possibly combined with the features of contrast-enhanced ultrasound (3, 4).

In addition to ultrasonographic findings, other findings of imaging modalities, including PET/CT and MRI, are also provided in Figure 3.

The intraoperative discovery showed that the mass was removed completely after dissociating the mass in the subcutaneous connective tissue and adipose tissue layer carefully. There was a capsule in the resected tumor, which has soft tissue and hemorrhagic necrotic foci inside.

Pathological examination showed that the size of the grayish-yellow and grayish-brown nodular mass was 3.5 × 2.5 × 2.5 cm, which had a complete and smooth capsule. The incanus and grayish-brown section plane were solid with moderate texture and hardness. Immunohistochemistry showed that PAX8 was positive, 2SC was positive, AKR1B10 was positive, AMACR was positive, CA9 was negative, CK7 was negative, TTF-1 was negative, and the targeted area was weakly positive with loss of FH gene expression, while the control is positive. The pathological findings were consistent with the

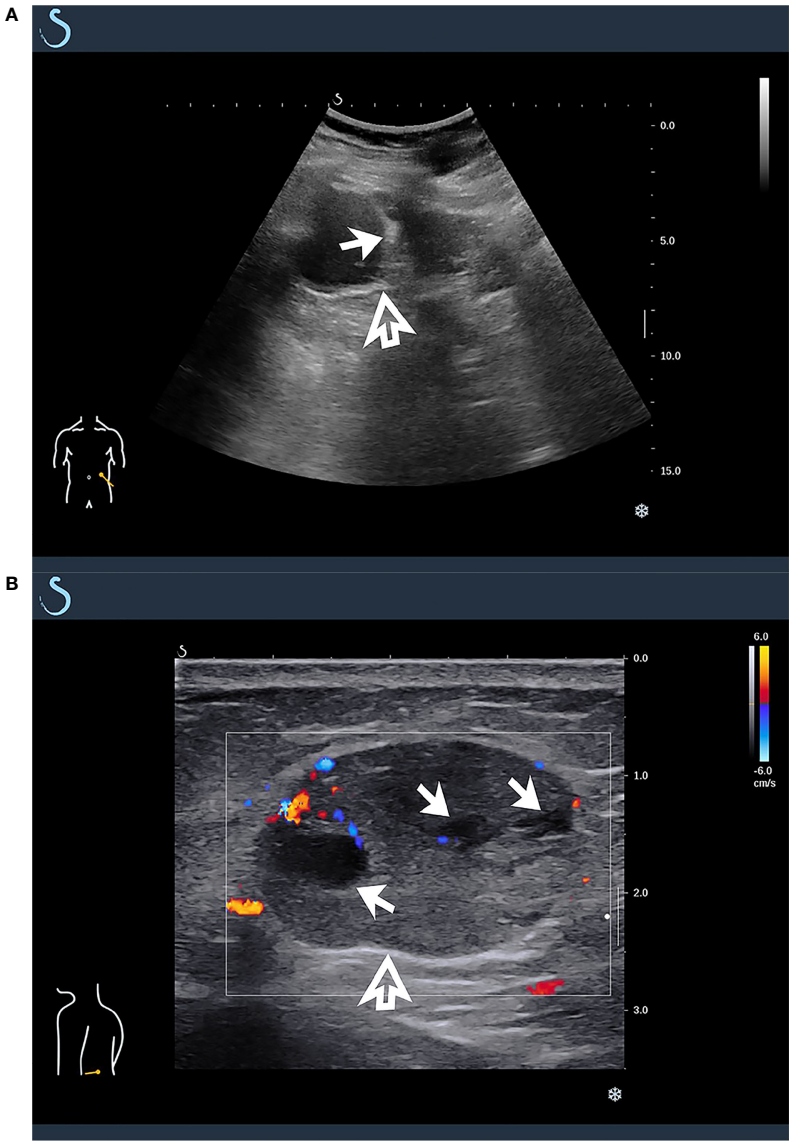

FIGURE 1
Ultrasonographic findings of masses in retroperitoneum and abdominal wall. **(A)** A multicystic mass was found in retroperitoneum of left renal region by grayscale using low-frequency transducer (hollow arrow), which featured multiple septa inside the cystic component (solid arrow). **(B)** By high-frequency probe, a hypoechoic mass was detected in abdominal wall near the left waist, and there were punctiform and linear blood flow signals in color Doppler (hollow arrow), which featured patchy anechoic areas inside the mass (solid arrow).

metastasis of FH gene-deficient renal cell carcinoma, accounting for about 80% of the tumor (Figure 4).

Discussion

Fumarate hydratase-deficient renal cell carcinoma (FH-d RCC) is a rare subtype of RCC associated with fumarate hydratase (FH) gene and hereditary leiomyomatosis and renal cell carcinoma (HLRCC) syndrome. HLRCC syndrome is a rare autosomal dominant disorder related to germline mutations of FH gene, which increases the risk of developing skin leiomyoma, uterine leiomyoma, and renal cell carcinoma (5, 6). In the latest 2016 edition of WHO renal tumor classification, HLRCC-associated RCC is listed as a new independent subtype of RCC (7).

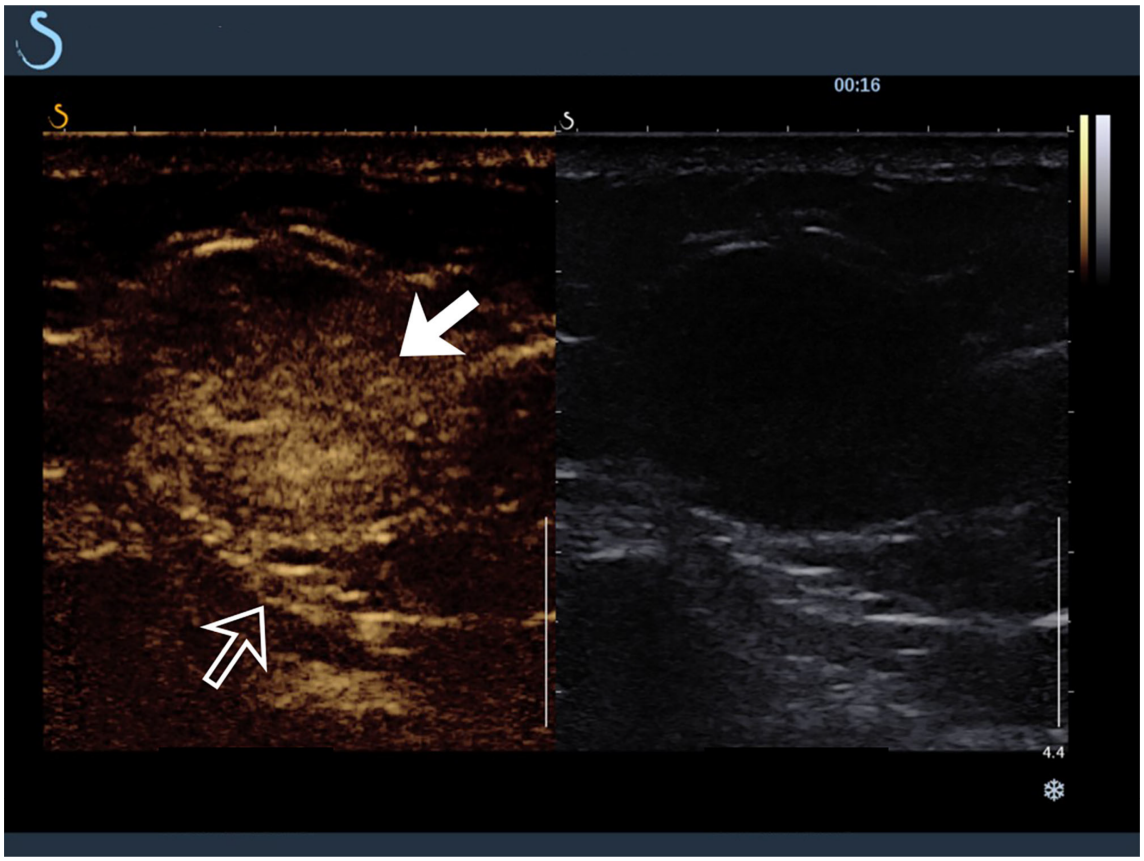

FIGURE 2
Contrast-enhanced ultrasound findings of mass in abdominal wall near the left waist (hollow arrow). The hypoechoic mass showed rapid hyperenhancement in arterial phase (solid arrow).

In humans, the FH protein is encoded by FH gene, which is located on the q-arm of chromosome 1 (8). FH gene participates in the mitochondrial tricarboxylic acid cycle (9). In tumor tissues, heterozygous deletion of FH gene locus often results in complete loss of FH function. The most immediate effect is the accumulation of intracellular fumarate, which at high concentrations directly alters various cellular signaling pathways (8). Pyruvate has difficulty completing the tricarboxylic acid cycle in the cell, and the process of oxidative phosphorylation and energy supply inside the mitochondria is correspondingly difficult to unfold, and the energy supply can only rely on anaerobic glycolysis, which in turn leads to pseudo-hypoxia. There is an inextricable relationship between tumor development and pseudo-hypoxia (10).

At present, most studies focus on clinicopathology, molecular analysis, treatments, and so on of FH-d RCC. Yang et al. (11) investigated the multidetector computed tomography (MDCT) features of FH-d RCC, and Nikolovski et al. (12) evaluated the imaging features of FH-d RCC on CT, MRI, and FDG PET. However, the clinical imaging findings of metastasis of FH-d RCC, such as imaging of ultrasound, are rarely involved in reports.

FH-d RCC is different from ordinary familial RCC. It is highly aggressive, prone to local progression and metastasizing, and has a poor prognosis (13, 14). Studies by Muller et al. and Pan et al. showed that the median survival for metastatic FH-d RCC was about 18 months (15, 16). In this case, the patient underwent radical nephrectomy because of FH-d RCC, and tumors have been recurring and metastasizing in multiple organs 7 months after the operation. By using axitinib for the targeted therapy (200 mg ivggt q21d) and sintilimab (5mg bid) for the immunotherapy, the basic conditions of the patient improved gradually. To date, the patient has undergone 14 months (a total of 18 cycles of sintilimab) of treatment with this regimen, and the patient was very satisfied with our treatment plans.

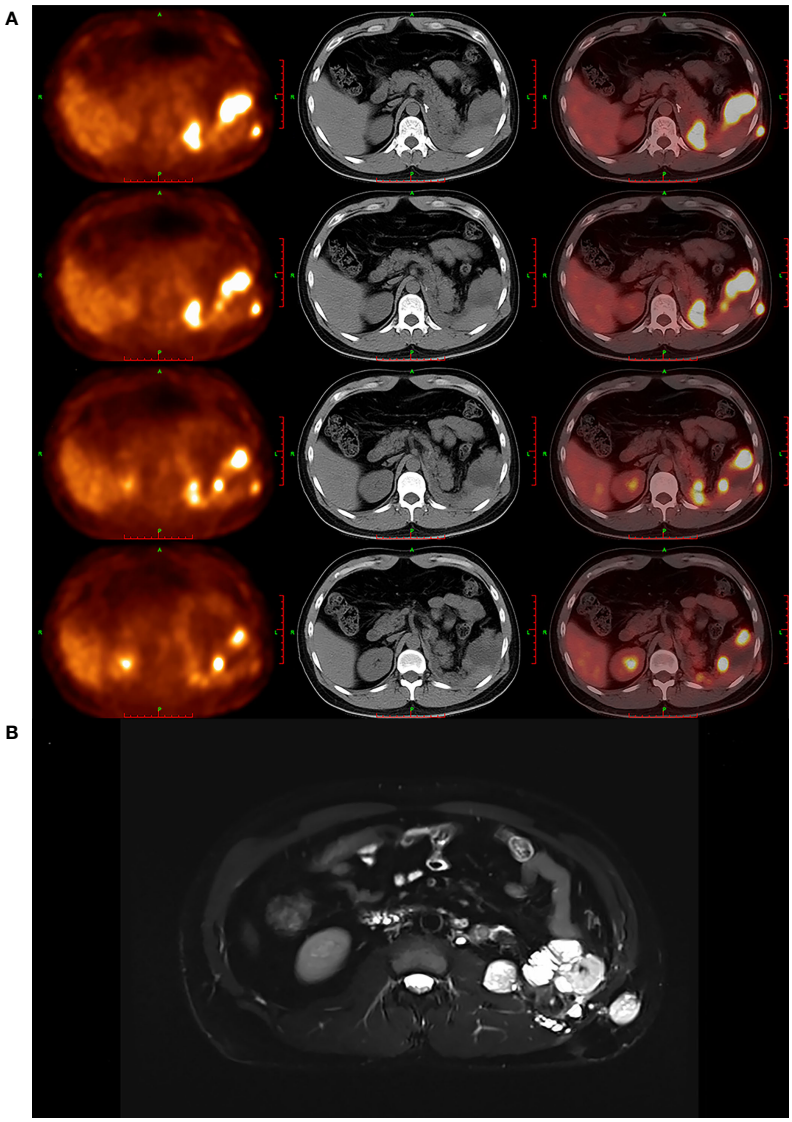

FIGURE 3
PET/CT and MRI findings of masses. **(A)** PET/CT images showed that multiple soft-tissue-density nodules and masses were found in left renal and adrenal region, perisplenic region, left retroperitoneum, left intraabdominal fascia, and left abdominal wall, which featured high uptake of ^{18}F-FDG abnormally. **(B)** MRI images showed that multiple nodules and masses were found in left renal and adrenal regions, perisplenic region, left retroperitoneum, left vertebral fascia, subcutaneous and muscular layer of left posterior abdominal wall, anterior part of left psoas major muscle, and left iliac fossa, which suggested that the tumor has recurred and metastasized likely.

The imaging features of the tumor or metastasis are unclear as a result of scarcity. The metastases of recurring lesions were reported, which displayed features by ultrasonography. In this case, by grayscale ultrasound, the mass features a septum in the cystic component or patchy anechoic areas in the hypoechoic mass. Relatively circumscribed margin, relatively regular shape, and heterogeneous echo in the mass could provide some clues for the diagnosis. In color Doppler and power Doppler, tiny punctiform and linear blood flow signals may indicate some characteristics of blood supply in the tumor. In contrast-enhanced ultrasound, the features of tumor perfusion, in this case, are distinctive. Hyperenhancement of the whole lesion was observed in the arterial phase, which contradicts ultrasonographic findings in color Doppler and power Doppler. Meanwhile, the tumor detected heterogeneous enhancement with fireworks-like enhancement, which showed punctiform hyperenhancement

10.3389/fonc.2022.896477

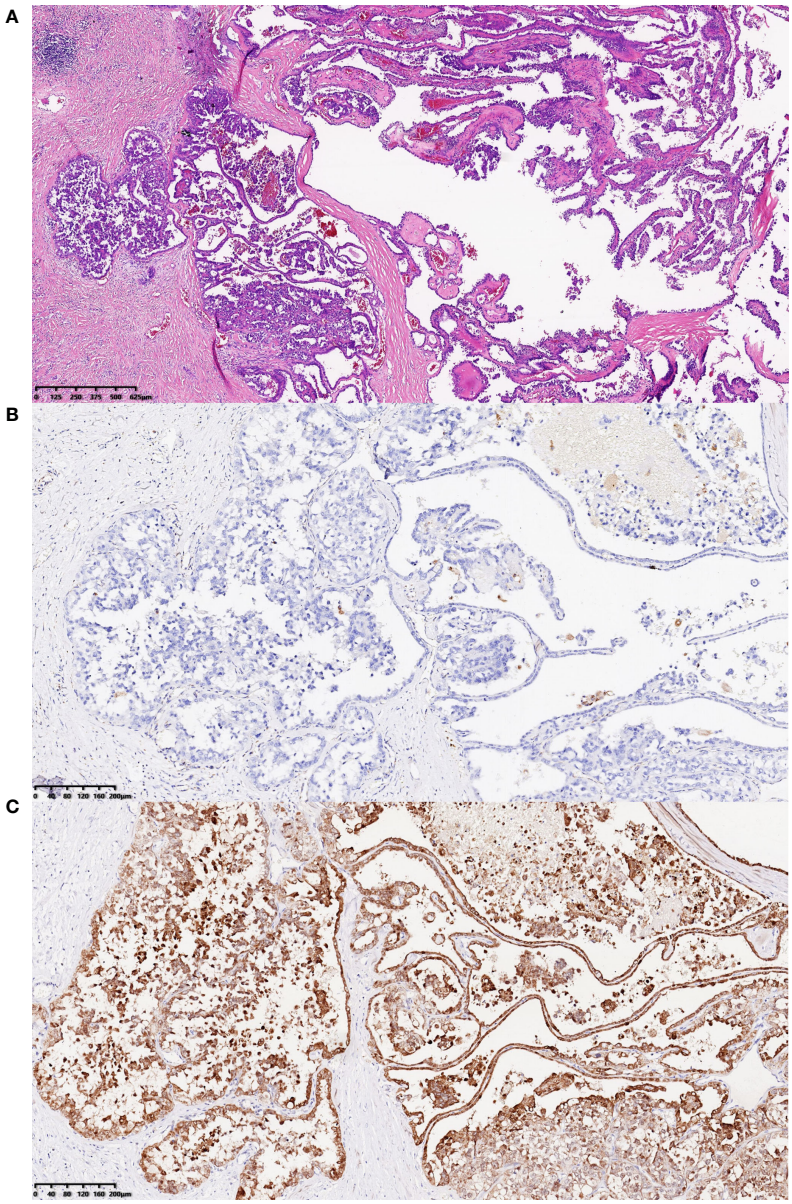

FIGURE 4
H&E staining results and immunohistochemistry staining results for FH gene and 2SC. **(A)** H&E staining results showed that the tumor cells in abdominal wall near the left waist, the majority of which were arranged into papillary shape, featured abundant and eosinophilic cytoplasm, round or oval enlarged nuclei with marked eosinophilic nucleoli, and perinucleolar halo (hematoxylin and eosin staining; magnification, ×40). **(B, C)** The tumor cells in abdominal wall near the left waist were visualized by immunohistochemistry staining for FH gene and 2SC, which revealed that the expression of FH protein was lost and 2SC was cytoplasmic positive (magnification, both ×100).

firstly from the center of the mass and then spread outward like fireworks in spite of patchy anechoic areas, which should present non-enhancement normally.

FH-d RCC is an infrequent renal malignant tumor, which is difficult to diagnose before the operation, and multimodal ultrasonography for the disease is even rarer. In this case, multimodal ultrasonographic features of metastatic lesions were described in detail, including grayscale, color Doppler, power Doppler, and contrast-enhanced ultrasound. Regrettably, there is no multimodal ultrasonography for the primary foci of FH-d RCC in this case report, and more cases are needed to obtain a more comprehensive understanding of the disease.

Data availability statement

The original contributions presented in the study are included in the article/Supplementary Material. Further inquiries can be directed to the corresponding author.

Ethics statement

The studies involving human participants were reviewed and approved by West China Hospital, Sichuan University. The patients/participants provided their written informed consent to participate in this study.

Author contributions

XZ, YZ, and YL contributed the part of ultrasound. PS, ZL, and HZ provided the clinical case. MZ, NC contributed the part of pathology. JY contributed the part of MRI. RH contributed the part of PET/CT. DC acted as corresponding author. All authors contributed to the article and approved the submitted version.

Conflict of interest

The authors declare that the research was conducted in the absence of any commercial or financial relationships that could be construed as a potential conflict of interest.

Publisher's note

Supplementary material

The Supplementary Material for this article can be found online at: https://www.frontiersin.org/articles/10.3389/fonc.2022.896477/full#supplementary-material

References

1. Choyke PL, Glenn GM, Walther MM, Zbar B, Linehan WM. Hereditary renal cancers. *Radiology* (2003) 226(1):33–46. doi: 10.1148/radiol.2261011296

2. Chen YB, Brannon AR, Toubaji A, Dudas ME, Won HH, Al-Ahmadie HA, et al. Hereditary leiomyomatosis and renal cell carcinoma syndrome-associated renal cancer: recognition of the syndrome by pathologic features and the utility of detecting aberrant succination by immunohistochemistry. *Am J Surg Pathol* (2014) 38(5):627–37. doi: 10.1097/PAS.0000000000000163

3. Israel GM, Bosniak MA. An update of the bosniak renal cyst classification system. *Urology* (2005) 66(3):484–8. doi: 10.1016/j.urology.2005.04.003

4. Najafi A, Wildt M, Hainc N, Hohmann J. Evaluation of cystic and solid renal lesions with contrast-enhanced ultrasound: A retrospective study. *Ultrasound Int Open* (2021) 7(1):E25–34. doi: 10.1055/a-1522-8969

5. Lucia CA, Emeline C, Luigi C, Carmen RF, Laurence C, Brigitte L, et al. Response to systemic therapy in fumarate hydratase–deficient renal cell carcinoma. *Eur J Cancer* (2021) 151:106–14. doi: 10.1016/j.ejca.2021.04.009

6. Yu YF, He SM, Wu YC, Xiong SW, Shen Q, Li YY, et al. Clinicopathological features and prognosis of fumarate hydratase deficient renal cell carcinoma. *Jounal Peking Univ (health sciences)* (2021) 53(4):640–6. doi: 10.19723/j.issn.1671-167X.2021.04.003

7. Holger M, Antonio LC, Peter AH, Victor ER, Thomas MU. The 2016 WHO classification of tumours of the urinary system and male genital organs-part a: renal, penile, and testicular tumours. *Eur Urol* (2016) 70(1):93–105. doi: 10.1016/j.eururo.2016.02.029

8. Ooi A. Advances in hereditary leiomyomatosis and renal cell carcinoma (HLRCC) research [J]. *Semin Cancer Biol* (2020) 61:158–66. doi: 10.1016/j.semcancer.2019.10.016

9. Linehan WM, Rouault TA. Molecular pathways: fumarate hydratase-deficient kidney cancer-targeting the warburg effect in cancer [J]. *Clin Cancer Res: an Off J Am Assoc Cancer Res* (2013) 19(13):3345–52. doi: 10.1158/1078-0432.CCR-13-0304

10. Pollard P, Wortham N, Barclay E, Alam A, Elia G, Manek S, et al. Evidence of increased microvessel density and activation of the hypoxia pathway in tumours from the hereditary leiomyomatosis and renal cell cancer syndrome [J]. *J Pathol* (2005) 205(1):41–9. doi: 10.1002/path.1686

11. Yang L, Li XM, Hu YJ, Zhang MN, Yao J, Song B. Multidetector CT characteristics of fumarate hydratase-deficient renal cell carcinoma and papillary type II renal cell carcinoma. *Korean J Radiol* (2021) 22(12):1996–2005. doi: 10.3348/kjr.2021.0212

12. Nikolovski I, Carlo MI, Chen YB, Vargas HA. Imaging features of fumarate hydratase-deficient renal cell carcinomas: A retrospective study. *Cancer Imaging* (2021) 21(1):24. doi: 10.1186/s40644-021-00392-9

13. Sun GX, Zhang XM, Liang JY, Pan XY, Zhu S, Liu ZH, et al. Integrated molecular characterization of fumarate hydratase-deficient renal cell carcinoma. *Clin Cancer Res* (2021) 27(6):1734–43. doi: 10.1158/1078-0432.CCR-20-3788

14. Du Y, Dang ZY, Li ZP. Advances in diagnosis and treatment of hereditary leiomyomatosis and renal cell carcinoma (HLRCC). *Pract J Cancer* (2021) 36 (7):1215–8. doi: 10.3969/j.issn.1001-5930.2021.07.043

15. Pan XY, Zhang MN, Yao J, Zeng H, Nie L, Gong J, et al. Fumaratehydratase-deficient renal cell carcinoma: A clinicopathological and molecular study of 13 cases. *J Clin Pathol* (2019) 72(11):748–54. doi: 10.1136/jclinpath-2019-205924

16. Muller M, Ferlicot S, Guillaud-Bataille M, Le Teuff G, Genestie C, Deveaux S, et al. Reassessing the clinical spectrum associated with hereditary leiomyomatosis and renal cell carcinoma syndrome in French FH mutation carriers. *Clin Genet* (2017) 92(6):606–15. doi: 10.1111/cge.13014

frontiers | Frontiers in Oncology

TYPE Case Report
PUBLISHED 26 October 2022
DOI 10.3389/fonc.2022.1013066

OPEN ACCESS

EDITED BY
Yue Chen,
Southwest Medical University, China

REVIEWED BY
Huipan Liu,
The Affiliated Hospital of Southwest Medical University, China
Tulay Kus,
University of Gaziantep, Turkey
Zhanwen Huang,
The Affiliated Hospital of Southwest Medical University, China

*CORRESPONDENCE
Jingmian Zhang
13722858079@163.com
Xinming Zhao
Xinm_zhao@163.com

†These authors have contributed equally to this work and share first authorship

SPECIALTY SECTION
This article was submitted to Cancer Imaging and Image-directed Interventions, a section of the journal Frontiers in Oncology

RECEIVED 06 August 2022
ACCEPTED 11 October 2022
PUBLISHED 26 October 2022

CITATION
Li T, Jiang X, Zhang Z, Chen X, Wang J, Zhao X and Zhang J (2022) Case Report: ^{68}Ga-FAPI PET/CT, a more advantageous detection mean of gastric, peritoneal, and ovarian metastases from breast cancer. *Front. Oncol.* 12:1013066. doi: 10.3389/fonc.2022.1013066

Case Report: ^{68}Ga-FAPI PET/CT, a more advantageous detection mean of gastric, peritoneal, and ovarian metastases from breast cancer

Tianyue Li[1,2†], Xiaojing Jiang[1†], Zhaoqi Zhang[1], Xiaolin Chen[1], Jianfang Wang[1], Xinming Zhao[1,2*] and Jingmian Zhang[1,2*]

[1]Department of Nuclear Medicine, The Fourth Hospital of Hebei Medical University, Shijiazhuang, China, [2]Hebei Provincial Key Laboratory of Tumor Microenvironment and Drug Resistance, Shijiazhuang, China

Breast cancer is the most common malignant tumor in adult women. Its common metastatic sites are lymph nodes, bones, lungs, the liver, and the brain. It is so rare for a patient with breast cancer to have metastases of the gastrointestinal tract, peritoneum, and ovary at the same time that the clinical reporting rate is low. We present a case of a 61-year-old woman who underwent right mastectomy and chemoradiotherapy 3 years ago because of mixed invasive ductal-lobular breast cancer. This time, she came to the hospital due to the symptom of stomach discomfort for 2 weeks. The gastroscopy biopsy result showed gastric metastasis from breast cancer. Then, ^{18}F-FDG imaging and ^{68}Ga-FAPI PET/CT imaging were performed for further diagnosis; ^{68}Ga-FAPI PET/CT demonstrated a significantly elevated FAPI activity in the thickened gastric wall, peritoneum, and bilateral adnexal areas, which was superior to that of ^{18}F-FDG. Finally, a biopsy of suspicious lesions was taken for pathological and histochemical examination, which confirmed that, in addition to the gastric metastasis, the peritoneum and bilateral ovaries were all consistent with metastatic breast cancer.

KEYWORDS

^{18}F-FDG, ^{68}Ga-FAPI, PET/CT, breast cancer, gastric metastasis, peritoneal carcinomatosis, ovarian metastasis

Case presentation

A 61-year-old woman presented at a gastrointestinal surgery clinic with the symptom of stomach discomfort for 2 weeks. She underwent right modified radical mastectomy and axillary lymph node dissection for invasive ductal-lobular breast cancer (stage pT1cN1M0) 3 years ago, followed by chemotherapy (docetaxel 120 mg, doxorubicin 40

mg, and cyclophosphamide 80 mg every 21 days for a total of six cycles) and 5 weeks of radiotherapy (a total dose of 50 Gy in 25 fractions). Moreover, she has been taking anastrozole up to now. Meanwhile, she also brought her local gastroscopic biopsy result, which showed gastric metastasis from breast cancer. The patient underwent subsequent auxiliary examinations to assess her general condition. Laboratory examination revealed increased levels of CA125 and CA153, which were 46.46 U/ml (reference range 0–25.0) and 158.20 U/ml (reference range 0–24.0), respectively. Contrast-enhanced computed tomography (CECT) demonstrated that the thickening muscularis and mucosa at the distal end of the antrum had moderate enhancement. Pelvic ultrasound demonstrated abnormal changes in the bilateral adnexal areas, but the nature of these changes was uncertain. The patient was then referred to the nuclear medicine department for positron emission tomography/computed tomography (PET/CT) imaging to further evaluate whether there was metastasis in other parts of her body.

Fluorine 18 (18F) fluorodeoxyglucose (FDG) PET/CT (Figure 1) results revealed slight FDG activity in the thickened gastric wall (SUVmax 3.8) and an abnormal mass in the right adnexal area (SUVmax 3.0). There was no obvious abnormal FDG uptake in the peritoneum or the left adnexal area. In order to assist in making a diagnosis, the patient was recruited in the gallium 68 (68Ga)-conjugated fibroblast-activation protein inhibitor (FAPI) PET/CT clinical trial of malignant tumor approved by the institutional review committee of our hospital after the patient's written informed consent was obtained (No. 2021069). Compared with ^{18}F-FDG, ^{68}Ga-FAPI PET/CT (Figure 2) results demonstrated significantly elevated FAPI activity in the thickened gastric wall (SUVmax 9.8) and a mass in the right adnexal area (SUVmax 11.6). Furthermore, ^{68}Ga-FAPI PET/CT showed extensive peritoneal carcinomatosis with FAPI uptake (SUVmax 3.9) and a mass in the left adnexal area with moderate FAPI activity (SUVmax 6.5).

In view of these auxiliary examination results, the patient underwent abdominopelvic exploration and pathological examination. In addition to gastric metastasis, histopathological and immunohistochemical examinations of bilateral adnexectomy and peritoneal nodule confirmed that both the peritoneum and bilateral ovaries had metastases from breast cancer (Figure 3). Subsequently, she received three consecutive days of intraperitoneal hyperthermic perfusion chemotherapy (paclitaxel 120 mg once a day). She is in a fair condition at present, and we will continue to follow her up in the future.

Discussion

Gastrointestinal metastases can sometimes be seen in patients with cancers of the breast, kidney, lung, and

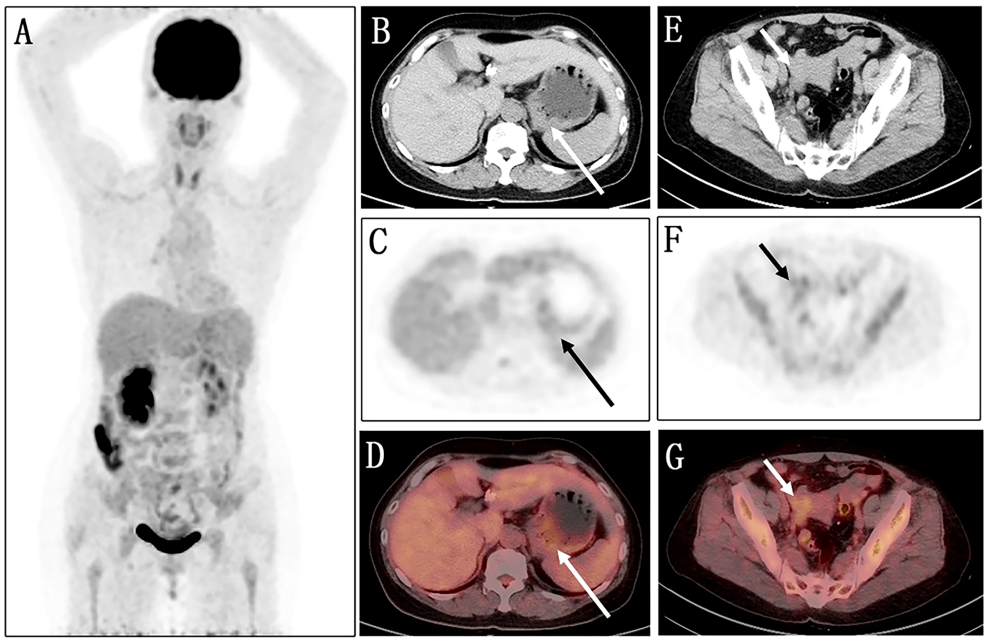

FIGURE 1
Images of ^{18}F-FDG PET/CT. **(A)** No obvious abnormality is found in the maximum intensity projection (MIP) image. **(B–D)** The axial images of the abdominal cavity reveal slight FDG activity in the thickened gastric wall (long arrows; SUV_{max} 3.8). **(E–G)** Similarly, the axial images of the pelvic cavity show an abnormal mass with a slight FDG uptake in the right adnexal area (short arrows; SUV_{max} 3.0).

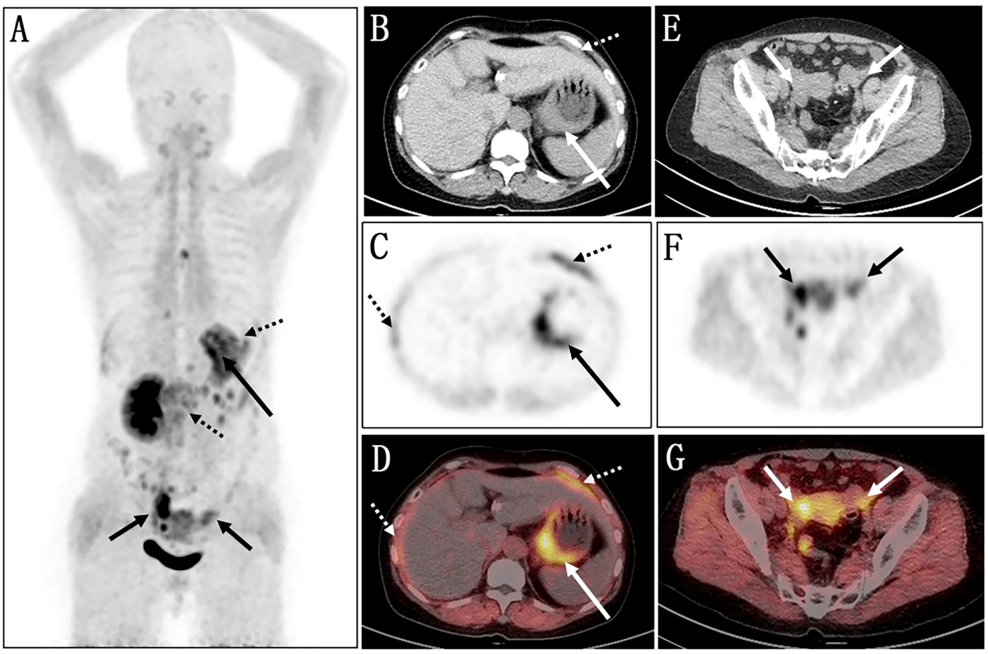

FIGURE 2
Images of ^{68}Ga-FAPI PET/CT. **(A)** The MIP image shows several lesions with varying degrees of FAPI uptake. **(B–D)** Axial views of abdominal cavity demonstrate significantly elevated FAPI activity in the thickened gastric wall (long arrows; SUV_{max} 9.8). **(E–G)** The axial images of pelvic cavity reveal abnormal FAPI uptake in the bilateral adnexal areas (short arrows; SUV_{max} of right 11.6, SUV_{max} of left 6.5). **(C, D)** Furthermore, ^{68}Ga-FAPI PET/CT showed extensive peritoneal carcinomatosis with FAPI uptake (dotted arrows; SUV_{max} 3.9).

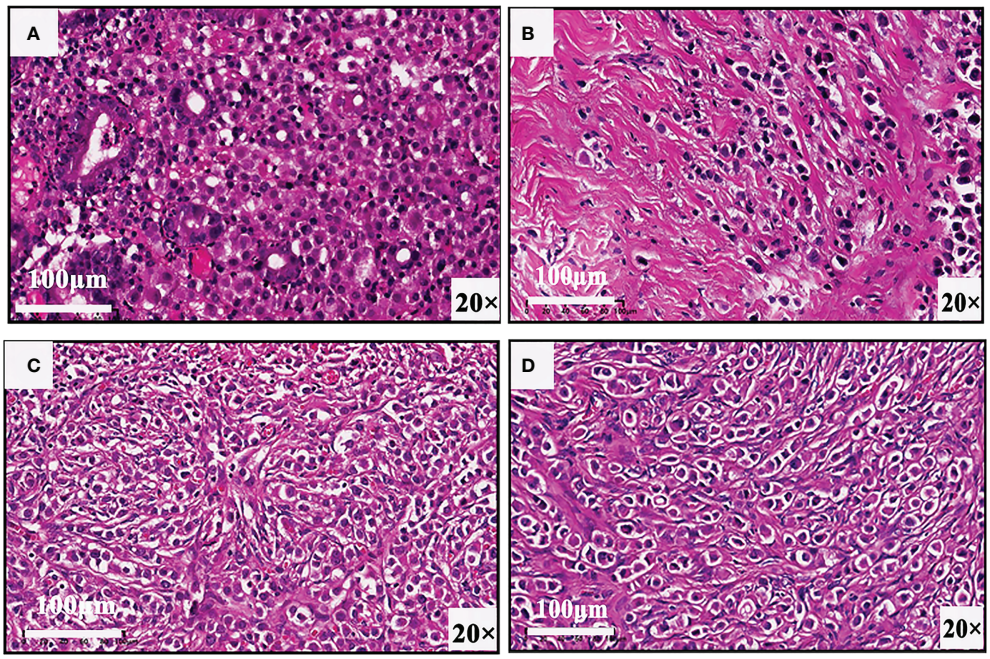

FIGURE 3
Biopsy results of **(A)** gastric wall, **(B)** pelvic nodule, **(C)** right ovary, and **(D)** left ovary confirm that there are gastric, peritoneal, and ovarian metastases from breast cancer.

malignant melanoma. Breast cancer is the second type of cancer (after lung cancer) that determines gastrointestinal metastasis (1). Notably, different histological types of primary breast cancer tend to have different metastasis sites. Compared with invasive ductal cancer, metastases from breast cancer to the gastrointestinal tract, peritoneum, ovaries, and uterus are more likely to occur in invasive lobular cancer (2, 3). However, this is a case of mixed breast cancer. When breast cancer metastasizes to the gastrointestinal tract, the onset is hidden, and there are often no special manifestations. Some patients with breast cancer will even get hospitalized with gastrointestinal discomfort as the first symptom (4). The tumor cells of gastric metastasis from breast cancer usually grow diffusely under the mucosa and muscularis, resulting in localized or diffuse gastric wall thickening, which is difficult to be distinguished from primary gastric malignancies (5, 6). Pathological examination and immunohistochemistry are gold standards for diagnosis. Additionally, research shows that HNF4A alone could be a marker for distinguishing primary gastric cancer from breast metastasis (7).

Ovarian metastasis is frequently encountered during the course of breast cancer, concerning one woman in five among those suffering from the disease. These secondary ovarian lesions are usually small and bilateral with a non-cystic pattern and are more likely to be from the primary infiltrating lobular carcinoma of the breast (8). Previous studies suggest that the size of the tumor, positive lymph nodes, and the histological type are all related to the occurrence of ovarian metastasis from breast cancer. Researchers also emphasize the importance of measuring the level of the breast marker CA153 and the ovarian marker CA125 in the serum (9). Similarly, pathological and immunohistochemical results are the gold standard for the diagnosis of ovarian metastasis of breast cancer. Bilateral, solid, small-sized, and highly vascularized masses are characteristic features of ovarian metastasis on macroscopic examination (10).

Peritoneal metastasis from breast cancer is a challenging clinical presentation. There is a lack of knowledge syntheses and specific recommendations for the management of breast cancer peritoneal metastases. The majority of pathology and imaging reports demonstrate that breast cancer peritoneal metastasis is mainly associated with invasive lobular carcinoma and the following intrinsic subtypes: HER2-enriched, luminal B, and basal-like (11, 12). Therefore, for patients with breast cancer, doctors should pay attention to identifying these metastatic cancers to develop correct treatment plans, and ^{68}Ga-FAPI PET/CT will stand out in the process of auxiliary diagnosis.

Most patients with peritoneal metastasis have poor prognosis, with only a minority of the patients having a survival time of more than 6 months (11, 12). In addition, research shows that the median survival time until the gastric involvement was 19 months (range, 0–41 months) (13). At present, there are still few original studies on the prognosis of gastric, peritoneal, and ovarian metastases of breast cancer.

FAPI, a newly developed tumor imaging target, can specifically bind to FAP *in vivo*, which is overexpressed in cancer-associated fibroblasts in many primary solid tumors and metastases. Many recent studies have demonstrated that ^{68}Ga-FAPI is superior to ^{18}F-FDG in tumor detection in many types. Compared with ^{18}F-FDG, ^{68}Ga-FAPI shows several advantages, including a better tumor-to-background ratio, independence of blood glucose levels, rapid renal clearance, and feasibility of rapid image acquisition (14, 15). Many recent studies have demonstrated that ^{68}Ga-FAPI is superior to ^{18}F-FDG in the detection of many types of tumors, especially some malignant lesions of the gastrointestinal tract and peritoneum, with higher tracer uptake in most primary and metastatic lesions. One of the possible reasons is that ^{18}F-FDG PET/CT imaging is often interfered by non-specific gastrointestinal physiological uptake in the abdomen and the pelvis, which may cause diagnostic bias, whereas the uptake of ^{68}Ga-FAPI is not affected by this. Moreover, ^{18}F-FDG may appear false negative in some malignant lesions with inactive glucose metabolism, such as gastrointestinal tumors with more signet ring cells and mucinous tissue in which ^{68}Ga-FAPI will show great advantages (16–21). This case may be an example that can guide physicians in making better treatment strategies.

Conclusion

Gastric and ovarian metastases of breast cancer can present with clinical and imaging characteristics resembling primary malignancy. Even pathological changes are difficult to identify, and immunohistochemistry is helpful for differential diagnosis. These similarities can cause significant diagnostic difficulties, with a subsequent therapeutic delay and a potential adverse outcome. However, how to accurately evaluate tumor staging and restaging before treatment is an important basis for clinical decision-making. Therefore, patients with a history of breast cancer should be considered for the possibility of developing distant metastasis if abnormal changes are found in the above parts of the body. It is worth noting that PET/CT can detect regional metastatic lymph nodes and distant metastasis through one-stop imaging, which is becoming more and more significant in clinical staging and restaging of tumors. In particular, for malignant tumors in the abdomen and the pelvis, such as gastrointestinal tumors and peritoneal carcinoma, whether primary or metastatic, ^{68}Ga-FAPI may have a greater advantage over ^{18}F-FDG, with a higher detection rate.

Data availability statement

The original contributions presented in the study are included in the article/supplementary material. Further inquiries can be directed to the corresponding authors.

Ethics statement

This study was approved by the institutional review committee of our hospital (No.2021069). The patients/participants provided their written informed consent to participate in this study.

Author contributions

TL and XJ were involved in the drafting and final editing of the report. They contributed equally to this work and share first authorship. ZZ and XC processed the images, and JW followed up with the patient. XZ and JZ, the corresponding authors, designed the study. All authors contributed to the article and approved the submitted version.

Funding

This work was financially supported by the Hebei Provincial Department of Science and Technology in China (No. 20377728D).

Acknowledgments

Thanks are due to all authors for assistance with the case report and the valuable discussion. In addition, funding from the Hebei Provincial Department of Science and Technology in China is gratefully acknowledged.

Conflict of interest

The authors declare that the research was conducted in the absence of any commercial or financial relationships that could be construed as a potential conflict of interest.

Publisher's note

All claims expressed in this article are solely those of the authors and do not necessarily represent those of their affiliated organizations, or those of the publisher, the editors and the reviewers. Any product that may be evaluated in this article, or claim that may be made by its manufacturer, is not guaranteed or endorsed by the publisher.

References

1. De Palma GD, Masone S, Rega M, Simeoli I, Donisi M, Addeo P, et al. Metastatic tumors to the stomach: Clinical and endoscopic features. *World J Gastroenterol* (2006) 12(45):7326–8. doi: 10.3748/wjg.v12.i45.7326

2. Xu L, Liang S, Yan N, Zhang L, Gu H, Fei X, et al. Metastatic gastric cancer from breast carcinoma: A report of 78 cases. *Oncol Lett* (2017) 14(4):4069–77. doi: 10.3892/ol.2017.6703

3. Bertozzi S, Londero AP, Cedolini C, Uzzau A, Seriau L, Bernardi S, et al. Prevalence, risk factors, and prognosis of peritoneal metastasis from breast cancer. *Springerplus* (2015) 4:688. doi: 10.1186/s40064-015-1449-x

4. Zhang LL, Rong XC, Yuan L, Cai LJ, Liu YP. Breast cancer with an initial gastrointestinal presentation: A case report and literature review. *Am J Transl Res* (2021) 13(11):13147–55.

5. Hong J, Kim Y, Cho J, Lim SW, Park SE, Kim HK, et al. Clinical features and prognosis of breast cancer with gastric metastasis. *Oncol Lett* (2019) 17(2):1833–41. doi: 10.3892/ol.2018.9754

6. Koike K, Kitahara K, Higaki M, Urata M, Yamazaki F, Noshiro H. Clinicopathological features of gastric metastasis from breast cancer in three cases. *Breast Cancer* (2014) 21(5):629–34. doi: 10.1007/s12282-011-0284-3

7. Juca P, Correa S, Vignal GM, Accioly MTS, Lustosa SAS, Abdelhay E, et al. Hnf4a expression as a potential diagnostic tool to discriminate primary gastric cancer from breast cancer metastasis in a Brazilian cohort. *Diagn Pathol* (2017) 12 (1):43. doi: 10.1186/s13000-017-0635-2

8. Wang G, Jin X, Zhu H, Wang S, Ding J, Zhang Y, et al. (68)Ga-Nota-Fapi-04 Pet/Ct in a patient with primary gastric diffuse Large b cell lymphoma: Comparisons with [(18)F] fdg Pet/Ct. *Eur J Nucl Med Mol Imaging* (2021) 48 (2):647–8. doi: 10.1007/s00259-020-04946-0

9. Zhao L, Chen S, Lin L, Sun L, Wu H, Lin Q, et al. [(68)Ga]Ga-Dota-Fapi-04 improves tumor staging and monitors early response to chemoradiotherapy in a patient with esophageal cancer. *Eur J Nucl Med Mol Imaging* (2020) 47(13):3188–9. doi: 10.1007/s00259-020-04818-7

10. Testa AC, Ferrandina G, Timmerman D, Savelli L, Ludovisi M, Van Holsbeke C, et al. Imaging in gynecological disease (1): Ultrasound features of metastases in the ovaries differ depending on the origin of the primary tumor. *Ultrasound Obstet Gynecol* (2007) 29(5):505–11. doi: 10.1002/uog.4020

11. Beniey M. Peritoneal metastases from breast cancer: A scoping review. *Cureus* (2019) 11(8):e5367. doi: 10.7759/cureus.5367

12. Tuthill M, Pell R, Guiliani R, Lim A, Gudi M, Contractor KB, et al. Peritoneal disease in breast cancer: A specific entity with an extremely poor prognosis. *Eur J Cancer* (2009) 45(12):2146–9. doi: 10.1016/j.ejca.2009.04.027

13. Jmour O, Belaid A, Mghirbi F, Behi K, Doghri R, Benna F. Gastric metastasis of bilateral breast cancer. *J Gastrointest Oncol* (2017) 8(1):E16–20. doi: 10.21037/jgo.2016.10.03

14. Cermik TF, Ergul N, Yilmaz B, Mercanoglu G. Tumor imaging with 68ga-Dota-Fapi-04 Pet/Ct: Comparison with 18f-fdg Pet/Ct in 22 different cancer types. *Clin Nucl Med* (2022) 47(4):e333–e9. doi: 10.1097/RLU.0000000000004073

15. Ballal S, Yadav MP, Moon ES, Kramer VS, Roesch F, Kumari S, et al. Biodistribution, pharmacokinetics, dosimetry of [(68)Ga]Ga-Dota.Sa.Fapi, and the head-to-Head comparison with [(18)F]F-fdg Pet/Ct in patients with various cancers. *Eur J Nucl Med Mol Imaging* (2021) 48(6):1915–31. doi: 10.1007/s00259-020-05132-y

16. Chang MC, Chen JH, Liang JA, Huang WS, Cheng KY, Kao CH. Pet or Pet/Ct for detection of peritoneal carcinomatosis: A meta-analysis. *Clin Nucl Med* (2013) 38(8):623–9. doi: 10.1097/RLU.0b013e318299609f

17. Elboga U, Sahin E, Kus T, Cayirli YB, Aktas G, Okuyan M, et al. Comparison of (68)Ga-fapi Pet/Ct and (18)Fdg Pet/Ct modalities in gastrointestinal system malignancies with peritoneal involvement. *Mol Imaging Biol* (2022) 24(5):789–97. doi: 10.1007/s11307-022-01729-x

18. Fan C, Guo W, Su G, Chen B, Chen H. Widespread metastatic gastric signet-ring cell carcinoma shown by 68ga-fapi Pet/Ct. *Clin Nucl Med* (2021) 46(2):e78–e9. doi: 10.1097/RLU.0000000000003245

19. Fu L, Huang S, Wu H, Dong Y, Xie F, Wu R, et al. Superiority of [(68)Ga]Ga-Fapi-04/[(18)F]Fapi-42 Pet/Ct to [(18)F]Fdg Pet/Ct in delineating the primary tumor and peritoneal metastasis in initial gastric cancer. *Eur Radiol* (2022) 32 (9):6281–90. doi: 10.1007/s00330-022-08743-1

20. Guo W, Chen H. (68)Ga fapi Pet/Ct imaging in peritoneal carcinomatosis. *Radiology* (2020) 297(3):521. doi: 10.1148/radiol.2020202469

21. Pang Y, Zhao L, Luo Z, Hao B, Wu H, Lin Q, et al. Comparison of (68)Ga-fapi and (18)F-fdg uptake in gastric, duodenal, and colorectal cancers. *Radiology* (2021) 298(2):393–402. doi: 10.1148/radiol.2020203275

frontiers | Frontiers in Oncology

TYPE Case Report
PUBLISHED 27 October 2022
DOI 10.3389/fonc.2022.1005206

OPEN ACCESS

EDITED BY
Hiroyuki Tomita,
Gifu University, Japan

REVIEWED BY
Juan Piñeiro-Maceira,
Rio de Janeiro State University, Brazil
Pio Zeppa,
University of Salerno, Italy

*CORRESPONDENCE
Guojie Wang
wanggj5@mail.sysu.edu.cn
Jie Zhang
zhangjie201806@sina.com

†These authors have contributed equally to this work

SPECIALTY SECTION
This article was submitted to Cancer Imaging and Image-directed Interventions, a section of the journal Frontiers in Oncology

RECEIVED 28 July 2022
ACCEPTED 13 October 2022
PUBLISHED 27 October 2022

CITATION
Wang G, Zhou X, Luo J, Hu Q and Zhang J (2022) Case report: Malignant proliferating trichilemmal tumor of the thumb.
Front. Oncol. 12:1005206.
doi: 10.3389/fonc.2022.1005206

Case report: Malignant proliferating trichilemmal tumor of the thumb

Guojie Wang[1*†], Xuan Zhou[2†], Junqi Luo[1], Qiyi Hu[3] and Jie Zhang[4*]

[1]Department of Radiology, Fifth Affiliated Hospital of Sun Yat-sen University, Zhuhai, China,
[2]Department of Pathology, Fifth Affiliated Hospital of Sun Yat-sen University, Zhuhai, China,
[3]Department of Nuclear Medicine, Fifth Affiliated Hospital of Sun Yat-sen University, Zhuhai, China,
[4]Department of Radiology, Zhuhai People's Hospital, Zhuhai, China

Proliferating trichilemmal tumor is a very rare benign tumor that has the potential to transition into a malignant tumor. PTT most commonly affects the scalps of women above 60 years old and is frequently misdiagnosed due to its rarity. Herein, we present a case of a 68-year-old man with a malignant proliferating trichilemmal tumor on his right thumb. X-ray image showed a soft tissue mass on his thumb accompanied by bone destruction, while ^{18}F-FDG PET revealed a hypermetabolic mass in the first index with axillary lymph node metastasis.

KEYWORDS

malignant proliferating trichilemmal tumor, finger, PET/CT, 18-FDG, pathology

Introduction

Proliferating trichilemmal tumor (PTT) is a benign neoplasia originating from the outer root sheath of hair follicles. PTT generally affects older women in the head and neck region and is often misdiagnosed (1, 2). Previous studies have linked trauma and/or inflammation to PTT (3). PTT are benign tumors that can become cancerous, termed malignant proliferating trichilemmal tumor (MPTT) (1, 3). Here, we present an unusual case of MPTT that was detected on the thumb of an elderly man.

Case report

A 68-year-old man was diagnosed with a soft tissue mass at the distal end of his right thumb that had been present for 6 months but was overlooked due to the mild symptoms. Two months prior to admission, the lesion showed rapid growth accompanied by persistent

dull pain. Physical examination revealed swelling at the distal segment of the thumb, local skin flushing, and slight tenderness.

X-ray imaging identified a mass at the distal part of the thumb with bone destruction (Figure 1). In addition, ^{18}F-FDG PET/CT examination revealed a significantly high metabolic activity in the thumb and right axillary lymph nodes (Figure 2).

Eventually, we surgically excised the lesion, which was approximately 5.5 cm × 3.5 cm × 3.0 cm in size. Light microscopy revealed that there are many clumps composed of epithelial cells under the skin. The clumps are lobulated, the outer cells are arranged in a palisade shape, and there is trichilemmal keratinization in the center. Between outer cells and central trichilemmal keratinization, there are no granular layers. There are obvious cytological atypia and nuclear pleomorphism in the outer cells (Figure 3). Immunohistochemistry results were positive for P63, P40, CK14, and EMA, while the tumor cells were negative for CD34.

Taken together, the above findings support the diagnosis of MPTT. A needle biopsy performed on the right axillary lymph node confirmed the presence of metastatic MPTT. Adjuvant chemotherapy was planned after surgery, and the patient was discharged. After surgical resection, he was followed for 6 months, and there was no report of recurrence.

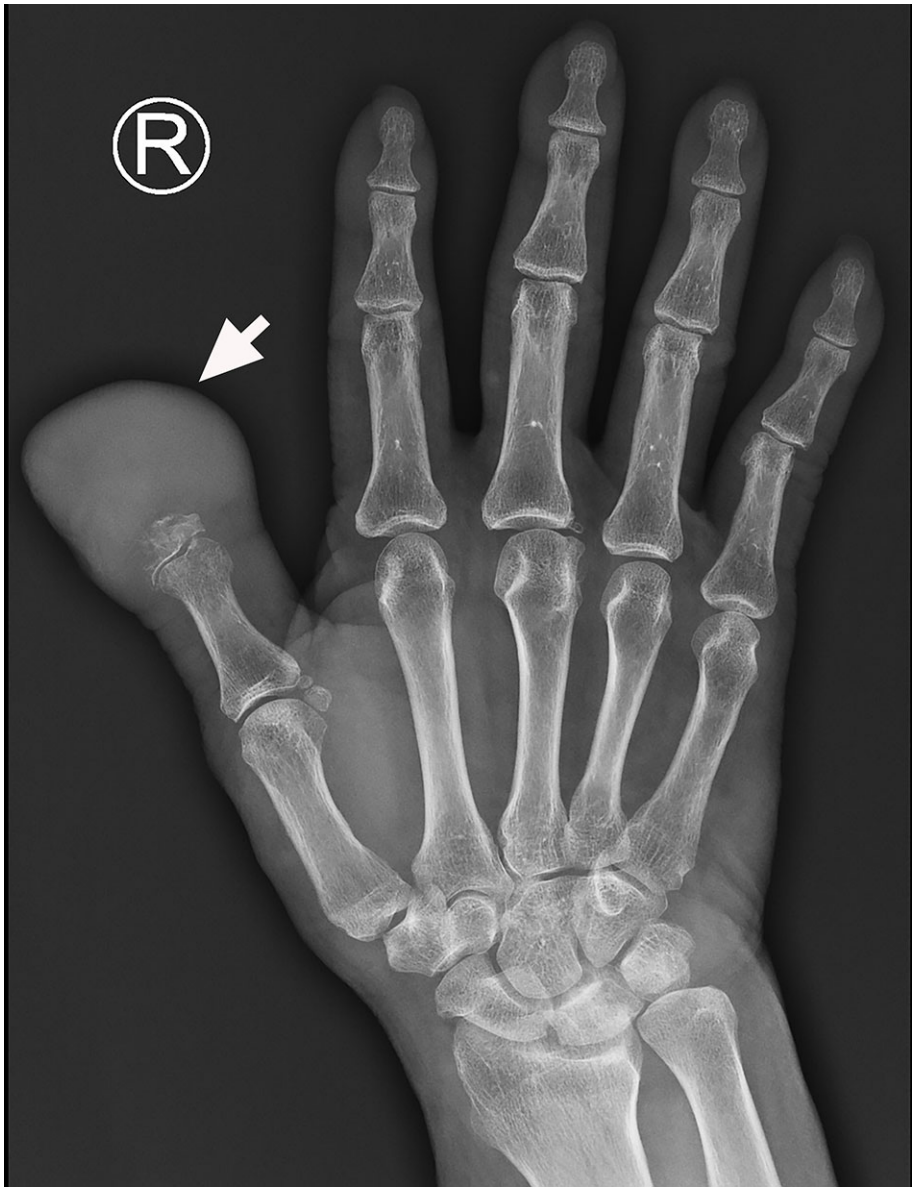

FIGURE 1
The X-ray image shows a mass at the distal end of the right thumb with marked phalanx destruction (arrow).

10.3389/fonc.2022.1005206

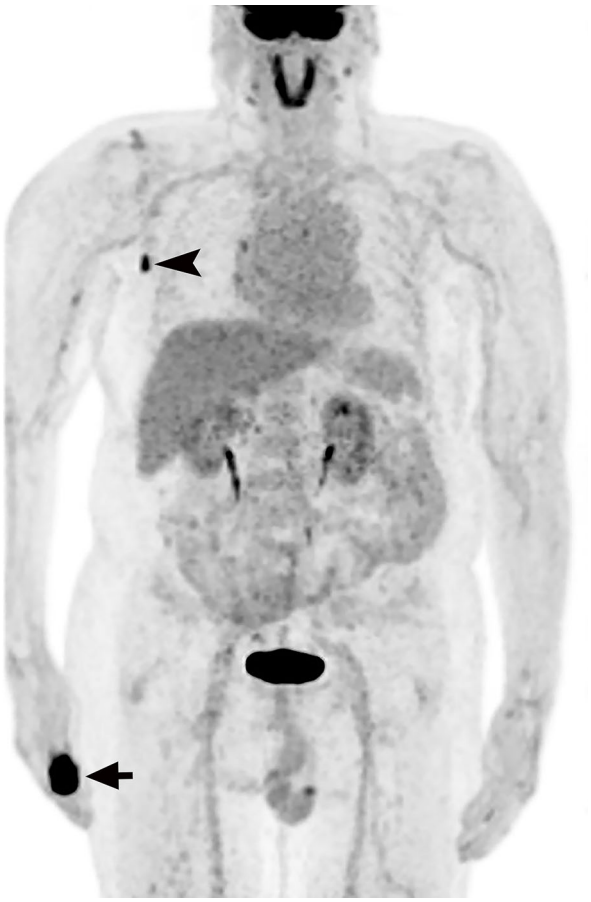

FIGURE 2
^{18}F-FDG PET reveals intense areas of ^{18}F-FDG uptake in the right thumb(arrow) and axillary lymph nodes (arrowhead).

Discussion

PTT are rare conditions that mainly occur in women above 60 years of age. Approximately 90% of cases occur on the scalp, with the remaining 10% located in regions such as the back, wrist, nose, and pudenda, to name a few (1). Even less common is PTT of the finger, which has been reported in the literature in only four cases. All four lesions were located in the subungual region (4–7). The researchers hypothesized that the subungual PTT was derived from the nail matrix, which could keratinize to a trichilemmal organization (5). PTT may also result from follicular units containing nail bed epithelium remaining in nails (8).

To the best of our knowledge, MPTT metastases have only been studied with ^{18}F-FDG PET in two patients previously (9, 10). In one case, ^{18}F-FDG PET was used to assess lymph node metastases caused by recurrent scalp MPTT (10). The other case underwent ^{18}F-FDG PET/CT to investigate lymph node metastases of a shoulder MPTT (9). MPTT intensified glucose avidity was present in all cases, suggesting that ^{18}F-FDG PET may be useful in the workup of MPTT patients, especially in cases where the tumor's malignancy potential is not clear.

The pathology of PTT is characterized by trichilemmal keratinization without granular layers. Trichilemmal Cysts, PTT, and MPTT are tumors with differentiation of hair follicles, which have a continuous pedigree from benign to malignant, one end of the tumor is a cystic tumor with a clear boundary, and the other end has malignant characteristics. When the tumor grows rapidly, has invasive growth and distant metastasis, and has a large number of nuclear pleomorphisms and obvious cytological atypia, MPTT should be considered. CD34 is a marker of outer hair root sheath differentiation and is negative in MPTT, which is also the point of differentiation between PTT and MPTT. Desmoplastic trichilemmomas are

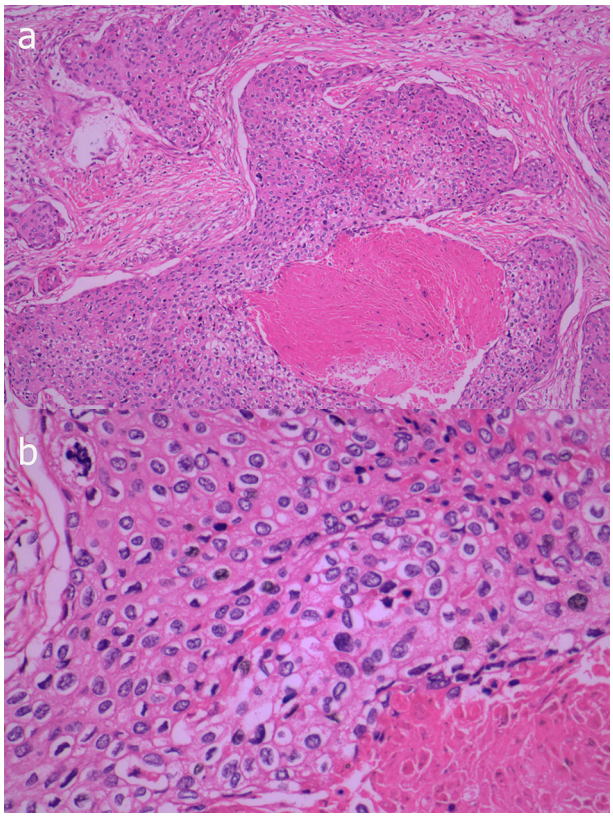

FIGURE 3
Photomicrograph shows many clumps composed of epithelial cells under the skin, the clumps are lobulated and the marginal cells are distributed in a palisade shape, with obvious keratinization in the center, but lacking a granular layer (**A**, HE×100). In the outer cells, there are obvious cytological atypia and nuclear pleomorphism (**B**, HE×400).

mostly found on the face, and similar to the trichilemmal tumor, it is characterized by subcutaneous tumor lobules and trichilemmal keratinization, and CD34 is positive. Furthermore, desmoplastic trichilemmomas have strips of epithelial cells growing at the edges (11). Trichilemmal keratinization is not seen in squamous cell carcinoma. Based on this, PTT can be differentiated from squamous cell carcinoma.

In conclusion, this is a rare case of MPTT in the thumb, and ^{18}F-FDG PET was useful in confirming axillary lymph node involvement in this rare neoplasia.

Data availability statement

The raw data supporting the conclusions of this article will be made available by the authors, without undue reservation.

Ethics statement

Written informed consent was obtained from the individual(s) for the publication of any potentially identifiable images or data included in this article.

Author contributions

GW, XZ, and JZ: manuscript writing. XZ: pathological review. GW, XZ, JL, QH, and JZ: manuscript revision. All authors contributed to the article and approved the submitted version.

Funding

This work was supported by the Science and Technology Program of Zhuhai (2220004000244) and the Medical Scientific Research Foundation of Guangdong Province(A2021449).

Conflict of interest

The authors declare that the research was conducted in the absence of any commercial or financial relationships that could be construed as a potential conflict of interest.

Publisher's note

References

1. Satyaprakash AK, Sheehan DJ, Sangüeza OP. Proliferating trichilemmal tumors: a review of the literature. *Dermatol Surg* (2007) 33(9):1102–8. doi: 10.1097/00042728-200709000-00011

2. Fieleke DR, Goldstein GD. Malignant proliferating trichilemmal tumor treated with mohs surgery: proposed protocol for diagnostic work-up and treatment. *Dermatol Surg* (2015) 41(2):292–4. doi: 10.1097/DSS.0000000000000269

3. Valerio E, Parro FHS, Macedo MP, et al. Proliferating trichilemmal cyst with clinical, radiological, macroscopic, and microscopic correlation. *Bras Dermatol* (2019) 94(4):452–4. doi: 10.1590/abd1806-4841.20198199

4. Melikoglu C, Eren F, Keklik B, et al. Trichilemmal cyst of the third fingertip: a case report. *Handb Surg* (2014) 19(1):131–3. doi: 10.1142/S0218810414720113

5. Kwon KE, Kim SJ, Kim JH, et al. Imaging sonographic findings of in a case of proliferating trichilemmal tumor of a finger: A case report. *J Clin Ultrasound* (2018) 46(3):215–7. doi: 10.1002/jcu.22500

6. El Hassani Y, Beaulieu JY, Tschanz E, et al. Localisation inhabituelle pulpaire d'un kyste trichilemmal proliférant [Proliferating trichilemmal tumor of the pulp of a finger: case report and review of the literature]. *Chir Main* (2013) 32(2):117–9. doi: 10.1016/j.main.2013.02.002

7. Ikegami T, Kameyama M, Orikasa H, et al. Trichilemmal cyst in the pulp of the index finger: a case report. *Handb Surg* (2003) 8(2):253–5. doi: 10.1142/S0218810403001765

8. Câmara de Oliveira M, Barcaui CB, Barcaui EO, et al. Melanonychia associated with subungual follicular inclusions: report of three cases. *Bras Dermatol* (2020) 95(2):217–20. doi: 10.1016/j.abd.2019.03.009

9. Leyendecker P, de Cambourg G, Mahé A, et al. 18F-FDG PET/CT findings in a patient with a proliferating trichilemmal cyst. *Clin Nucl Med* (2015) 40(7):598–9. doi: 10.1097/RLU.0000000000000742

10. Jung J, Cho SB, Yun M, et al. Metastatic malignant proliferating trichilemmal tumor detected by positron emission tomography. *Dermatol Surg* (2003) 29(8):872–4. doi: 10.1046/j.1524-4725.2003.29237.x

11. Afshar M, Lee RA, Jiang SI. Desmoplastic trichilemmoma–a report of successful treatment with mohs micrographic surgery and a review and update of the literature. *Dermatol Surg* (2012) 38(11):1867–71. doi: 10.1111/j.1524-4725.2012.02514.x

frontiers | Frontiers in Oncology

TYPE Case Report
PUBLISHED 11 November 2022
DOI 10.3389/fonc.2022.967294

OPEN ACCESS

EDITED BY
Andrea Ciarmiello,
Sant'Andrea University Hospital, Italy

REVIEWED BY
Giampiero Giovacchini,
Hospital Sant'Andrea, Italy
Francesca Tutino,
Sant'Andrea Hospital, La Spezia, Italy

*CORRESPONDENCE
Zhuo Shi
szxy_001@163.com
Meng Li
lmcams@163.com

SPECIALTY SECTION
This article was submitted to Cancer Imaging and Image-directed Interventions, a section of the journal Frontiers in Oncology

RECEIVED 12 June 2022
ACCEPTED 03 October 2022
PUBLISHED 11 November 2022

CITATION
Li J-W, Miao L, Zhao Z-G, Yang L, Shi Z and Li M (2022) Osteofibrous dysplasia-like adamantinoma: A case report and literature review. *Front. Oncol.* 12:967294. doi: 10.3389/fonc.2022.967294

Osteofibrous dysplasia-like adamantinoma: A case report and literature review

Jian-Wei Li[1], Lei Miao[1], Zhen-Guo Zhao[2], Lin Yang[3], Zhuo Shi[1*] and Meng Li[1*]

[1]Department of Diagnostic Radiology, National Cancer Center/ National Clinical Research Center for Cancer/Cancer Hospital, Chinese Academy of Medical Sciences and Peking Union Medical College, Beijing, China, [2]Department of Orthopaedics, National Cancer Center/National Clinical Research Center for Cancer/Cancer Hospital, Chinese Academy of Medical Sciences and Peking Union Medical College, Beijing, China, [3]Department of Pathology, National Cancer Center/National Clinical Research Center for Cancer/Cancer Hospital, Chinese Academy of Medical Sciences and Peking Union Medical College, Beijing, China

Abstract background: Osteofibrous dysplasia-like adamantinoma (OFD-like adamantinoma), classical adamantinoma and dedifferentiated adamantinoma were previously considered to be three subtypes of adamantinoma of long bones. In the 5th edition of the World Health Organization (WHO) classification of bone tumors in 2020, OFD-like adamantinoma was newly proposed and classified as an intermediate-locally aggressive tumor in other mesenchymal tumors of bone. OFD-like adamantinoma is rare, accounting for only 0.4% of all primary bone tumors. OFD-like adamantinoma is often misdiagnosed due to the insufficient understanding of it. Here we report a case of OFD-like adamantinoma treated in our hospital with a literature review.

Case presentation: The patient, a 14-year-old male, had swelling in his right leg with intermittent pain for one year. Plain radiography, computed tomography (CT) and magnetic resonance imaging (MRI) were performed. Based on the radiological and histological examinations, a diagnosis of OFD-like adamantinoma was suspected. After admission, the patient underwent tumor resection of the right tibia, free transplantation of the left fibula and internal fixation. After resection of the tumor, the wound recovered well, the vital signs were stable, and activity was normal. The patient has been followed up for more than a year with no recurrence or distant metastasis.

Conclusion: OFD-like adamantinoma is a rare primary bone tumor with nonspecific clinical features. Imaging examination can demonstrate the lesion and help diagnosis. The pathological discovery of epithelioid tissue is the key evidence for diagnosis.

KEYWORDS

bone tumor, osteofibrous dysplasia-like adamantinoma, plain radiography, computed tomography, magnetic resonance imaging

Introduction

Osteofibrous dysplasia-like adamantinoma, which is relatively rare to encounter in clinical practice, is also known as OFD-like adamantinoma and is a kind of low-grade malignant bone tumor that is different from classical adamantinoma and osteofibrous dysplasia (OFD). A case of OFD-like adamantinoma treated in our hospital is reported in this paper with a literature review.

Case description

A 14-year-old male patient had swelling in his right leg with intermittent pain for 1 year. The swelling of the lower leg was severe after exercise and could be relieved by rest. The previous month, he was treated at an external hospital, and the plain film radiography showed a lesion of the right tibia, so he came to our hospital for treatment. Physical examination: both lower limbs were equal in length, and obvious swelling or tenderness was not palpated in the right lower leg. The movement of both lower limbs and the muscle strength were normal. Plain radiography: the cortical expansive bone destruction of the anterior edge of the right upper tibia was irregular and lobulated, and the sclerotic edge could be seen. The long axis of the lesion was consistent with the tibia, with a maximum cross-sectional area of 2.1 × 1.9 cm and a length of approximately 7.5 cm, with no obvious periosteal reaction and no definite soft tissue mass. Computed tomography (CT): the lesion showed an eccentric polycystic expansive lucency area, and the bone cortex was expanded and thinned. Cortical interruption could be seen on some levels, and a small local lamellar periosteal reaction was observed in some parts. The lesion was associated with pathological fracture. Magnetic resonance imaging (MRI): the lesion of the upper right tibia showed a low signal on T1-weighted imaging (T_1WI), a high signal on T2-weighted imaging (T_2WI), and a high signal on diffusion-weighted imaging (DWI). The lesion showed significant enhancement on the postcontrast MRI scan. The preoperative imaging diagnosis was OFD of the upper right tibia with pathological fracture. After admission, the patient underwent tumor resection of the right tibia, free transplantation of the left fibula, and internal fixation. During the operation, the lesion was found to be located in the anterolateral bone cortex of the right tibia, and the tumor was white, flexible, and bleeding. The patient had good tolerance to the surgery with stable intraoperative condition. After resection of the tumor, the wound recovered well, the vital signs were stable, and activity was normal. Pathological examination showed a small amount of hyperplastic fibrous tissue and irregular woven bone and osteoblasts, in which scattered nest-like epithelial cells were seen. The immunohistochemistry results showed Ki-67 (+1%), SATB2 (+), CK19 (1+), AE1/AE3 (1+), CK18 (−), EMA (−), P63 (1+), S-100 (−), MDM2 (2+), SMA (−), and β-catenin (2+, cytoplasm) (Figure 1). The patient was recommended to be closely followed up and observed after the operation, avoiding weight bearing to prevent the aggravation of pathological fracture. The patient has been followed up for more than a year with no recurrence or distant metastasis.

Discussion

In addition to odontogenic epithelial tumors of the jaw, adamantinoma of long bones is the only truly primary epithelial tumor of bone. OFD-like adamantinoma, classical adamantinoma, and dedifferentiated adamantinoma were previously considered to be three subtypes of adamantinoma of long bones. In the 5th edition of the World Health Organization (WHO) classification of bone tumors in 2020, OFD-like adamantinoma was newly proposed and classified as an intermediate-locally aggressive tumor in other mesenchymal tumors of bone, while adamantinoma of long bones and dedifferentiated adamantinoma were classified as malignant tumors in other mesenchymal tumors of bone (1, 2). OFD-like adamantinoma is rare, accounting for only 0.4% of all primary bone tumors (3).

OFD-like adamantinoma grows slowly, with an average onset at 14 years of age, and there is no significant sex difference (4). Most patients experience clinical manifestations of swelling, pain, or pathological fracture (5). Under the pathological microscope, osteoblasts surround the bone fibrous stroma with needle-woven bone, which is characterized by nested epithelial cell clusters or scattered isolated epithelial cells under the background of OFD. Immunostaining can show cytokeratin (CK) positivity. The diagnosis should be further confirmed by immunohistochemistry (6–8). In this case, CK14 and AE1/AE3 were expressed in the tumor, suggesting that it was derived from epithelial tissue.

The location of OFD-like adamantinoma is characteristic and is mostly located in the shaft of the tibia (7). It is an intracortical lesion that occurs especially in the anterior cortex. Keeney et al. found that some sample cases (approximately 13%) were associated with ipsilateral fibular lesions (9). OFD-like adamantinoma is a locally invasive bone tumor with both benign and malignant features. Plain radiography shows eccentric cystic expansive bone destruction, which can be osteolytic or osteolytic sclerotic mixed type. The edge can be more often irregular. Periosteal reactions and soft tissue masses are rare, and anterior tibial anterior tibial bowing can be seen. Compared with plain radiography, CT, especially on thin layers with multiplanar reformation (MPR) reconstruction, can better show the details of cortical destruction and soft tissue density in the area of bone destruction and help detect subtle pathological fractures. The MRI signal is nonspecific. Soft tissue in the damaged area shows a slightly low signal on T_1WI and an uneven high signal on T_2WI, and the postcontrast scan shows heterogeneous enhancement. The superiority of MRI can better reflect the cystic and solid components of the tumor and the involvement of the medullary cavity, soft tissue, and the

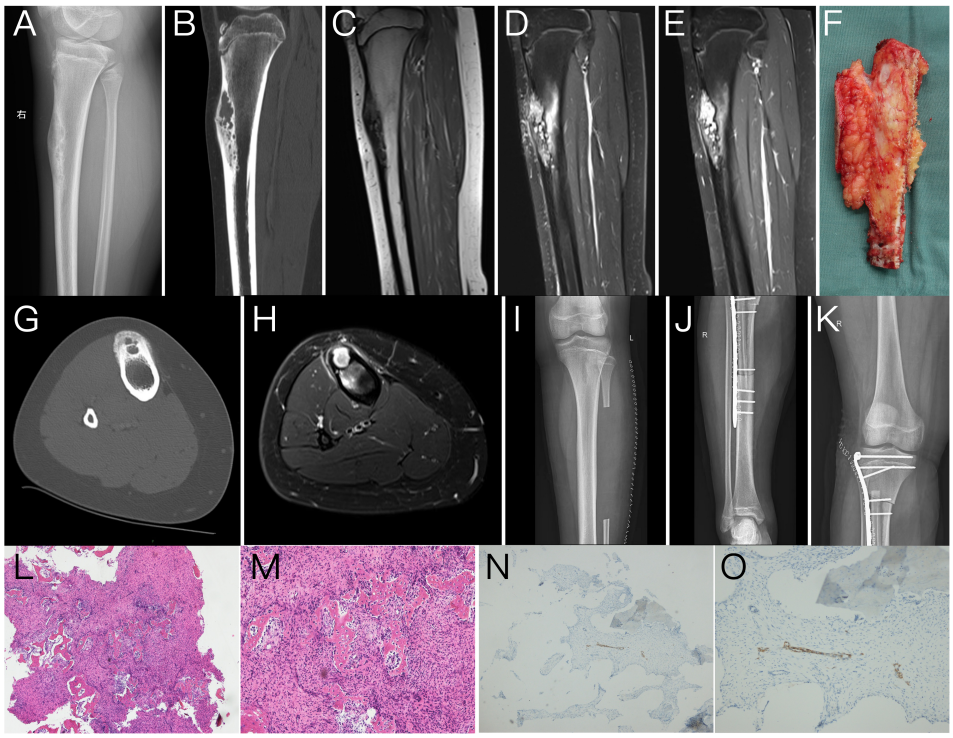

FIGURE 1
Lateral plain radiography of the tibia **(A)** showed a polycystic expansive bone destruction area in the anterior cortex of the upper segment of the right tibia with a sclerotic edge that was irregular and lobulated, and the long axis of the lesion was consistent with the tibia. The sagittal reformation image of CT **(B)** and the axial image of CT **(G)** clearly showed that the lesion is an eccentric polycystic expansive transparent area while the bone cortex expands and thins. Cortical interruption could be seen in some layers with a small periosteal reaction in some parts, and cortical hyperplasia, sclerosis, and cortical destruction could be visualized around the lesions. MRI showed abnormal signal lesions of the upper tibia on the right side with low signal intensities on T1-weighted images (T_1WI) **(C)** and high signal intensities on sagittal and axial T2-weighted images (T_2WI) **(D, H)**. The lesions were significantly enhanced on postcontrast scans **(E)**. The postoperative plain radiography of the lower limb **(I–K)** showed postoperative changes of tumor resection of the right tibia, free transplantation of the left fibula, and internal fixation. The gross specimen during the operation **(F)** showed a sagittal view of the tumor and the tibia, which had a good comparison with the lateral plain radiography and sagittal CT and MRI images **(A–E)**. Tumor pathological HE sections **(L, M)** showed irregularly woven bone trabeculae surrounded by osteoblasts, with many fibrous matrix and small nests of epithelial cells. Immunohistochemistry **(N, O)** showed nests of small tumor cells positive for cytokeratin CK19.

surrounding edema. The imaging examination of this case was comprehensive: the plain radiography, CT, and plain/postcontrast MRI findings were basically consistent with the imaging features of OFD-like adamantinoma. In this case, a small periosteal reaction was observed, which may be related to pathological fracture.

The histological and imaging features of OFD, OFD-like adamantinoma, and adamantinoma of long bones are closely related. They were previously considered to belong to the same disease pedigree (10), but it is difficult to distinguish them. OFD, also known as ossifying fibroma, is a benign disease whose age of onset, location, and imaging features are similar to those of OFD-like adamantinoma. It is often difficult to distinguish these conditions by imaging methods alone (11). Based on preoperative imaging, this case was diagnosed as the more common OFD, and the diagnosis of OFD-like adamantinoma was confirmed only after pathological microscopic observation and immunohistochemical detection of epithelial components. Adamantinoma of long bones is a low-grade malignant tumor. Compared with the features of OFD, invasive/malignant features such as the longitudinal length of the lesion, involvement of the medullary cavity, and moth-eaten margins may indicate a diagnosis of OFD-like adamantinoma (10). Some studies have shown that OFD-like adamantinoma can progress to adamantinoma. Hatori et al. speculated that OFD-like adamantinoma may be the precursor lesion of adamantinoma of long bones, but no research has confirmed this (3). Two cases of newly diagnosed OFD-like adamantinoma reported by Hazelbag in 1994 developed into adamantinoma of long bones when they recurred locally (12). Retrospective analysis found that there was a possibility of misdiagnosis by needle biopsy histology at the first diagnosis, which suggested that a biopsy of the lesion should be taken extensively and from multiple sites, and immunohistochemistry should be added to aid in the diagnosis when necessary. OFD-like adamantinoma has a

better outcome than classic adamantinoma, but long-term follow-up is necessary due to the possibility of local recurrence and late complications (13).

In conclusion, OFD-like adamantinoma is rare, and its clinical features are not specific. Imaging examination can demonstrate the lesion well and provide valuable help for diagnosis and differential diagnosis, but the final diagnosis often requires multidisciplinary consultation (14). The pathological discovery of epithelioid tissue is the key evidence for diagnosis.

Data availability statement

The original contributions presented in the study are included in the article/supplementary material. Further inquiries can be directed to the corresponding author.

Ethics statement

The study involving human participants was reviewed and approved by Cancer Hospital, Chinese Academy of Medical Sciences. Written informed consent requirements were waived due to the retrospective character of this study.

Author contributions

Z-GZ, LM, ZS, ML performed the data acquisition. ML, J-WL, LM performed the radiological images analysis. LY performed the histological analysis. ML, J-WL, LM performed the manuscript preparation. All authors contributed to the article and approved the submitted version.

Conflict of interest

The authors declare that the research was conducted in the absence of any commercial or financial relationships that could be construed as a potential conflict of interest.

Publisher's note

References

1. The WHO Classification of Tumours Editorial Board. *Who classification of tumours soft tissue and bone tumours. 5th Ed.* Lyon: World Health Organization (2020).

2. Choi JH, Ro JY. The 2020 who classification of tumors of bone: An updated review. *Adv Anat Pathol* (2021) 28(3):119–38. doi: 10.1097/PAP.0000000000000293

3. Hatori M, Watanabe M, Hosaka M, Sasano H, Narita M, Kokubun S. A classic adamantinoma arising from osteofibrous dysplasia-like adamantinoma in the lower leg: A case report and review of the literature. *Tohoku J Exp Med* (2006) 209(1):53–9. doi: 10.1620/tjem.209.53

4. Bethapudi S, Ritchie DA, Macduff E, Straiton J. Imaging in osteofibrous dysplasia, osteofibrous dysplasia-like adamantinoma, and classic adamantinoma. *Clin Radiol* (2014) 69(2):200–08. doi: 10.1016/j.crad.2013.09.011

5. Gleason BC, Liegl-Atzwanger B, Kozakewich HP, Connolly S, Gebhardt MC, Fletcher JA, et al. Osteofibrous dysplasia and adamantinoma in children and adolescents: A clinicopathologic reappraisal. *Am J Surg Pathol* (2008) 32(3):363–76. doi: 10.1097/PAS.0b013e318150d53e

6. Most MJ, Sim FH, Inwards CY. Osteofibrous dysplasia and adamantinoma. *J Am Acad Orthopaedic Surgeons* (2010) 18(6):358–66. doi: 10.5435/00124635-201006000-00008

7. Kahn LB. Adamantinoma, osteofibrous dysplasia and differentiated adamantinoma. *Skeletal Radiol* (2003) 32(5):245–58. doi: 10.1007/s00256-003-0624-2

8. Ishida T, Iijima T, Kikuchi F, Kitagawa T, Tanida T, Imamura T, et al. A clinicopathological and immunohistochemical study of osteofibrous dysplasia, differentiated adamantinoma, and adamantinoma of long bones. *Skeletal Radiol* (1992) 21(8):493–502. doi: 10.1007/BF00195230

9. Keeney GL, Unni KK, Beabout JW, Pritchard DJ. Adamantinoma of long bones. a clinicopathologic study of 85 cases. *Cancer* (1989) 64(3):730–37. doi: 10.1002/1097-0142(19890801)64:3<730::aid-cncr2820640327>3.0.co;2-p

10. Khanna M, Delaney D, Tirabosco R, Saifuddin A. Osteofibrous dysplasia, osteofibrous dysplasia-like adamantinoma and adamantinoma: Correlation of radiological imaging features with surgical histology and assessment of the use of radiology in contributing to needle biopsy diagnosis. *Skeletal Radiol* (2008) 37 (12):1077–84. doi: 10.1007/s00256-008-0553-1

11. Ratra A, Wooldridge A, Brindley G. Osteofibrous dysplasia-like adamantinoma of the tibia in a 15-Year-Old girl. *Am J Orthop* (2015) 44(10):E411.

12. Hazelbag HM, Taminiau AH, Fleuren GJ, Hogendoorn PC. Adamantinoma of the long bones. a clinicopathological study of thirty-two patients with emphasis on histological subtype, precursor lesion, and biological behavior. *J Bone Joint Surg Am* (1994) 76(10):1482–99. doi: 10.2106/00004623-199410000-00008

13. Deng Z, Gong L, Zhang Q, Hao L, Ding Y, Niu X. Outcome of osteofibrous dysplasia-like versus classic adamantinoma of long bones: A single-institution experience. *J Orthop Surg Res*. (2020) 15(1):268. doi: 10.1186/s13018-020-01769-5

14. Kamal AF, Anshori F, Kodrat E. Osteofibrous dysplasia-like adamantinoma versus osteofibrous dysplasia in children: A case report of challenging diagnosis. *Int J Surg Case Rep* (2021) 80:4. doi: 10.1016/j.ijscr.2021.01.093

frontiers | Frontiers in Oncology

TYPE Case Report
PUBLISHED 02 December 2022
DOI 10.3389/fonc.2022.1013017

OPEN ACCESS

EDITED BY
Xin-Wu Cui,
Huazhong University of Science and Technology, China

REVIEWED BY
Aleksandra Gilis-Januszewska,
Jagiellonian University Medical College, Poland
Malgorzata Trofimiuk-Muldner,
Jagiellonian University Medical College, Poland

*CORRESPONDENCE
Xiaoyan Chang
13683662636@163.com
Ke Lv
lvke@163.com

†These authors have contributed equally to this work

SPECIALTY SECTION
This article was submitted to Cancer Imaging and Image-directed Interventions, a section of the journal Frontiers in Oncology

RECEIVED 06 August 2022
ACCEPTED 14 November 2022
PUBLISHED 02 December 2022

CITATION
Shao Y, Gui Y, Cheng Y, Xu J, Chang X and Lv K (2022) Case report: Peritumoral hepatic steatosis in a patient with a metastatic somatostatin-producing oligosymptomatic neuroendocrine neoplasm.
Front. Oncol. 12:1013017.
doi: 10.3389/fonc.2022.1013017

Case report: Peritumoral hepatic steatosis in a patient with a metastatic somatostatin-producing oligosymptomatic neuroendocrine neoplasm

Yuming Shao[1†], Yang Gui[1†], Yuejuan Cheng[2], Jia Xu[3], Xiaoyan Chang[4*] and Ke Lv[1*]

[1]Department of Ultrasound, Peking Union Medical College Hospital, Chinese Academy of Medical Sciences and Peking Union Medical College, Beijing, China, [2]Department of Medical Oncology, Peking Union Medical College Hospital, Chinese Academy of Medical Sciences and Peking Union Medical College, Beijing, China, [3]Department of Radiology, Peking Union Medical College Hospital, Chinese Academy of Medical Sciences and Peking Union Medical College, Beijing, China, [4]Department of Pathology, Peking Union Medical College Hospital, Chinese Academy of Medical Sciences and Peking Union Medical College, Beijing, China

Neuroendocrine neoplasms (NENs) comprise a heterogeneous collection of tumors derived from various neuroendocrine cells and are divided into functioning NEN and non-functioning NEN. Some NENs present with mild symptoms and can secrete somatostatin. These neoplasms are known as somatostatin-producing oligosymptomatic NENs. In this report, we describe a case of metastatic somatostatin-producing oligosymptomatic NEN with peritumoral hepatic steatosis and review the relevant literature. The patient was a 45-year-old woman who presented with mild steatorrhea and melena. A computed tomography scan revealed an enlarged pancreas protruding into the duodenum. Pathology after total pancreatectomy showed a grade 2 pancreatic NEN with positive somatostatin immunostaining. Enlarging masses on the liver were observed after the operation. Ultrasound examination revealed several lesions in the liver, with inner hypoechoic areas that showed rapid enhancement and fast washout on contrast-enhanced ultrasonography and with outer hyperechoic areas with continuous iso-enhancement. Therefore, the inner hypoechoic areas seen on contrast-enhanced ultrasonography were suspected to be true metastases. A biopsy confirmed this suspicion and indicated that the outer areas were peritumoral liver steatosis. This case highlights the importance of the imaging pattern described in this report for accurate diagnosis of metastatic NEN to avoid incorrect estimation of tumor size or a missed diagnosis on biopsy.

KEYWORDS

pancreas, neuroendocrine neoplasm, somatostatin, peritumoral steatosis, case report

Introduction

As found in various organs, neuroendocrine neoplasms (NENs) are a group of neural crest tumors, at least 70% of which are of gastroenteropancreatic origin (1). Somatostatin-producing oligosymptomatic NEN is a subtype of pancreatic NEN. In this report, we describe a patient who had somatostatin-producing oligosymptomatic NEN with metastasis to the liver and peritumoral hepatic steatosis. This is the first report on the unique pathological and imaging features of this specific subtype of tumor.

Case presentation

A 45-year-old Chinese woman with mild steatorrhea and melena was admitted to our hospital after pathological examination of a biopsy of the pancreas confirmed grade 2 pancreatic NEN. The patient had no other signs or manifestations, such as abdominal pain, weight loss, jaundice, palpitations, hunger, reflux, or skin rash. Computed tomography (CT) examination of the abdomen and pelvis revealed an irregularly shaped pancreas. No abnormality was apparent in the liver or other organs (Figure 1A). Total pancreatectomy had originally been recommended but was refused by the patient. Eight months later, the melena worsened. A CT examination showed a more enlarged pancreas, part of which was protruding into the duodenum (Figures 1B, C). Physical examination did not reveal any important clinical findings. Preoperative laboratory investigations, including for CA199, CEA, CA125, insulin, C-peptide, fasting serum glucose, somatostatin, glucagon, and gastrin, were normal. Screening of the parathyroid glands and adenohypophysis was negative. The family and psychosocial history was normal. Total pancreatectomy and splenectomy were performed *via* an open approach, and R0 resection was achieved. The pathological results were consistent with grade 2 pancreatic NEN with 2 mitoses/2 mm^2 and a Ki-67 proliferation index of 5%. Immunostaining of chromogranin A, synaptophysin, and somatostatin was positive, but immunostaining of insulin, gastrin, and glucagon was negative (Figures 2A, B). In view of the clinical findings not being strong or distinctive enough for somatostatinoma and mild steatorrhea being the only sign present early in the clinical course, the final diagnosis was somatostatin-producing oligosymptomatic NEN.

The patient was followed up regularly after surgery at 3-month intervals with magnetic resonance imaging (MRI) of the abdomen every 6 months. At 1.5 years postoperatively, multiple small patchy and nodular lesions with opposite signals on axial T1-weighted in-phase and out-of-phase MRI were detected in the liver for the first time (Figure 1D). In view of the indeterminate nature of these lesions at that time, continued follow-up was recommended. The volumes of the lesions continued to increase after a further 6 months and 1 year (Figures 1E, F). Given that the lesions showed opposite signals

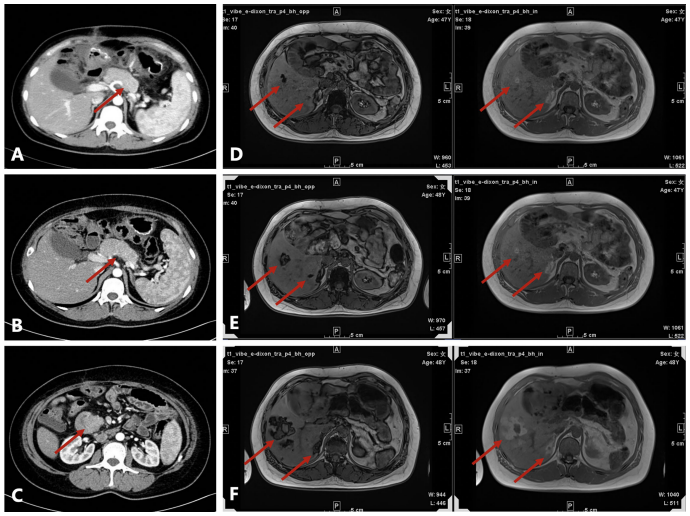

FIGURE 1
Radiological evaluation before and after surgery. **(A)** Irregularly shaped pancreas seen on contrast-enhanced computed tomography (CT) at the first admission. **(B)** Enlarged pancreas on contrast-enhanced CT before surgery. **(C)** Head of the pancreas protruding into the duodenum on contrast-enhanced CT before surgery. **(D–F)** Axial T1-weighted in-phase and out-of-phase images obtained during follow-up (D, 1.5 years after surgery; E, 2 years after surgery; F, 2.5 years after surgery). There were several patchy and nodular high-signal lesions in the right lobe of the liver on the in-phase image. Note a significant signal drop in these lesions on the opposed-phase image. The lesions gradually enlarged during follow-up. A nodule inside the largest lesion was detected in the last follow-up scan.

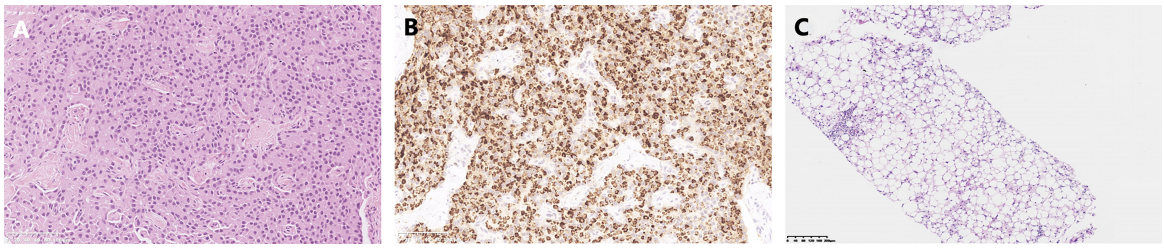

FIGURE 2
Pathological results. **(A)** Hematoxylin-eosin staining of the pancreatic neuroendocrine neoplasm. **(B)** Somatostatin immunostaining. **(C)** Biopsy of the liver metastases.

on in-phase and out-of-phase T1-weighted MRI and were enlarging during follow-up, metastatic tumor with fatty changes was strongly suspected. We then performed a comprehensive ultrasonographic investigation of the liver lesions. A conventional ultrasound scan revealed several irregularly shaped hyperechoic lesions in the liver. The largest lesion measured 6.7 × 3.9 cm and was located in the right lobe. A hypoechoic area with a diameter of 2.2 cm was observed inside this hyperechoic lesion (Figure 3A). Contrast-enhanced ultrasonography (CEUS) was then performed to confirm the exact location of the lesion and to avoid the possibility of a false-negative biopsy result. CEUS of the inner hypoechoic area showed rapid enhancement in the arterial phase and early washout in the portal venous phase with hypo-enhancement in the delayed phase. However, continuous iso-enhancement or hypo-enhancement was seen in the peripheral area (Figures 3B–D). The patient had no discomfort, and her liver function tests were normal. A real-time ultrasound-guided biopsy was performed to ensure extraction of both the peripheral hyperechoic and inner hypoechoic areas and to clarify the nature of the lesions. Histologic evaluation showed a small number of NEN cells and peritumoral liver cells with fatty change (Figure 2C).

Therefore, a diagnosis of liver metastasis of NEN was made. Three months later, the patient was started on sulfatinib, a small-molecule drug that targets the vascular endothelial growth factor and fibroblast growth factor receptors, as part of a clinical trial. The patient was followed up intensively at monthly intervals. Grade 1 hypertension and abnormal liver function were documented as adverse effects. Clinical evaluation in July 2022

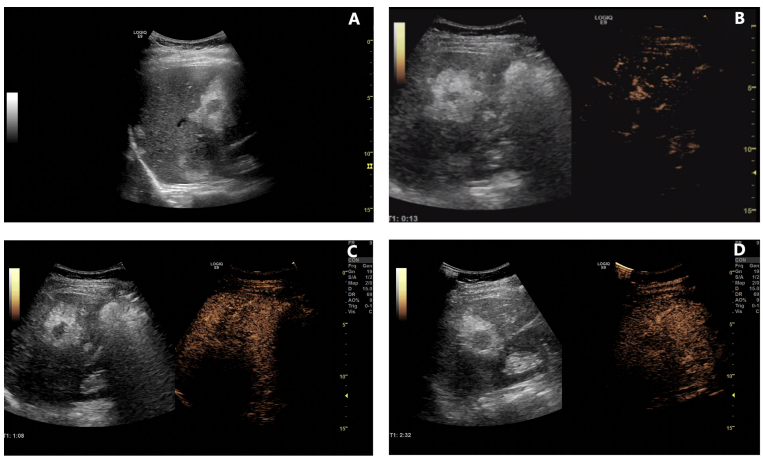

FIGURE 3
Contrast-enhanced ultrasonography of lesions in the liver. **(A)** B-mode ultrasound examination revealed several lesions with an inner hypoechoic area and outer hyperechoic area. **(B–D)** Contrast-enhanced ultrasonographic scans [**(B)**, 13 s in the arterial phase; **(C)**, 68 s in the portal venous phase; **(D)**, 152 s in the delayed phase] showed rapid enhancement in the arterial phase, early washout in the portal venous phase, and hypo-enhancement in the delayed phase in the inner hypoechoic area. However, the peripheral area was continuously iso-enhancing or hypo-enhancing.

(40 months after biopsy of the liver lesions) revealed stable disease. Timeline showing the course of the disease is in Figure 4.

Discussion

This report describes a patient with metastatic NEN to the liver who had unique pathological and imaging features. The hepatic metastases were surrounded by liver cells showing fatty changes. Ultrasonography showed that these lesions contained a hypoechoic area in the center of a hyperechoic area. CEUS was able to distinguish the actual boundary of the metastases and to guide liver biopsy. To the best of our knowledge, this is the first report of metastatic somatostatin-producing oligosymptomatic NEN with peritumoral liver steatosis.

Pancreatic NENs are divided into functioning and non-functioning tumors. Functioning NENs can secrete a large amount of hormones, causing specific clinical hormone hypersecretion syndromes, including insulinoma, glucagonoma, somatostatinoma, gastrinoma, and VIPoma as well as serotonin-producing tumors and adrenocorticotropic hormone-producing tumors. Non-functioning tumors are not associated with clinical hormone hypersecretion syndromes. However, some may still produce biogenic hormones and stain on immunochemistry. The levels of these hormones, which include glucagon, pancreatic polypeptide, somatostatin, and chromogranin, are insufficient to cause clinical symptoms (2). Tumors that demonstrate immunohistochemical labeling with somatostatin but are not associated with symptoms of somatostatinoma syndrome, such as diabetes, cholelithiasis, or diarrhea/steatorrhea, should be classified as somatostatin-producing well-differentiated NEN rather than somatostatinoma (3). The patient in this report presented with only mild steatorrhea, had no other obvious clinical manifestations of somatostatinoma syndrome, and did not have abnormal serum hormone levels. Therefore, this case should be designated as somatostatin-producing oligosymptomatic NEN.

Although the imaging features of liver metastases vary because of the heterogenous origins of the primary tumors, the ultrasonogram in this case showed features that are not often encountered, which made diagnosis difficult. The outer hyperechoic area may be mistaken for tumor tissue and the inner hypoechoic area may be interpreted as liquidation, necrosis, or mucin secretion. Under these circumstances, the tumor volume may be overestimated or the diagnosis missed if the biopsy extracts tissue only from the outer hyperechoic area. However, CEUS may have unique advantages that overcome the abovementioned problems to some extent. In this case, the enhancement pattern in the outer area seemed to indicate normal or relatively normal hepatic tissue, whereas that in the inner area was consistent with the hyper-enhancement typical of metastatic lesions. Furthermore, the results of CEUS helped to generate the biopsy strategy.

CEUS is useful in the evaluation of liver metastases. In a meta-analysis that included 828 lesions, the overall sensitivity of CEUS was 91% (4). Several studies have clearly shown that CEUS allows better imaging of the liver, especially in cases with superficial metastases and where there are lesions along the ligamentum teres (5, 6). Similarly, intraoperative CEUS has been shown to have better diagnostic performance than conventional ultrasound for detection of small liver metastases (7). CEUS is also comparable with contrast-enhanced CT and contrast-enhanced MRI in detection of liver metastases (8, 9). The enhancement pattern of liver metastases in the arterial phase is related to the degree of arterial perfusion. Hypervascular metastases, including NENs, have been reported to show a complete hyper-enhancement pattern in the arterial phase and hypo-enhancement and even non-enhancement in the portal and delayed phases (10). This enhancement pattern was also seen in our case.

Most of the relevant literature on use of CEUS for detection of liver metastases has involved patients with a gastroenteric

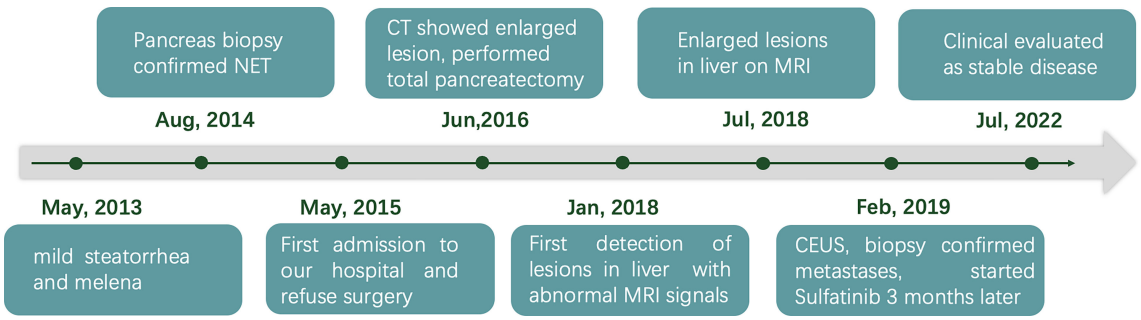

FIGURE 4
Timeline showing the course of the disease.

tumor as the primary. Few studies have included patients with pancreatic NEN, for which the imaging features have been unclear (5). We searched PubMed, Embase, and Google Scholar databases to determine whether peritumoral hepatic steatosis was a unique feature of metastatic pancreatic NEN. The search identified nine cases, the clinical and imaging characteristics of which are shown in Table 1 (11–18). The patients' ages at the time of diagnosis of metastatic liver lesions were 27–77 years, with a slight female predominance. The time interval between diagnosis of the primary tumor and liver metastases was up to 10 years but mostly less than 5 years. Ultrasonography, CT, and MRI were used to detect metastases in these reports, and our case is the first in which CEUS was used. In terms of imaging features, the fatty infiltration pattern was likely a focal rim surrounding the metastatic tumor in most of the reported cases, including in our case, although there was one report of a wedge-shaped lesion with steatosis distal to the portal flow (11). Most studies did not report the size of the lesions; those that did reported the size of the inner area to be less than 2 cm. In terms of pathological subtype, seven of the nine reported cases were insulinoma and two were non-functioning NEN. Insulin immunostaining was positive for one of the non-functioning NEN and negative for all common hormones, including insulin, gastrin, somatostatin, and glucagon, in the other.

The mechanism *via* which peritumoral hepatic steatosis develops in patients with metastatic NEN is still uncertain. However, the insulin produced by insulinomas may explain the steatosis around the metastases. Insulin is known to be important in the pathogenesis of hepatic steatosis. A higher level of insulin could inhibit oxidation of free fatty acids and activate genes associated with *de novo* lipogenesis, leading to accumulation of fat in hepatocytes (19). The phenomenon of local steatosis caused by insulin has also been observed in patients with intraperitoneal insulin delivery (20) and those with intraportal islet transplantation (21). In contrast, glucagon facilitates oxidation of fatty acids in hepatocytes and accordingly favors lipolysis (22). There has been a report of a patient with a history of diffuse non-alcoholic fatty liver disease who was found to have metastatic glucagonoma surrounded by a steatosis-deficient zone with an imaging pattern that was also opposite to that of insulinoma (13).

The theory of local hormone production could explain some cases of insulinoma and the reported case of non-functioning NEN with positive insulin staining, which also produced insulin in the area surrounding the tumor (11). However, this theory could not explain our case or the case that produced no hormones. Somatostatin can regulate blood glucose levels under physiological conditions by inhibiting insulin and glucagon secretion from the pancreas (23). However, our patient had undergone total pancreatectomy before liver metastasis was recognized. Furthermore, one report mentioned that a localized decrease in portal flow was one of the causes of focal fatty infiltration (11). Because the imaging features of the lesion in that case were not consistent with those in most of the other reports, this suspicion may also be imperfect. Although we could not confirm the cause of focal steatosis in our patient pathologically, it was speculated that a change in the tumor microenvironment may have contributed to the fatty changes associated with the metastatic NEN.

This research has some limitations. First, somatostatin receptor scintigraphy, such as octreoscan or ^{68}Ga-DOTATOC positron emission tomography, was not performed before or after surgery. Therefore, there is a small possibility that micrometastases were missed. Second, the mechanism for the development of the peritumoral steatosis remains unclear.

TABLE 1 Brief review of metastatic NEN cases with peritumoral liver steatosis in the literature and this case.

Characteristics	Hoshiba (11)	Sohn (12)	Fregeville (13)	Sumiyoshi (14)	Takeshita (15)	Atwell (16)	Atwell (16)	Borghei (17)	Muramae (18)	This case
Age*	64	27	30	44	69	74	58	54	77	49
Gender	F	M	F	F	F	M	M	F	F	F
Time interval**	9 years	NA	2 years	NA	0	0	3 years	0	3 years	4 years
Pathology	N-F	Insul	Insul	Insul	Insul	Insul	Insul	N-F	Insul	N-F
Immunohistochemistry***	Insulin	NA	NA	NA	Insulin	NA	NA	All negative	NA	Somat-ostatin
Imaging procedures	US/CT	MRI	CT/MRI	US/MRI	CT/MRI	US/CT	US/CT	CT	US/CT/ MRI	MRI/ CEUS
Imaging feature	Wedge	Rim	Rim	Rim	Rim	Rim	Rim	Rim	Rim	Rim
Inner area size	1cm	1.2cm	NA	NA	0.5cm	NA	NA	2cm	NA	2.2cm
Overall size	NA	1.9cm	NA	NA	3cm	NA	NA	NA	NA	6.7cm

M, male; F, female; N-F, non-functioning neuroendocrine neoplasm; Insul, insulinoma; NA, not acquired; US, ultrasound; CT, computed tomography; MRI, magnetic resonance imaging.
*Age at diagnosing liver metastasis.
**Time between the diagnosis of primary tumor and metastasis.
***Common hormones for NEN immunohistochemistry clinically, including insulin, gastrin, somatostatin, and glucagon. NA means the results were not mentioned in the original article, rather than negative.

In summary, this is the first report of peritumoral liver steatosis in a patient with metastatic somatostatin-producing oligosymptomatic NEN. Peritumoral liver steatosis may be a specific pathological and imaging feature observed in metastatic NENs. Awareness of this feature is conducive to an early and accurate diagnosis. CEUS and other imaging procedures may help to distinguish tumor size and guide biopsy of metastases.

Data availability statement

The original contributions presented in the study are included in the article/Supplementary Material. Further inquiries can be directed to the corresponding authors.

Ethics statement

Written informed consent was obtained from the individual (s) for the publication of any potentially identifiable images or data included in this article.

Author contributions

YS and YG contributed equally to this study and should be regarded as co-first authors. YS and YG collected the imaging and clinical data, designed the study, and interpreted the results. YS drafted the manuscript. YG performed the US and CEUS scan. YC followed up the patient and collected the clinical data. JX perform the CT and MRI scans. XC performed the pathological analysis and interpreted the results. KL designed the study, perform the CEUS and biopsy. All authors contributed to the article and approved the submitted version.

Funding

This study was funded by National Natural Science Foundation (82171968 to KL) and the Chinese Academy of Medical Sciences Innovation Fund for Medical Sciences (CIFMS), CAMS Innovation Fund for Medical Sciences (CIFMS) (award number: 2020-I2M-C&T-B-039 to KL) The funder's role was collecting the clinical and imaging data, and open access publication fees.

Conflict of interest

The authors declare that the research was conducted in the absence of any commercial or financial relationships that could be construed as a potential conflict of interest.

Publisher's note

References

1. Kloppel G. Neuroendocrine neoplasms: Dichotomy, origin and classifications. *Visc Med* (2017) 33(5):324–30. doi: 10.1159/000481390

2. Guilmette JM, Nose V. Neoplasms of the neuroendocrine pancreas: An update in the classification, definition, and molecular genetic advances. *Adv Anat Pathol* (2019) 26(1):13–30. doi: 10.1097/PAP.0000000000000201

3. Garbrecht N, Anlauf M, Schmitt A, Henopp T, Sipos B, Raffel A, et al. Somatostatin-producing neuroendocrine tumors of the duodenum and pancreas: incidence, types, biological behavior, association with inherited syndromes, and functional activity. *Endocr Relat Cancer* (2008) 15(1):229–41. doi: 10.1677/ERC-07-0157

4. Friedrich-Rust M, Klopffleisch T, Nierhoff J, Herrmann E, Vermehren J, Schneider MD, et al. Contrast-enhanced ultrasound for the differentiation of benign and malignant focal liver lesions: a meta-analysis. *Liver Int* (2013) 33 (5):739–55. doi: 10.1111/liv.12115

5. Konopke R, Kersting S, Bergert H, Bloomenthal A, Gastmeier J, Saeger HD, et al. Contrast-enhanced ultrasonography to detect liver metastases : a prospective trial to compare transcutaneous unenhanced and contrast-enhanced ultrasonography in patients undergoing laparotomy. *Int J Colorectal Dis* (2007) 22(2):201–7. doi: 10.1007/s00384-006-0134-5

6. Quaia E, D'Onofrio M, Palumbo A, Rossi S, Bruni S, Cova M. Comparison of contrast-enhanced ultrasonography versus baseline ultrasound and contrast-enhanced computed tomography in metastatic disease of the liver: diagnostic performance and confidence. *Eur Radiol* (2006) 16(7):1599–609. doi: 10.1007/s00330-006-0192-7

7. Itabashi T, Sasaki A, Otsuka K, Kimura T, Nitta H, Wakabayashi G. Potential value of sonazoid-enhanced intraoperative laparoscopic ultrasonography for liver assessment during laparoscopy-assisted colectomy. *Surg Today* (2014) 44(4):696–701. doi: 10.1007/s00595-013-0607-4

8. Larsen LP, Rosenkilde M, Christensen H, Bang N, Bolvig L, Christiansen T, et al. Can contrast-enhanced ultrasonography replace multidetector-computed tomography in the detection of liver metastases from colorectal cancer? *Eur J Radiol* (2009) 69(2):308–13. doi: 10.1016/j.ejrad.2007.10.023

9. Cantisani V, Ricci P, Erturk M, Pagliara E, Drudi F, Calliada F, et al. Detection of hepatic metastases from colorectal cancer: prospective evaluation of gray scale US versus SonoVue(R) low mechanical index real time-enhanced US as compared with multidetector-CT or gd-BOPTA-MRI. *Ultraschall Med* (2010) 31 (5):500–5. doi: 10.1055/s-0028-1109751

10. Larsen LP. Role of contrast enhanced ultrasonography in the assessment of hepatic metastases: A review. *World J Hepatol* (2010) 2(1):8–15. doi: 10.4254/wjh.v2.i1.8

11. Hoshiba K, Demachi H, Miyata S, Matsui O, Takashima T, Tsuji M, et al. Fatty infiltration of the liver distal to a metastatic liver tumor. *Abdom Imaging* (1997) 22(5):496–8. doi: 10.1007/s002619900246

12. Sohn J, Siegelman E, Osiason A. Unusual patterns of hepatic steatosis caused by the local effect of insulin revealed on chemical shift MR imaging. *AJR Am J Roentgenol* (2001) 176(2):471–4. doi: 10.2214/ajr.176.2.1760471

13. Fregeville A, Couvelard A, Paradis V, Vilgrain V, Warshauer DM. Metastatic insulinoma and glucagonoma from the pancreas responsible for specific peritumoral patterns of hepatic steatosis secondary to local effects of

insulin and glucagon on hepatocytes. *Gastroenterology* (2005) 129(4):1150,365. doi: 10.1053/j.gastro.2005.08.033

14. Sumiyoshi S, Kobayashi Y, Souda K, Takehara Y, Nakamura H. Images of interest. hepatobiliary and pancreatic: Insulinoma metastases with focal hepatic steatosis. *J Gastroenterol Hepatol* (2005) 20(4):650. doi: 10.1111/j.1440-1746.2005.03871.x

15. Takeshita A, Yamamoto K, Fujita A, Hanafusa T, Yasuda E, Shibayama Y. Focal hepatic steatosis surrounding a metastatic insulinoma. *Pathol Int* (2008) 58 (1):59–63. doi: 10.1111/j.1440-1827.2007.02190.x

16. Atwell TD, Lloyd RV, Nagorney DM, Fidler JL, Andrews JC, Reading CC. Peritumoral steatosis associated with insulinomas: appearance at imaging. *Abdom Imaging* (2008) 33(5):571–4. doi: 10.1007/s00261-007-9278-1

17. Borghei P, Pan Z, Berland LL. Peritumoural steatosis in metastatic "non-functioning" neuroendocrine tumour of the pancreas. *Clin Radiol* (2012) 67 (10):1027–9. doi: 10.1016/j.crad.2012.02.014

18. Muramae N, Kobayashi T, Otsui K, Sakaguchi K. Focal hepatic steatosis caused by metastatic malignant insulinoma. *Intern Med* (2021) 60(4):653–4. doi: 10.2169/internalmedicine.5780-20

19. Daniel T, Ben-Shachar M, Drori E, Hamad S, Permyakova A, Ben-Cnaan E, et al. Grape pomace reduces the severity of non-alcoholic hepatic steatosis and the development of steatohepatitis by improving insulin sensitivity and reducing ectopic fat deposition in mice. *J Nutr Biochem* (2021) 98:108867. doi: 10.1016/j.jnutbio.2021.108867

20. Jang EC, Kim G, Kim YS, Yoon SA, Ku YM, Yang CW, et al. Hepatic subcapsular steatosis in a diabetic CAPD patient receiving intraperitoneal insulin. *Korean J Intern Med* (2006) 21(3):206–9. doi: 10.3904/kjim.2006.21.3.206

21. Markmann JF, Rosen M, Siegelman ES, Soulen MC, Deng S, Barker CF, et al. Magnetic resonance-defined periportal steatosis following intraportal islet transplantation: a functional footprint of islet graft survival? *Diabetes* (2003) 52 (7):1591–4. doi: 10.2337/diabetes.52.7.1591

22. Perry RJ, Zhang D, Guerra MT, Brill AL, Goedeke L, Nasiri AR, et al. Glucagon stimulates gluconeogenesis by INSP3R1-mediated hepatic lipolysis. *Nature* (2020) 579(7798):279–83. doi: 10.1038/s41586-020-2074-6

23. Luethy D, Johnson AL, Stefanovski D, Boston RC, Orsini JA. Glucose and insulin response after intravenous and subcutaneous somatostatin administration in healthy horses. *J Vet Pharmacol Ther* (2019) 42(5):541–7. doi: 10.1111/jvp.12793

frontiers | Frontiers in Oncology

TYPE Case Report
PUBLISHED 02 February 2023
DOI 10.3389/fonc.2023.1093196

OPEN ACCESS

EDITED BY
Antonio Bottari,
Università degli Studi di Messina, Italy

REVIEWED BY
DiMing Cai,
Sichuan University, China
Jiangfeng Wu,
Dongyang People's Hospital, China

*CORRESPONDENCE
Ying Huang
huangying712@163.com

SPECIALTY SECTION
This article was submitted to Cancer Imaging and Image-directed Interventions, a section of the journal Frontiers in Oncology

RECEIVED 08 November 2022
ACCEPTED 20 January 2023
PUBLISHED 02 February 2023

CITATION
Zhang YQ, Wang XY and Huang Y (2023) The findings on the CEUS of diffuse large B cell lymphoma in abdomen: A case report and literature review.
Front. Oncol. 13:1093196.
doi: 10.3389/fonc.2023.1093196

The findings on the CEUS of diffuse large B cell lymphoma in abdomen: A case report and literature review

Yu-Qing Zhang, Xin-Yue Wang and Ying Huang*

Department of Ultrasound, Shengjing Hospital of China Medical University, Shenyang, China

Background: PET-CT is the first choice for the imaging diagnosis of intraperitoneal lymphomas. Contrast-enhanced ultrasound (CEUS) is rare in the diagnosis of intraperitoneal nodal lymphoma.

Case summary: A 62-year-old man was admitted for examination with "right upper abdominal pain". Ultrasound was used to refer to the masses in the hilar region, spleen, and anterior sacral region respectively. The masses were all hypoechoic, and blood flow signals could be detected by CDFI. Laboratory tests of CA125 were within normal limits. CEUS examination was performed on the three masses respectively. The three masses showed different perfusion patterns. Thickened vessels appeared around the mass in the hilar region, a peripheral centrally directed perfusion pattern was observed in the splenic mass, and blood supply vessels appeared in the center of the presacral mass with a significant filling defect. They all showed a contrast pattern with rapid clearance and hypoenhancement compared with the surrounding areas. Ultrasound guided needle biopsy revealed non-Hodgkin's lymphoma, diffuse large B-cell lymphoma, non-germinal center origin. After biopsy, the patient was treated with R-CHOP regimen for chemotherapy, and the tumor disappeared by routine ultrasound review after 5 cycles of chemotherapy.

Conclusion: To the best of our knowledge, this report is the first to describe the findings of CEUS in intraperitoneal nodal lymphoma. CEUS has various manifestations in intraperitoneal nodal lymphoma. Future studies are still needed to explore the diagnostic features of CEUS in intraperitoneal nodal lymphoma.

KEYWORDS

non-Hodgkin's lymphoma, ultrasound, contrast-enhanced ultrasound (CEUS), time-intensity curve (TIC), Positron Emission Tomography- Computed Tomography (PET- CT)

Introduction

The incidence of lymphoma continues to rise worldwide. According to Global Cancer Statistics 2018, non-Hodgkin's lymphoma ranks 13th and 11th among all forms of malignancy in terms of morbidity and mortality (1). The diagnosis of lymphoma depends on pathology, and imaging examination can provide more staging information. The application of contrast-enhanced ultrasound (CEUS) in the diagnosis of lymphoma is rare in medicine. Intraperitoneal lymph node lymphoma is less common than superficial lymph nodes. Up to the present, no studies have reported the diagnosis of intraperitoneal nodal lymphoma by contrast-enhanced ultrasound.

Case presentation

Chief complaints

A 62-year-old male patient was admitted to the hospital because of "Pain in the right upper abdomen". Through CT upper abdominal plain scan, a mass in the hilar region could be seen clearly. Thus, further examination was recommended.

History of past illness

The patient had no medical history of other blood diseases, no low fever, no night sweats, and no significant weight loss. In 2015, he underwent cerebrovascular stenting for basilar artery stenosis, and recovered well after surgery. Rosuvastatin, Clopidogrel and Aspirin were taken orally to control the disease. In 2016, he underwent cholecystectomy due to gallstones, and no abdominal discomfort occurred after the operation. He had a history of hypertension for more than 20 years, and his blood pressure was well controlled without other chronic diseases at ordinary times.

Personal and family history

The patient smoked for more than 20 years and quit smoking for more than 10 years. Denied any history of alcohol use. No history of drug or food allergy.

Physical examination

There was a palpable mass in the anterior sacral area, which was hard and slightly tender. No tenderness, rebound pain, muscle tension in the rest of the place. All other vital signs were stable, blood pressure was not high, and no positive signs were detected.

Laboratory examinations

The patient's serum β2 microglobulin was 2.58mg/L at admission, which was higher than the normal value (0.7-1.8mg/L). Urinary β2 microglobulin 0.762 mg/L, higher than the normal value (< 0.24mg/L) thymidine kinase (TK1)0.33pmol/L, still in the normal range. Serum CA125 was 10.58U/mL, and there was no obvious abnormality.

Imaging examinations

Because a hilar mass was showed after scanning the upper abdomen through CT, the patient was scheduled for further examination through contrast-enhanced ultrasound (Figure 1). The ultrasound examination on abdomen was performed using a Resona9 ultrasound system (Mindray Medical International, China) equipped with an SC6-1U (1-6 MHZ) transducer. Conventional ultrasound examination showed a hypoechoic mass in the hilar region, the size of the mass was 4.65x5.33x3.91cm, the boundary was clear, the shape was irregular, and CDFI could detect blood flow signals. Another nearly-circular hypoechoic mass was found in the spleen. The size of the mass was 4.96x4.74x5.19cm, the boundary was clear, and the blood flow signal could be detected by CDFI. Another hypoechoic mass was seen in the anterior sacral area, with a size of 5.84x5.20x4.68cm, located below the bifurcation of the abdominal aorta, with clear boundary and irregular shape. There was no adhesion with the surrounding intestine. Blood flow signals could be detected by CDFI. Further CEUS diagnosis was recommended by the patient's physician and informed consent was obtained. Depth, gain, and focus are thoroughly adjusted to achieve optimal visualization according to the radiologist's habits. The timer was activated after a high-dose injection of 1.5 mL of Sonovue (Bracco, Italy) suspension (an ultrasound contrast agent) and 5 mL of saline (Bracco, Italy). CEUS examination was performed on all three masses. After conducting contrast-enhanced ultrasound, it showed that the blood vessels were thickened at the edge of the tumor in the hilar region, which were enhanced earlier than the surrounding tissues. The tumor showed diffusing snowflake enhancement inside, and showed uneven hypoenhancement after reaching the peak (compared with the liver tissue), and was rapid wash-out compared to that of the liver tissue. The splenic mass showed a peripheral enhancement pattern to the center, with uneven hypoenhancement. The enhancement was later than that of the normal spleen tissue, and rapid wash-out compared to normal spleen. There was no significant change in the lesion range after CEUS compared with the two-dimensional ultrasound. In the presacral mass, the central vessels of the mass were enhanced first, and the enhancement began later than the peripheral tissues, with uneven hypoenhancement. And there were obvious filling defects, and the clearance was earlier than that of the peripheral tissues. The boundary between the three masses and surrounding tissues was obvious (Figure 2). The time-intensity curve (TIC) showed that the ascending slope of the lesion was higher than that of the surrounding tissue, although the lesion was delayed hypoperfusion, which also suggested that the lesion area had more blood vessels and less resistance. The clearance time of the lesion was significantly earlier than that of the surrounding tissue, which was consistent with the characteristics of malignancy. The three masses did not have the same pattern of enhancement, and there were obvious filling defect areas in the presacral mass, while the enhancement was more uniform in the hilar region and the splenic

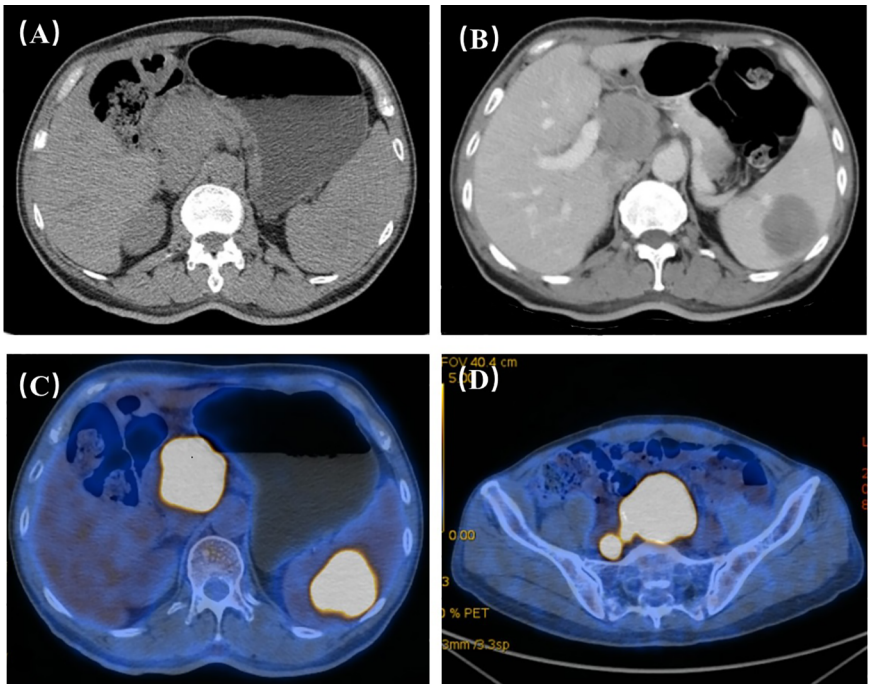

FIGURE 1
(A) Through plain scan of the upper abdomen, it clearly showed the masses in the hilar region, but the masses in the spleen were not obvious. **(B)** Through contrast-enhanced CT, it could show the masses in the hilar region and splenic region, and the masses showed progressive and uneven enhancement. The hilar region nodules: plain scan 30HU arterial phase, 40HU portal vein phase, 52HU delayed phase, 65HU; spleen nodules: plain scan 35HU arterial phase, 46HU portal vein phase, 52HU delayed phase, 63HU; upper abdominal enhancement suggested: Further examination is recommended for hilar and splenic masses. **(C, D)** FDG metabolism of hilar mass, splenic mass and presacral mass on PET-CT increased, and finally PET-CT suggested that the three were homologous and had a high possibility of lymphoma.

mass. Although the enhancement patterns of the three masses were different, they all showed rapid wash-out, which was consistent with the characteristics of malignant masses. Among them, the thickened vessels at the edge of the tumor in the hilar region were consistent with the CEUS features of lymphoma in previous studies (2). The CEUS pattern of splenic mass was basically consistent with the characteristics of nodular splenic infiltration of malignant lymphoma mentioned in the literature. The CEUS pattern of central vessel enhancement first in the presacral mass has not been confirmed in the literature in lymphoma, but considering that the patient had no medical history of other malignant tumors and considering homology with other masses. Finally, the patient was diagnosed lymphoma under the CEUS pattern combined with the patient's medical history.

Pathological findings and immunohistochemical staining

Puncture biopsy was performed on the patient's anterior sacral mass, and 16G automatic puncture biopsy needle (Bard, America) was used. The final pathological results suggested non-Hodgkin B-cell lymphoma, diffuse large B-cell lymphoma, and non-germinal center origin. Immunohistochemical results showed that CD20, CD21, CD19 were positive, Ki-67>90%, Bcl-2>90%, Bcl-6>80%.

Results of flow cytometry

Through flow cytometry, the results showed double clonal B mature lymphocytes.

Final diagnosis

The final diagnosis of this case was intranodal type diffuse large B-cell lymphoma with splenic infiltration.

Treatment

The patient was diagnosed with diffuse large B-cell lymphoma and received R-CHOP chemotherapy, namely rituximab, dexamethasone, vincristine, epirubicin, and cyclophosphamide, for a course of 8 cycles. After 4 cycles of chemotherapy, abdominal enhanced CT examination showed that the size of the hilar lesion was about 2.96x2.11cm, the presacral mass was unclear, and the size of the splenic mass was about 2.79x3.04cm. After 5 cycles of chemotherapy, conventional ultrasound scan of the whole abdomen showed no definite lesions.

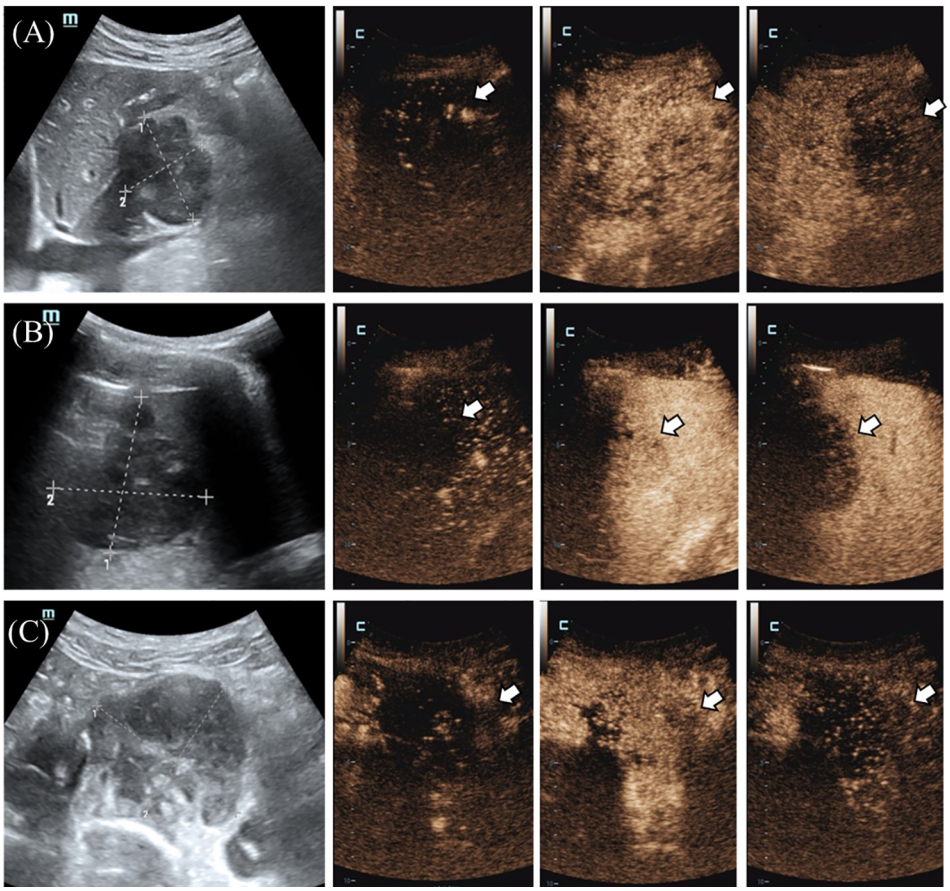

FIGURE 2
(A) The tumor in the hilar region showed thickened blood vessels, located at the edge of the tumor (indicated by the arrow), and was enhanced and cleared earlier than the surrounding tissue. **(B)** The splenic mass (shown by the arrow) showed a peripheral to central enhancement pattern with uneven hypoenhancement, which was enhanced later and cleared earlier than normal splenic tissue. **(C)** In the presacral mass (shown by the arrow), the central vessels of the mass were enhanced first, and the enhancement began later than the peripheral tissues, with uneven hypoenhancement, and there were obvious filling defects, and the clearance was earlier than the peripheral tissues.

Discussion

Diffuse large B-cell lymphoma (DLBCL) is the most prevalent subtype of non-Hodgkin lymphoma. Patients usually presented with progressive lymphadenopathy, extranodal disease, or presented with the both, which require treatments (3). The definitive diagnosis of lymphoma clinically depends on the detailed examination of tumor tissue. In addition to morphological characteristics, the accurate classification of lymphoma also requires specialized tests, including immunohistochemistry, flow cytometry, fluorescence *in situ* hybridization (FISH) and molecular testing (4, 5). Positron Emission Tomography-Computed Tomography (PET-CT) was used to evaluate organ involvement and clinical staging (6). However, PET-CT is often limited by the high cost of examination and the high radiation dose. In recent years, many studies have focused on more accurate diagnosis of lymphoma by imaging methods, further differentiating from other space-occupying lesions and prognosis evaluation (7–9). Different treatments from the most malignant tumors together with the negative prognosis, the timely diagnosis of lymphoma becomes necessary.

CEUS has the advantages of convenience and easy operation. Contrast-enhanced ultrasound can display the changes of microcirculation perfusion in real time. At present, contrast-enhanced ultrasound has been widely used (10). CEUS is rarely reported in the diagnosis of lymphoma compared with other diseases. Many studies in the literature focus on the CEUS features and differential diagnostic efficacy of superficial lymph nodes (11–13). It is rare to study abdominal lymph nodes.

In this case, under the CEUS mode the distribution of microvessels presented by different masses was different. Thickened blood vessels appeared around the mass in the hepatic portal area, which became the first perfusion area of the tumor. It may be caused by surrounding blood vessels in the invasive growth process of the tumor. The volume of the pre-sacral mass was large, and the rapid growth rate led to the lack of blood supply in the tumor. Due to the above the filling defect inside the mass was found by contrast-enhanced ultrasound. Due to the different growth location and size, the microvascular distribution of each homologous tumor is slightly different.

Superficial lymph nodes are the most common site of lymphomas, especially those in the head and neck. Contrast-enhanced ultrasound can clearly show the distribution of blood vessels in lymph nodes, which makes the diagnosis of superficial lymph nodes more accurate (Table 1). The studies on CEUS

TABLE 1 Contrast-enhanced ultrasound characteristics of superficial lymph node lymphoma reported in the literature.

Ref.	Year	Country	Type of literature	Gender (M/F)	Age	lymphoid neoplasms	CEUS feature	Conclusion	Contrast agent/ dosage
Shan-shan Yin et al.	2018	China	Research	71/74	53.1 ± 14.4	Not specified	The peripheral arrival time of lymphoma is significantly later than that of metastatic cancer lymph nodes, the central arrival time is earlier than that of metastatic cancer lymph nodes, and the ΔT is significantly shorter than that of metastatic cancer lymph nodes.	CEUS can provide additional information for the differential diagnosis of superficial lymph node enlargement.	SonoVue/ 1.0ml
Leopoldo Rubaltelli et al.	2004	Italy	Research	28/17	27-76	Not specified	CEUS of lymphoma shows intense but heterogeneous speckle-like enhancement in the early arterial phase.	CEUS is highly accurate in the differential diagnosis of benign and malignant lymph nodes.	Esatune/ 4.8ml
Ji Nie et al.	2020	China	Research	76/67	53.4 ± 12.9	Not specified	Quantitative analysis of CEUS parameters showed that the PI (and AUC were lower in lymphomas than in cancerous lymph nodes. Lymphomas tend to show homogeneous enhancement	Contrast-enhanced ultrasound is used for the differential diagnosis of head and neck lymphomas and cancerous lymph nodes.	SonoVue/ 2.4ml
Ming Yu et al.	2009	China	Research	48/46	46	Not specified	Of the 17 lymphomas, 9 showed homogeneous hyperenhancement and 6 showed absence of perfusion.	Contrast enhancement patterns and temporal intensity profiles provide valuable diagnostic information for the differential diagnosis of benign and malignant lymph nodes.	SonoVue/ 2.4ml
Xiaoyan Niu et al.	2018	China	Research	42/21	50	Not specified	In the current lymph nodes, ΔI, AUC, and AS showed positive associations with PET-CT values.	The real-time enhancement process and TIC parameters can provide comprehensive information regarding the activity of lymph nodes for further examination.	SonoVue/ 2.4ml
Wenbin Jiang et al.	2018	China	Research	42/21	50	Not specified	When lymphoma CEUS shows ΔT < 5.5 or AS > 2.58, it indicates advanced stage and aggressiveness of the lymphoma	The quantitative parameters of CEUS help to assess the different clinical and pathological patterns of extramedullary lymphoma.	SonoVue/ 2.4ml
Xuelei Ma et al.	2018	China	Research	43/18	50.8	Not specified	83.1% of lymphomas present with diffuse uniform hyperenhancement	The rapid distribution of highly enhanced patterns in CEUS can be a useful diagnostic criterion for both aggressive and non-aggressive lymphomas.	SonoVue/ 2.4ml
Shirong Liu et al.	2019	China	Research	18/14	40.67 ± 16.83	Not specified	Subperitoneal CEUS showed that the majority (6 of 7, 85.7%) of lymphomas exhibited heterogeneous perfusion and lymphatic tract distortion.	subcapsular CEUS may help to distinguish between benign and malignant lesions	SonoVue/ 2.0ml
Lei Xin et al.	2017	China	Research	12/23	50.5	Not specified	Quantitative CEUS parameters before and after the first three cycles of chemotherapy showed significant differences in AreaΔ, PIΔ, and IΔ in the overall response group compared to the no responsive group.	The results of this study suggest that quantitative analysis of CEUS may be a useful method for assessing treatment response to superficial lymph node enlargement	SonoVue/ 2.4ml

(Continued)

TABLE 1 Continued

Ref.	Year	Country	Type of literature	Gender (M/F)	Age	lymphoid neoplasms	CEUS feature	Conclusion	Contrast agent/ dosage
								in lymphoma before and after chemotherapy	
M. Kumagawa et al.	2021	Japan	Research	18/9	66	Not specified	Accordingly, changes in the ratio of PE < 1.09 and changes in the ratio of PI < 1.65, distinguished CR from non-CR accurately.	Changes in perfusion parameters assessed by CEUS may be able to assess the prognosis of patients with lymphoma	Daiichi-Sankyo/ 0.5ml

diagnosis of superficial lymph nodes are more mature. The study of Shan-Shan Yin et al. suggested that the CEUS findings of lymphoma are significantly different from those of lymph node metastasis and reactive lymph nodes. Through CEUS findings of lymphoma, it can mostly be seen the diffusing and even enhancement, and rarely be seen the non-perfusion filling defect areas. Lymph node metastases usually presented with centripetal enhancement, and non-perfusion filling defect area is more common. Reactive hyperplastic lymph nodes presented with uniform hyperenhancement due to vascular hyperplasia, and lymph node tuberculosis presented with unclear lymph node boundary (11). Much of the literature comes to similar conclusions (14–16). This may be related to angiogenesis and vascular distribution in the lesion. Due to the rapid growth rate of malignant metastases, immature neovascularization and non-vascular necrotic areas are common in metastatic lymph nodes, which hinders the distribution of contrast agent to these areas then leads to perfusion defects. In most lymphomas, blood vessels are highly hyperplastic, which makes the microvesicles of contrast agent easy to flow and rapidly distribute throughout the lesion, resulting in more uniform enhancement (16). Although the features of contrast-enhanced ultrasound in lymphoma have been unanimously agreed in many literatures, there are still some exceptions. In the study, Ming Yu et al. reported 6 cases of lymphoma without perfusion (17). Due to the uncertainty in the qualitative manifestations of contrast-enhanced ultrasound in lymphoma, literature studies have made focus on the quantitative analysis of contrast-enhanced ultrasound. Shan-shan Yin et al. also analyzed the arrival time parameters of contrast media and found that compared with lymphoma, the contrast had arrived earlier in metastatic cancer but spent longer to the center (11). Xiaoyan Niu et al. suggested that quantitative indicators of CEUS were correlated with PET-CT indicators, which had potential diagnostic value for lymphoma (18). CEUS has a high diagnostic value in the diagnosis of benign and malignant superficial lymph nodes, which has been confirmed by studies. However, CEUS still manifested similarities in lymph nodes with different pathologies, and the treatment of lymph node diseases is completely different. Therefore, more studies are devoted to further explore the more accurate diagnosis of lymphoma by CEUS. Liu SR et al. injected subcapsular contrast injection and observed that lymph nodes of lymphoma patients had lymphatic vessel distortion and uneven distribution of contrast agent, which was completely different from reactive proliferative lymph nodes with uniform distribution of contrast agent and lymph node metastasis with local concentration of contrast agent and lymphatic vessel rupture (19). Compared with intravenous contrast medium injection, subcapsular contrast medium injection has a better effect in identifying the types of lymph nodes, it requires higher technical requirements for the operator. Thus, this kind of injection cannot be popularized wider. The prognosis of different subtypes of lymphoma varies greatly. According to the growth pattern and prognosis of lymphoma, it can be divided into aggressive lymphoma and indolent lymphoma. Studies suggest that the contrast-enhanced ultrasonography of indolent lymphoma is more similar to that of reactive proliferative lymph nodes, presenting rapid uniform hyperenhancement (13). The later the stage, the more aggressive and malignant the lymphoma, the richer the blood vessels in the tumor, the higher the blood flow velocity, and the higher the RI. The difference of ΔT and AS between early and advanced lymphomas was statistically significant, suggesting that advanced lymphomas had abundant blood flow at the CEUS quantitative level (20). However, there was no significant difference in contrast-enhanced ultrasound performance between HL and NHL. Further analysis of the various subtypes of lymphoma by contrast-enhanced ultrasound is not available. Studies suggest that contrast-enhanced ultrasound has a high application value in evaluating the response of lymphoma to drugs after chemotherapy, and it can accurately respond to changes in the blood supply of the lesion after chemotherapy. For the lesions that responded to chemotherapy, the area under the curve of CEUS quantitative analysis before and after chemotherapy showed statistically significant difference in perfusion index (PI) (21). in the study of M. Kumagawa et al., peak enhancement (PE) and PI are considered to be the effective indicators for evaluating whether a patient has achieved a complete response after chemotherapy (22). The prediction of lesion response after chemotherapy can quickly make clear the next treatment plan of patients more quickly.

CEUS is relatively rare in the diagnosis of lymphomas in extranodal organs (Table 2). Through CEUS, it can well reflect the blood supply of the lesion and the distribution of microvessels, and has a good diagnostic efficiency for the differentiation of lymphoma from benign nodules of spleen (23–25). Lymphoma of the spleen is more common in secondary lymphoma invasion and formation, but primary lymphoma is rare to be seen. The findings of primary splenic lymphoma are similar to those of secondary CEUS, with early isoenhancement and early regression (26, 27). Other malignant tumors of the spleen are rare to be seen, and the differentiation of splenic lymphoma from other malignant tumors has not been reported. Christian Gorg et al. believe that CEUS has no added value in the diagnosis of splenic involvement in lymphoma and cannot improve the diagnostic accuracy of

10.3389/fonc.2023.1093196

TABLE 2 Contrast-enhanced ultrasound characteristics of lymphoma involving extranodal organs reported in the literature.

Ref.	Year	Country	Type of literature	Gender (M/F)	Age	Organ involved	lymphoid neoplasms	CEUS feature	Conclusion	Contrast agent/ dosage
Marco Picardi et al.	2009	Italy	Research	53/47	30/ 32	spleen	Hodgkin lymphoma	After contrast material injection, most malignant nodules had clear intralesional vessels with isoenhanced and fine intralesional microcirculation with hypoenhanced appearance in the parenchymal phase.	Harmonic compound US with contrast enhancement for the characterization of possible nodules provides a higher sensitivity in the detection of splenic involvement by Hodgkin lymphoma.	Sonovue/ 2.4ml
Stefano Ballestri et al.	2014	Japan	Case	F	73	spleen	Not mentioned	Arterial phase at 15 s. initially, inhomogeneous parenchymal enhancement. Splenic lesions are isoechoic compared to the surrounding parenchyma. Parenchymal phase at 35 s. Hypoenhancement of the lesion.	CEUS was able to correctly identify as malignant.	Sonovue/ Not mentioned
Marco Picardi et al.	2022	Italy	Research	43/34	48	spleen	Not specified	The enhancement pattern of lymphoma characterized by isoenhancement in the arterial phase followed by wash-out appearance that had early onset and marked degree.	It is important indications of CEUS for assessing the spleen at risk of lymphomatous invasion.	Sonovue/ 2.4ml
Tom Sutherland et al.	2010	Australia	Case	M	66	spleen	diffuse large B cell lymphoma	In the early phase, the mass demonstrated homogenous enhancement similar to the surrounding normal spleen and was isoenhanced for the first 20 seconds. Rapid wash-out then occurred with the mass being hypoenhanced relative to normal spleen in the parenchymal phase and becoming subsequently.	With second-generation sonographic contrast agents, the enhancement characteristics of the primary splenic lymphoma in our case were identical to those of secondary splenic lymphoma described in the literature with early contrast enhancement and rapid progressive washout.	Definity/ 1.5ml
Zhang W et al.	2022	China	Research	20/29	31-73	spleen	Not specified	It mostly showed uniform enhancement when checking Splenic lymphoma by CEUS, which could be low or high enhancement, but not septal	Contrast-enhanced ultrasound is valuable for the differential diagnosis of splenic lymphoma and splenic tuberculosis.	SonoVue/ 2.4ml

(Continued)

10.3389/fonc.2023.1093196

TABLE 2 Continued

Ref.	Year	Country	Type of literature	Gender (M/F)	Age	Organ involved	lymphoid neoplasms	CEUS feature	Conclusion	Contrast agent/ dosage
								enhancement within lesions. Spacer enhancement can be used to distinguish splenic lymphoma from splenic tuberculosis.		
Christian Görg et al.	2009	Germany	Research	27/24	20-83	spleen	Not specified	During the arterial phase focal lesions were hypoenhancement or isoenhancement, During the parenchymal phase focal lesions were hypoenhancement.	CEUS has no clear advantage for diagnosis of splenic lymphoma involvement.	Sonovue/ 2.4ml
Francesco Giuseppe Foschi et al.	2010	America	Case	M	62/58	liver	MALT	Contrast-enhanced ultrasonography showed that the nodular lesion had mild inhomogeneous hyperenhancement in the arterial phase and wash-out in the portal and late phases.	There is no imaging pattern on CEUS is specific for PHL.	Sonovue/ 2.4ml
Yuki Yamashita et al.	2021	Japan	Case	F	66	liver	MALT	After Sonazoid injection, the tumor was depicted as a homogeneously hyper-enhanced lesion with penetrating vessels in the early arterial phase, which began to wash out in 15 seconds. The tumor was hypo-enhanced in the portal and late phases on CEUS.	Primary hepatic extranodal marginal zone lymphoma of MALT presenting image findings different from those of typical hepatocellular carcinoma along with the vessel penetration sign.	Sonazoid/ Not mentioned
C. Trenker et al.	2013	Germany	Research	22/16	60.1	liver	Not specified	The present study shows hypoenhancement in the portal phase in n = 36 (94.7%) cases. In n = 2 (5.3%) cases hepatic lymphoma presented isoechogenic enhancement in the portal phase. In n = 38 (100%) cases lymphoma lesions exhibited hypoenhancement during the late phase.	The application of CEUS can help to find the right diagnosis. A discrimination between malignant liver lesions, such as liver lymphomas, metastasis or HCC, remains impossible.	Sonovue/ 2.5ml

(Continued)

TABLE 2 Continued

Ref.	Year	Country	Type of literature	Gender (M/F)	Age	Organ involved	lymphoid neoplasms	CEUS feature	Conclusion	Contrast agent/ dosage
Corinna Trenker et al.	2015	Germany	Research	M	75	Pulmonary	Not specified	pulmonary lymphomas surprisingly showed a PA vascularization pattern in all but 1 case. the typical"wash-out" sign that has been understood to be a sign of malignancy was detected in 3 patients, whereas 3 patients also showed isoechoic parenchymal enhancement.	Definite differentiation from other malignant or benign pulmonary lesions cannot be achieved by CEUS	Sonovue/ 2.4ml
Lulu Yang et al.	2021	China	Research	8/23	65	Thyroid	Not specified	For most of the PTL lesions, contrast agent entered in a centripetal way and presented as hypoenhancement, as well as heterogeneous. In CUES mode, PTL had significant lower values of PI and AUC than those of NHT.	CEUS is an efficient diagnostic tool in the differential diagnosis of PTL and NHT for patients with diffuse HT.	Sonovue/ 2.0ml
Li Yang et al.	2022	China	Case	M	59	Testicular	Not specified	the PTL lesions presented by a hyperenhancement by enlarged range in CEUS along with a nonbranching linear vascular pattern on microvascular US.	Combined with straight vascular signs on grey-scale US and painless testicular mass of physical examination, it can provide some help for early non-invasive diagnosis of PTL.	Sonovue/ 2.4ml
Guntram Lock et al.	2016	Germany	Case series	M	59	Testicular	Not specified	On CEUS, all lymphoma lesions show marked hyperenhancement.	the key sonographic features of testicular lymphoma are as follows:(1) sharply demarcated homogeneous hypoechoic testicular lesions with marked hypervascularization on colorcoded sonography; (2) a rapid (<7 seconds) filling time of contrast bubbles; and (3) a straight parallel course of intralesional vessels in most cases, as shown by contrast-enhanced sonography.	Sonovue/ 2.4ml

conventional ultrasound for splenic involvement (28). CEUS has been used to identify space-occupying lesions of the liver. Intrahepatic lymphoma, as an uncommon intrahepatic malignant tumor, is less common than other malignant tumors. Similar to the spleen, liver lymphomas secondary to intra nodal lymphomas is usually to be seen, primary liver lymphomas are rare. Primary liver lymphoma is often associated with HBV and HCV virus infections. HBV infection-related MALT was more common in primary liver

lymphoma (29). More studies are needed to determine whether viral infection affects the progression of liver lymphoma. Color Doppler ultrasound often shows multiple vascular channels in malignant liver lymphoma, which is called "vascular penetration sign". Contrast-enhanced blood vessels were first observed in the arterial phase of CEUS, and there were still angiograms in the Kupffer phase. This feature is significantly different from the typical contrast-enhanced ultrasound findings of other liver malignant tumors. However, liver malignant lymphoma also has rich blood supply CEUS findings that are not similar to other malignant tumors and cannot be differentiated from other diseases (30, 31). C. Trenker et al. also concluded that the differential diagnosis of hepatic malignant lymphoma from other malignant tumors could not be completed by CEUS in their study of CEUS findings in 38 cases of lymphoma (32). The renal lymphoma was mainly nodular type. It presented mostly hypoenhancement or isoenhancement in the arterial phase and hypoenhancement in the parenchymal phase through CEUS. Contrast-enhanced ultrasound has certain value in the differential diagnosis of renal lymphoma and benign nodules (33). The findings of CEUS in lymphoma with extranodal organ invasion are relatively uniform, and there is little difference between different extranodal organs. There are also extranodal organs with specificity through CEUS, and the literature studies are mainly based on case reports. One case serially reported the contrast-enhanced ultrasound findings of 6 cases of intrapulmonary lymphoma. 83% of the lymphomas were mainly supplied by pulmonary artery, which was not consistent with the findings of other pulmonary malignancies (34). There is a correlation between thyroid lymphoma and nodular Hashimoto's thyroiditis. Lulu Yang et al. found that the combination of CEUS features and quantitative indicators has a good diagnostic efficacy in differentiating thyroid lymphoma from nodular Hashimoto's thyroiditis (35), However, more studies are needed to confirm whether it can be widely used in clinical practice. Primary testicular lymphoma is rare, and it is difficult to distinguish lymphoma from other testicular lesions by conventional two-dimensional ultrasound or color Doppler. Literature studies have suggested that testicular lymphoma is mostly characterized by rapid high-enhancement contrast-enhanced ultrasound, which is more extensive than gray-scale ultrasound. An 80% increase in blood flow shows a straight vessel pattern with nonbranched increased vascular hyperplasia (36, 37). Most of the studies related to the diagnosis of extranodal organ lymphoma by CEUS are limited to the differentiation of other space-occupying lesions from benign or malignant. However, it seems that it is still difficult to distinguish lymphoma from other malignant tumors by CEUS. Contrast-enhanced ultrasound does not appear to contribute to the diagnosis of extranodal lymphoma subtypes.

The value of CEUS in the diagnosis and prognostic assessment of superficial intra nodal lymphoma has been validated. However, its diagnostic value for lymphoma with extranodal organ invasion seems to need further research and verification.

Conclusion

CEUS findings of this case of intraperitoneal nodular lymphoma showed hypoperfusion in the early stage of enhancement compared with the delayed perfusion of surrounding tissues, and rapid clearance. The pattern of lesion initiation enhancement is varied. To the best of our knowledge, this report is the first to describe CEUS findings of intraperitoneal nodal lymphoma. CEUS is rarely used in the diagnosis of lymphoma compared with other diseases. The value of CEUS for intraperitoneal nodal lymphoma still needs to be confirmed by subsequent studies.

Data availability statement

The original contributions presented in the study are included in the article/Supplementary material. Further inquiries can be directed to the corresponding author.

Ethics statement

Written informed consent was obtained from the individual(s) for the publication of any potentially identifiable images or data included in this article.

Author contributions

YZ: Paper writing, patient information collection, literature review; XW: Paper writing, information collection; YH: Writing instruction, implementation of intervention, information collection. All authors contributed to the article and approved the submitted version.

Conflict of interest

The authors declare that the research was conducted in the absence of any commercial or financial relationships that could be construed as a potential conflict of interest.

Publisher's note

All claims expressed in this article are solely those of the authors and do not necessarily represent those of their affiliated organizations, or those of the publisher, the editors and the reviewers. Any product that may be evaluated in this article, or claim that may be made by its manufacturer, is not guaranteed or endorsed by the publisher.

References

1. Bray F, Ferlay J, Soerjomataram I, Siegel RL, Torre LA, Jemal A. Global cancer statistics 2018: GLOBOCAN estimates of incidence and mortality worldwide for 36 cancers in 185 countries. *CA: Cancer J Clin* (2018) 68(6):394–424. doi: 10.3322/caac.21492

2. Kong J, Fu JJ, Yang W, Sun Y, Wang S, Bai J, et al. Contrast-enhanced ultrasound features of mediastinal lymphomas and thymic epithelial tumors. *J Clin ultrasound JCU*. (2020) 48(1):19–28. doi: 10.1002/jcu.22782

3. Shankland KR, Armitage JO, Hancock BW. Non-Hodgkin lymphoma. *Lancet (London England)* (2012) 380(9844):848–57. doi: 10.1016/S0140-6736(12)60605-9

4. Vockerodt M, Yap LF, Shannon-Lowe C, Curley H, Wei W, Vrzalikova K, et al. The Epstein-Barr virus and the pathogenesis of lymphoma. *J pathology*. (2015) 235(2):312–22. doi: 10.1002/path.4459

5. Li S, Young KH, Medeiros LJ. Diffuse large b-cell lymphoma. *Pathology*. (2018) 50 (1):74–87. doi: 10.1016/j.pathol.2017.09.006

6. Cheson BD, Fisher RI, Barrington SF, Cavalli F, Schwartz LH, Zucca E, et al. Recommendations for initial evaluation, staging, and response assessment of Hodgkin and non-Hodgkin lymphoma: the lugano classification. *J Clin Oncol Off J Am Soc Clin Oncol* (2014) 32(27):3059–68. doi: 10.1200/JCO.2013.54.8800

7. Shen J, Xue L, Zhong Y, Wu YL, Zhang W, Yu TF. Feasibility of using dynamic contrast-enhanced MRI for differentiating thymic carcinoma from thymic lymphoma based on semi-quantitative and quantitative models. *Clin radiology*. (2020) 75 (7):560.e19–.e25. doi: 10.1016/j.crad.2020.02.010

8. Fu F, Sun X, Li Y, Liu Y, Shan Y, Ji N, et al. Dynamic contrast-enhanced magnetic resonance imaging biomarkers predict chemotherapeutic responses and survival in primary central-nervous-system lymphoma. *Eur radiology*. (2021) 31(4):1863–71. doi: 10.1007/s00330-020-07296-5

9. Tanaka T, Akiyoshi H, Nishida H, Mie K, Lin LS, Iimori Y, et al. Contrast-enhanced computed tomography findings of canine primary renal tumors including renal cell carcinoma, lymphoma, and hemangiosarcoma. *PloS One* (2019) 14(11):e0225211. doi: 10.1371/journal.pone.0225211

10. Yusuf GT, Fang C, Huang DY, Sellars ME, Deganello A, Sidhu PS. Endocavitary contrast enhanced ultrasound (CEUS): a novel problem solving technique. *Insights into imaging*. (2018) 9(3):303–11. doi: 10.1007/s13244-018-0601-x

11. Yin SS, Cui QL, Fan ZH, Yang W, Yan K. Diagnostic value of arrival time parametric imaging using contrast-enhanced ultrasonography in superficial enlarged lymph nodes. *J ultrasound Med Off J Am Institute Ultrasound Med* (2019) 38(5):1287–98. doi: 10.1002/jum.14809

12. Spiesecke P, Neumann K, Wakonig K, Lerchbaumer MH. Contrast-enhanced ultrasound (CEUS) in characterization of inconclusive cervical lymph nodes: a meta-analysis and systematic review. *Sci Rep* (2022) 12(1):7804. doi: 10.1038/s41598-022-11542-9

13. Ma X, Ling W, Xia F, Zhang Y, Zhu C, He J. Application of contrast-enhanced ultrasound (CEUS) in lymphomatous lymph nodes: A comparison between PET/CT and contrast-enhanced CT. *Contrast media Mol imaging*. (2019) 2019:5709698. doi: 10.1155/2019/5709698

14. Rubaltelli L, Khadivi Y, Tregnaghi A, Stramare R, Ferro F, Borsato S, et al. Evaluation of lymph node perfusion using continuous mode harmonic ultrasonography with a second-generation contrast agent. *J ultrasound Med Off J Am Institute Ultrasound Med* (2004) 23(6):829–36. doi: 10.7863/jum.2004.23.6.829

15. Stramare R, Scagliori E, Mannucci M, Beltrame V, Rubaltelli L. The role of contrast-enhanced gray-scale ultrasonography in the differential diagnosis of superficial lymph nodes. *Ultrasound quarterly*. (2010) 26(1):45–51. doi: 10.1097/RUQ.0b013e3181cf4469

16. Nie J, Ling W, Yang Q, Jin H, Ou X, Ma X. The value of CEUS in distinguishing cancerous lymph nodes from the primary lymphoma of the head and neck. *Front Oncol* (2020) 10:473. doi: 10.3389/fonc.2020.00473

17. Yu M, Liu Q, Song HP, Han ZH, Su HL, He GB, et al. Clinical application of contrast-enhanced ultrasonography in diagnosis of superficial lymphadenopathy. *J ultrasound Med Off J Am Institute Ultrasound Med* (2010) 29(5):735–40. doi: 10.7863/jum.2010.29.5.735

18. Niu X, Jiang W, Zhang X, Ding Z, Xue H, Wang Z, et al. Comparison of contrast-enhanced ultrasound and positron emission Tomography/Computed tomography (PET/CT) in lymphoma. *Med Sci monitor Int Med J Exp Clin Res* (2018) 24:5558–65. doi: 10.12659/MSM.908849

19. Liu SR, Liu C, Jing HM, Miao LY, Cui LG, Qian LX, et al. Subcapsular injection of ultrasonic contrast agent distinguishes between benign and malignant lymph node lesions exhibiting homogeneous enhancement in intravenous contrast-enhanced ultrasound images. *Ultrasound Med Biol* (2020) 46(3):582–8. doi: 10.1016/j.ultrasmedbio.2019.12.004

20. Jiang W, Xue H, Wang Q, Zhang X, Wang Z, Zhao C. Value of contrast-enhanced ultrasound and PET/CT in assessment of extramedullary lymphoma. *Eur J Radiol*. (2018) 99:88–93. doi: 10.1016/j.ejrad.2017.12.001

21. Xin L, Yan Z, Zhang X, Zang Y, Ding Z, Xue H, et al. Parameters for contrast-enhanced ultrasound (CEUS) of enlarged superficial lymph nodes for the evaluation of therapeutic response in lymphoma: A preliminary study. *Med Sci monitor Int Med J Exp Clin Res* (2017) 23:5430–8. doi: 10.12659/MSM.907293

22. Kumagawa M, Matsumoto N, Miura K, Ogawa M, Takahashi H, Hatta Y, et al. Correlation between alterations in blood flow of malignant lymphomas after induction chemotherapies and clinical outcomes: a pilot study utilising contrast-enhanced ultrasonography for early interim evaluation of lymphoma treatment. *Clin radiology*. (2021) 76(7):550.e9–.e17. doi: 10.1016/j.crad.2021.02.007

23. Picardi M, Soricelli A, Pane F, Zeppa P, Nicolai E, De Laurentiis M, et al. Contrast-enhanced harmonic compound US of the spleen to increase staging accuracy in patients with Hodgkin lymphoma: a prospective study. *Radiology*. (2009) 251(2):574–82. doi: 10.1148/radiol.2512081293

24. Picardi M, Giordano C, Trastulli F, Leone A, Della Pepa R, Pugliese N, et al. Sulfur exafluoride contrast-enhanced ultrasound showing early wash-out of marked degree identifies lymphoma invasion of spleen with excellent diagnostic accuracy: A monocentric study of 260 splenic nodules. *Cancers* (2022) 14(8):1927. doi: 10.3390/cancers14081927

25. Zhang W, Yang G, Zhang X, Ni T. The role of contrast-enhanced ultrasound in differentiating splenic tuberculosis from splenic lymphoma. *Front Oncol* (2022) 12:891815. doi: 10.3389/fonc.2022.891815

26. Sutherland T, Temple F, Hennessy O, Lee WK. Contrast-enhanced ultrasound features of primary splenic lymphoma. *J Clin ultrasound JCU*. (2010) 38(6):317–9. doi: 10.1002/jcu.20699

27. Ballestri S, Lonardo A, Romagnoli D, Losi L, Loria P. Primary lymphoma of the spleen mimicking simple benign cysts: contrast-enhanced ultrasonography and other imaging findings. *J Med ultrasonics (2001)*. (2015) 42(2):251–5. doi: 10.1007/s10396-014-0579-z

28. Görg C, Faoro C, Bert T, Tebbe J, Neesse A, Wilhelm C. Contrast enhanced ultrasound of splenic lymphoma involvement. *Eur J radiology*. (2011) 80(2):169–74. doi: 10.1016/j.ejrad.2009.11.012

29. Yamashita Y, Joshita S, Kobayashi H, Wakabayashi SI, Sugiura A, Yamazaki T, et al. Primary hepatic extranodal marginal zone lymphoma of mucosa-associated lymphoid tissue in a patient with chronic hepatitis b virus infection: Case report and summary of the literature. *Medicina (Kaunas Lithuania)* (2021) 57(3):280. doi: 10.3390/medicina57030280

30. Foschi FG, Dall'Aglio AC, Marano G, Lanzi A, Savini P, Piscaglia F, et al. Role of contrast-enhanced ultrasonography in primary hepatic lymphoma. *J ultrasound Med Off J Am Institute Ultrasound Med* (2010) 29(9):1353–6. doi: 10.7863/jum.2010.29.9.1353

31. Sawatzki M, Meyenberger C, Brand S, Semela D. Contrast-enhanced ultrasound (CEUS) has excellent diagnostic accuracy in differentiating focal liver lesions: results from a Swiss tertiary gastroenterological centre. *Swiss Med weekly* (2019) 149:w20087. doi: 10.4414/smw.2019.20087

32. Trenker C, Kunsch S, Michl P, Wissniowski TT, Goerg K, Goerg C. Contrast-enhanced ultrasound (CEUS) in hepatic lymphoma: retrospective evaluation in 38 cases. *Ultraschall der Med (Stuttgart Germany 1980)*. (2014) 35(2):142–8. doi: 10.1055/s-0033-1350179

33. Trenker C, Neesse A, Görg C. Sonographic patterns of renal lymphoma in b-mode imaging and in contrast-enhanced ultrasound (CEUS)–a retrospective evaluation. *Eur J radiology*. (2015) 84(5):807–10. doi: 10.1016/j.ejrad.2014.12.027

34. Trenker C, Wilhelm C, Neesse A, Rexin P, Görg C. Contrast-enhanced ultrasound in pulmonary lymphoma: A small pilot study. *J ultrasound Med Off J Am Institute Ultrasound Med* (2018) 37(12):2943–7. doi: 10.1002/jum.14651

35. Yang L, Zhao H, He Y, Zhu X, Yue C, Luo Y, et al. Contrast-enhanced ultrasound in the differential diagnosis of primary thyroid lymphoma and nodular hashimoto's thyroiditis in a background of heterogeneous parenchyma. *Front Oncol* (2020) 10:597975. doi: 10.3389/fonc.2020.597975

36. Yang L, Tao Y, Weixin Z, Meiling B, Jing H. Contrast-enhanced and microvascular ultrasound imaging features of testicular lymphoma: report of five cases and review literature. *BMC urology*. (2022) 22(1):6. doi: 10.1186/s12894-022-00957-1

37. Lock G, Schmidt C, Schröder C, Löning T, Dieckmann KP. Straight vessel pattern and rapid filling time: Characteristic findings on contrast-enhanced sonography of testicular lymphoma. *J ultrasound Med Off J Am Institute Ultrasound Med* (2016) 35 (7):1593–9. doi: 10.7863/ultra.15.05049

frontiers | Frontiers in Oncology

TYPE Case Report
PUBLISHED 21 February 2023
DOI 10.3389/fonc.2023.1092044

OPEN ACCESS

EDITED BY
Antonio Bottari,
Università degli Studi di Messina, Italy

REVIEWED BY
Mikel Gorostidi,
University of the Basque Country, Spain
Elisa Piovano,
AOU Città della Salute e della Scienza di Torino - Presidio Sant'Anna - Obstetrics and Gynecology Unit n 3, Italy

*CORRESPONDENCE
Daniela Fischerova
daniela.fischerova@vfn.cz

SPECIALTY SECTION
This article was submitted to Cancer Imaging and Image-directed Interventions, a section of the journal Frontiers in Oncology

RECEIVED 07 November 2022
ACCEPTED 20 January 2023
PUBLISHED 21 February 2023

CITATION
Fischerova D, Scovazzi U, Sousa N, Hovhannisyan T, Burgetova A, Dundr P, Němejcová K, Bennett R, Vočka M, Frühauf F, Kocian R, Indrielle-Kelly T and Cibula D (2023) Primary retroperitoneal nodal endometrioid carcinoma associated with Lynch syndrome: A case report. *Front. Oncol.* 13:1092044. doi: 10.3389/fonc.2023.1092044

Primary retroperitoneal nodal endometrioid carcinoma associated with Lynch syndrome: A case report

Daniela Fischerova[1*], Umberto Scovazzi[2], Natacha Sousa[3], Tatevik Hovhannisyan[4], Andrea Burgetova[5], Pavel Dundr[6], Kristýna Němejcová[6], Rosalie Bennett[6], Michal Vočka[7], Filip Frühauf[1], Roman Kocian[1], Tereza Indrielle-Kelly[8] and David Cibula[1]

[1]Department of Obstetrics and Gynecology, First Faculty of Medicine, Charles University and General University Hospital in Prague, Prague, Czechia, [2]Department of Gynecology and Obstetrics, Ospedale Policlinico San Martino and University of Genoa, Genova, Italy, [3]Department of Gynecology and Obstetrics, Hospital de Braga, Braga, Portugal, [4]Department of Gynecology and Gynecologic Oncology, Nairi Medical Center (MC), Yerevan, Armenia, [5]Department of Radiology, First Faculty of Medicine, Charles University and General University Hospital in Prague, Prague, Czechia, [6]Department of Pathology, First Faculty of Medicine, Charles University and General University Hospital in Prague, Prague, Czechia, [7]Department of Oncology, First Faculty of Medicine, Charles University, Prague, Czechia, [8]Department of Obstetrics and Gynecology, Burton Hospitals National Health System (NHS), West Midlands, United Kingdom

We report a rare case of primary nodal, poorly differentiated endometrioid carcinoma associated with Lynch syndrome. A 29-year-old female patient was referred by her general gynecologist for further imaging with suspected right-sided ovarian endometrioid cyst. Ultrasound examination by an expert gynecological sonographer at tertiary center revealed unremarkable findings in the abdomen and pelvis apart from three iliac lymph nodes showing signs of malignant infiltration in the right obturator fossa and two lesions in the 4b segment of the liver. During the same appointment ultrasound guided tru-cut biopsy was performed to differentiate hematological malignancy from carcinomatous lymph node infiltration. Based on the histological findings of endometrioid carcinoma from lymph node biopsy, primary debulking surgery including hysterectomy and salpingo-oophorectomy was performed. Endometrioid carcinoma was confirmed only in the three lymph nodes suspected on the expert scan and primary nodal origin of endometroid carcinoma developed from ectopic Müllerian tissue was considered. As a part of the pathological examination immunohistochemistry analysis for mismatch repair protein (MMR) expression was done. The findings of deficient mismatch repair proteins (dMMR) led to additional genetic testing, which revealed deletion of the entire EPCAM gene up to exon 1-8 of the MSH2 gene. This was unexpected considering her insignificant family history of cancer. We discuss the diagnostic work-up for patients presenting with metastatic lymph node infiltration by cancer of unknown primary and possible reasons for malignant lymph node transformation associated with Lynch syndrome.

KEYWORDS

Lynch syndrome, hereditary nonpolyposis, ultrasonography, biopsy, adenocarcinoma, lymph nodes, genetic testing, immunohistochemistry

1 Introduction

Patients with malignant infiltration of lymph nodes and negative history of malignancy represent a diagnostic challenge. The infiltration of lymph nodes can be related to metastases of cancer of unknown primary site (CUP) (1), lymphoproliferation (2), melanomas (3, 4), and others. There are also rare cases of carcinomas arising primarily from lymph nodes, associated with malignant transformation of ectopic epithelial tissue, such as carcinoma arising in endosalpingeosis (5).

CUP accounts for approximately 3–5% of all malignant neoplasms (6). It represents a heterogeneous group of metastatic tumors for which no primary site is detected following a full diagnostic work-up and in 30% of all CUP patients even at autopsy (6). More than 50% of CUP patients present with multiple sites of involvement, and the single site CUP are most commonly in the liver, lymph nodes, peritoneum, lungs, bones, and brain (6). Although iliac lymph node metastases are usually related to gynecological cancers (uterine cervix, endometrium, the tubes, and ovaries) or colorectal cancer, their involvement with unknown primary cancer in women is rare (7).

There are recommendations available regarding the diagnosis, treatment, and follow-up of CUP (8, 9). Primary tumor can be anticipated based on the regional drainage of the infiltrated lymph node(s). Obtaining histology from the infiltrated lymph nodes using tru-cut biopsy or fine-needle aspiration (FNA) can be done under ultrasound guidance. These initial steps help direct search for primary tumor and choose appropriate treatment strategy (7, 10–14). The recommended whole-body imaging for targeted search for primary source of tumor dissemination is positron emission tomography combined with computed tomography (PET-CT) or whole-body diffusion-weighted magnetic resonance imaging (15, 16). The addition of a more extended tumor marker profile can also be considered (16).

Less likely, *de novo* primary nodal malignant transformation has been reported in literature associated with malignant transformation of ectopic epithelial tissue, such as serous carcinoma arising in endosalpingeosis, for example, a case of a serous borderline tumor or a high-grade serous carcinoma within an inguinal lymph node without known primary tumor (17, 18).

The occurrence of carcinoma in younger patients can be associated with hereditary syndromes characterized by germline mutation with higher risk of cancer development. A possible source of endometrioid carcinoma, which can be associated with Lynch or Cowden syndrome, can be the uterus or ovary, or endometriosis in any localization (19). Hereditary breast and ovarian cancer (HBOC) syndrome is associated with no or low risk of endometrial cancer, however, of different histotype, mainly endometrial serous carcinoma (20, 21). Lynch syndrome is an autosomal dominant disorder caused by a germline mutation in one of several DNA mismatch repair (MMR) genes (mostly *MSH2*, *MLH1*, *MSH6*, and *PMS2*), and it is not only the most common cause of inherited colorectal cancer but it also accounts for approximately 3% of endometrial cancer (mainly endometrioid carcinoma often located in the lower uterine segment) (22–25). Atypical manifestations related to Lynch syndrome were also described in literature, as Lynch syndrome–associated squamous cell CUP in retroperitoneal lymph node (26) and primary peritoneal endometrioid carcinoma after prophylactic gynecological surgery (27). There was also a case of an incidental endometrioid carcinoma of unknown primary isolated in the external iliac lymph nodes at risk reducing hysterectomy and bilateral salpingo-oophorectomy in a Lynch syndrome carrier with no history other than previous hyperplastic polyp (28).

We describe a rare case of a 29-year-old female patient presenting with infiltrated lymph nodes in the right obturator fossa with no visible primary source.

2 Case summary

A 29-year-old patient was referred for an expert ultrasound examination to gynecologic oncology center for hypoechogenic round lesion, presumed endometrioma. The patient did not have any symptoms suggestive of endometriosis. Apart from two Caesarean sections and tonsillectomy, her surgical history was unremarkable. She suffered from multiple sclerosis treated with immunosuppressive therapy (Interferon β) and bicuspid aortal valve. Her grandmother died the aged of 50 of pancreatic cancer, and her great grandfather succumbed to colorectal cancer at unknown age.

Ultrasound examination performed at gynecologic oncology center by experienced sonographer revealed normal gynecologic findings of the uterus and adnexa, smooth peritoneum, small amount of free fluid, and neither adhesions in the pelvis nor other signs related to endometriosis (Figure 1). Lateral to the right ovary, there were three bulky lymph nodes detected in the right obturator fossa, which were misinterpreted by the referring physician as endometrioma (Figure 2 and Videoclip 1). Systematic ultrasound examination of pelvic and abdominal lymph nodes revealed no other suspicious lymph nodes in the retroperitoneum or groins. Expert sonographer detected two inhomogeneous lesions of 24 and 25 mm in the segment 4b of liver parenchyma, considered to be metastatic spread on gray scale ultrasound (Supplementary Figure S1 and Videoclip 2). During the same visit, ultrasound-guided tru-cut biopsy of infiltrated lymph nodes was performed. To briefly describe ultrasound-guided tru-cut biopsy using a transvaginal approach, no patient preparation, fasting, or routine administration of analgesics or antibiotics is required for this minimally invasive approach in the outpatient setting (Supplementary Figure S2 and Videoclip 3). The entire procedure is performed with the patient in the lithotomy position. The sonographer selects a safe site for biopsy from a lesion that is not necrotic or cystic, so that an adequate sample can be obtained for histologic analysis and immunohistochemical evaluation. After ruling out possible contraindications (in particular the use of anticoagulant drugs) and to ensure the safety of the procedure, a needle guide attached to the probe is used; a disposable needle (30 cm/18 Gauge) is inserted into the automated biopsy device, then the needle is inserted into the needle guide and the needle tip is inserted through the vaginal wall into the pelvis in close proximity to the infiltrating lymph nodes and aligned with the lesion.

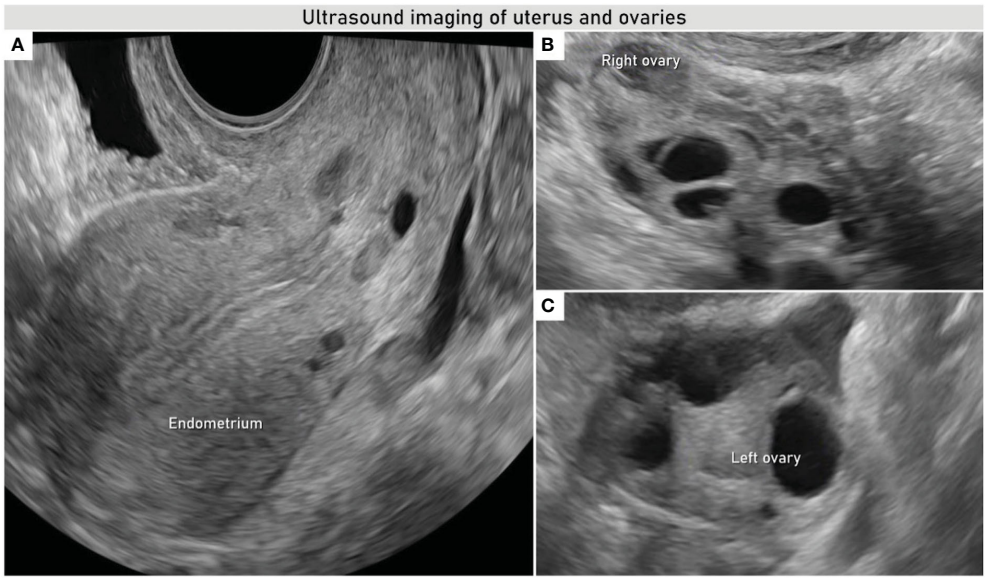

FIGURE 1
Transvaginal ultrasound evaluation of uterus and adnexa. Uniform endometrium **(A)** and right and left ovaries of normal appearance **(B, C)**.

A penetration depth between 15 and 22 mm is selected, and the procedure is performed with continuous monitoring of patient comfort and needle position on the ultrasound machine monitor. Collection of two to three core samples allows for better adequacy and accuracy of histological analysis. The procedure takes several minutes. After biopsy, the biopsy site is checked for internal bleeding ("fountain sign"), and the intensity of the external per vaginal bleeding is checked. The patient is instructed and discharged home. The result of the histopathological examination is available within 72h (7, 10, 12).

In addition to the collection of the biopsy, a tumor marker profile was obtained during the same appointment and additional imaging tests were scheduled. Tumor marker profile included cancer antigen 125 (CA 125), carcinoembryonic antigen (CEA), cancer antigen 19-9 (CA 19-9), cancer antigen 15-3 (CA 15-3), and cytokeratine fraction 21-1 (CYFRA 21-1).The PET-CT was chosen for targeted search of

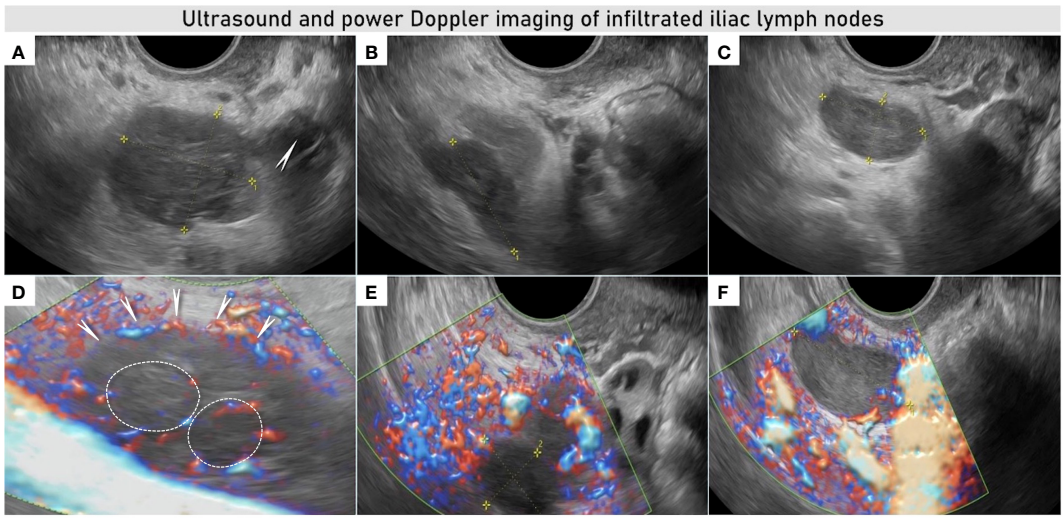

FIGURE 2
Ultrasound and power Doppler imaging of infiltrated lymph nodes in the right obturator fossa. Transvaginal ultrasound imaging demonstrates three bulky lymph nodes: first iliac lymph node (29 × 26 × 31 mm) infiltrated by tumor nodules located in the close proximity to the right ovary (arrow) **(A)** with visible transcapsular vessels penetrating the lymph node from the outside (arrows) and ring-shaped vessels marked with white circles **(D)**. Second iliac lymph node (25 × 13 × 21 mm) was lateral to the first one, infiltrating the pelvic side wall and internal iliac vessels up to the interiliac bifurcation with infiltration of the external iliac vein **(B)**, this lymph node was less vascularized on color Doppler images **(E)**. Third infiltrated node (26 × 13 × 30 mm) was located deeper in the pelvis, near the right lateral parametrium **(C)**, with transcapsular vessels on color Doppler image **(F)** See also Videoclip 1.

primary tumor. Magnetic resonance imaging of the liver was added for closer characterization of liver lesions and their potential resectability.

Results were presented to the multidisciplinary team. Tumor markers CA 125, CEA, CA 19-9, CA15-3, and CYFRA 21-1 were in normal range. The PET-CT showed metabolic accumulation of 18F-fluorodeoxyglucose (18F-FDG) in the right obturator fossa (Figure 3) but no other metabolically active lesions in the body including the liver (Supplementary Figure S1). On MRI, the liver lesions showed enhancement in the early stage with persistence to late stage suggesting the lesions to be more likely adenoma or focal nodular hyperplasia (Supplementary Figure S1). Tru-cut biopsy revealed a poorly differentiated tumor composed of solid sheets of polygonal eosinophilic cells with marked nuclear pleomorphism, conspicuous mitotic activity, and necrotic areas (Supplementary Figure S3).

Immunohistochemically, the tumor cells showed positive expression of PAX8 and CK7, loss of expression of PTEN, ARID1A, and p53 wild-type expression. This immunoprofile suggested Müllerian differentiation favoring endometrioid or clear cell carcinoma, since loss of PTEN and ARID1A is found in 40 and 50% of these cases (29). The markers used for distinction between endometrioid and clear cell carcinoma showed ambiguous results. HNF1β was mostly weakly to moderately positive (strong positivity is more typical for clear cell carcinomas). In Supplementary Figure S4, positive expression of CK7 and HNF1β were demonstrated. Napsin A, which is used as another marker of clear cell carcinoma with intermediate sensitivity, was negative. On the other hand, ER and PR were negative, which favor a diagnosis of clear cell carcinoma (30). In addition, WT1 showed negativity as a marker used to rule out the derivation from adnexal serous carcinoma. The morphology and immunophenotype of the tumor were not quite characteristic for either clear cell or endometroid carcinoma. However, due to the immunohistochemical findings, the first differential diagnosis was poorly differentiated endometrioid carcinoma and second possibility was eosinophilic variant of clear cell carcinoma. Due to the absence of primary origin of invasive carcinoma on the imaging (including PET-CT), we considered either a primarily nodal tumour arising from endometriosis or occult spread from another source (e.g. from the endometrium or ovary).

Since the patient's reproductive plan was complete and the possibility of fertility preservation was not considered, the treatment plan would not have differed if additional biopsy specimens, such as endometrial biopsy, had been performed before definitive surgery. Surgical treatment including hysterectomy and bilateral salpingo-oophorectomy with extirpation of the infiltrating lymph nodes and systemic dissection of the pelvic and paraaortic lymph nodes was chosen.

Intraoperative assessment revealed no suspicious findings except the enlarged lymph nodes in the right obturator fossa. These were infiltrating the right pelvic side wall, including right internal iliac vessels and partially external iliac right vein, psoas muscle as well as S2–S3 rami of the lumbosacral plexus. The extent of the infiltration was not evident in any preoperative imaging assessment. Therefore, the senior surgeon was requested to join the intervention, and a laterally extended endopelvic resection was performed on the right side, including resection of the internal iliac vein, partial resection of the external iliac vein, psoas muscle, periostium of the pubic bone, and S2–S3 rami (divisions) of the lumbosacral plexus. Total abdominal hysterectomy with bilateral salpingoophorectomy, pelvic, and paraaortic lymph node dissection were carried out with no visible residual tumor left at the end of surgery.

Histological evaluation of the final specimen from the uterus and adnexa did not reveal any cancer, and all 36 lymph nodes removed during the dissection did not show malignant cells. The three infiltrated lymph nodes in the right obturator fossa were confirmed

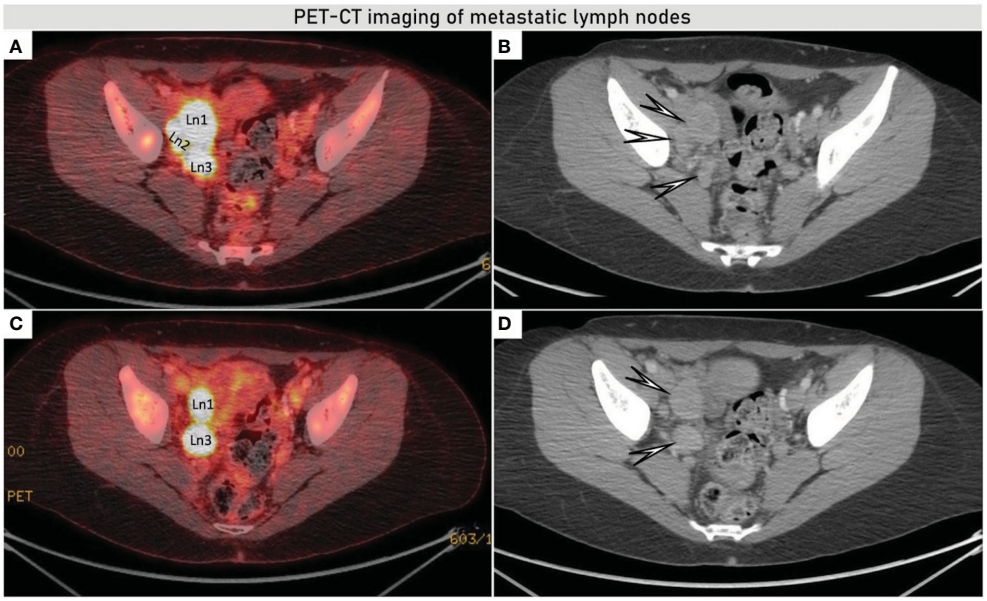

FIGURE 3
Axial fused PET-CT showed increased accumulation of 18F-FDG in the bulky iliac lymph nodes on the right obturator fossa of up to 36 × 25 mm **(A, C)**, morphologic images from CECT demonstrating enlarged nodes in the right obturator fossa (white arrows) **(B, D)**. PET-CT (positron emission tomography combined with computed tomography), CECT (contrast enhanced computed tomography), and 18F-FDG (18F- fluorodeoxyglucose).

to have extensive involvement by poorly differentiated cancer (Figure 4) with loss of MSH2 and MSH6 protein expression. There were no signs of endometriosis in the affected lymph nodes (e.g., neither hemosiderin nor signs of active bleeding).

Based on the finding of deficient mismatch repair proteins (dMMR), which is indicative of genetic disorders and Lynch syndrome in particular (31), genetic testing was recommended. This revealed an inherited deletion of the entire *EPCAM* gene up to exon 1-8 of the *MSH2* gene corresponding to Lynch syndrome. Patient underwent adjuvant combined chemotherapy consisting of paclitaxel and carboplatin (six cycles). As expected, after the resection of the right iliac veins, the patient developed transient lymphoedema of the right leg, which resolved spontaneously within a few weeks. No neurological sequelae were reported, as the integrity of the ventral part of the lumbosacral plexus was preserved. For the first 5 years, follow-up is planned to be in our gynecological oncology center with physical examination and pelvic and abdominal ultrasound imaging (controls every 3 months for the first 2 years; every 4 months in the third year; every 6 months for the fourth and fifth years). After the fifth year, yearly controls with a general gynecologist based on the patients individual surveillance plan. In addition, patient surveillance for lifetime risk of Lynch syndrome-associated colorectal cancer (30-73%) and gastric cancer (up to 18%) will be provided at a specialised centre for hereditary cancer syndromes, including annual colonoscopy and gastroduodenoscopy every 3 years (32).

Informed consent was obtained from the patient for publication of this article.

3 Discussion

This is the first case of nodal malignancy without evident gynecological or relevant medical history, documenting a young patient journey from the incidental finding of enlarged lymph nodes in the right obturator fossa to the diagnosis of a primary nodal, poorly differentiated endometrioid carcinoma after extensive diagnostic work-up and surgery. Patient is in complete clinical remission after 36 months postoperatively (Supplementary Figure 5).

In the diagnostic approach to lymphadenopathy, a vast array of diseases and drugs ought to be considered. The prevalence of nodal malignancy is approximately 0.4% in young population and 4% in adults (33). The region of the metastatic lymph nodes and its area of drainage can often be used to guide us toward a potential location of the pathology. Current evidence on evaluation and differential diagnosis of metastatic lymph nodes recommends a thorough medical history and physical examination as well as systematic work-up including biopsy of the most suspicious lymph node/-s, tumor marker profile, imaging, and other tests as appropriate (33). In this case, the young female patient had no relevant medical history besides multiple sclerosis treated with interferon-β. Her family history showed insignificant oncologic risk and her physical examination was unremarkable.

Ultrasound imaging offers high resolution of the pelvis with the endovaginal probe, permitting above else a meticulous scanning of the pelvic lymph node morphological and vascular architecture. This allows an accurate differentiation between benign and malignant transformations of lymph nodes with the possibility to perform ultrasound-guided biopsy (7, 10, 11). The Vulvar International Tumor Analysis (VITA) consensus opinion provides a guide for standardized assessment and description of lymph nodes using ultrasound (34). In this case, the expert sonographer identified three enlarged lymph nodes in the right obturator fossa with sonographic features of malignant changes such as subcapsular such as subcapsular tumor nodules contrasting against the residual non-infiltrated lymphoid tissue. The color Doppler demonstrated ring-shaped vessels around the subcapsular tumor nodules as well as transcapsular flow (Figures 2, 4 and Videoclips 1, 4). In addition, two suspicious intraparenchymal liver lesions were described on the ultrasound (Supplementary Figure S1 and Videoclip 2). An alternative technique to evaluate lymph node is PET-CT, which provides not only metabolic information but also a systemic staging. PET-CT confirmed the ultrasound findings showing high metabolism rate in the pelvic nodes but no enhanced metabolic activity in the hepatic lesions neither showed a possible primary tumor site.

To differentiate lymphoproliferative disease from secondary cancer metastases and to direct us to the possible primary source, tru-cut biopsy was performed, enabling a histologic diagnosis with high accuracy. In this case, poorly differentiated carcinoma was found in the lymph nodes with immunoprofile, suggesting endometrioid carcinoma differentiation. After an extensive histological examination of the specimen from hysterectomy and bilateral salpingo-oophorectomy, the primary source of tumor spread from uterus or adnexa was excluded and only nodal infiltration by endometrioid carcinoma was confirmed. Due to the result of histopathology and the young age, we have included MMR analysis to exclude Lynch syndrome. In tumor cells MLH1, PMS2 expression was retained in nuclei whereas MSH2 and MSH6 expression was lost, suggesting microsatellite instability (MSI, dMMR). These findings were highly suspicious of Lynch syndrome. Genetic testing was performed, which confirmed patient was a Lynch syndrome carrier of *EPCAM* gene deletion up to exon 1-8 of the *MSH2* gene. Lynch syndrome is inherited *via* a pathogenic germline variant in one of the four mismatch repair (MMR) genes *MLH1*, *MSH2*, *MSH6*, and *PMS2*. A second somatic hit affecting the remaining functional allele of the same MMR gene leads to DNA MMR deficiency. Thus, MMR deficiency is a major driving force in Lynch syndrome carcinogenesis.

Given the negative findings from hysterectomy and bilateral salpingo-oophorectomy, we considered primary malignant transformation of ectopic Müllerian tissue inside the lymph node. Regarding primary nodal malignant infiltration, to our knowledge, there are only a few case reports of Lynch syndrome–associated carcinoma with retroperitoneal lymph node infiltration (26, 28). Most similar case was reported by Koual et al. (28) on a 50-year-old patient with Lynch syndrome with previous history of a hyperplastic polyp who underwent prophylactic hysterectomy and bilateral salpingo-oophorectomy. During the surgery a nodule in the broad ligament was excised, revealing a nodal endometrioid adenocarcinoma within the pelvic lymph nodes, with no evident primary tumor (28).

Our case report represents the first case of nodal malignancy without evident gynecological pathology even after extensive work-up and with no possible link in the past history, unlike the Koual's case where the endometrial hyperplasia may have caused a possible spillage or spread of undetected malignant cells in the lymph nodes.

10.3389/fonc.2023.1092044

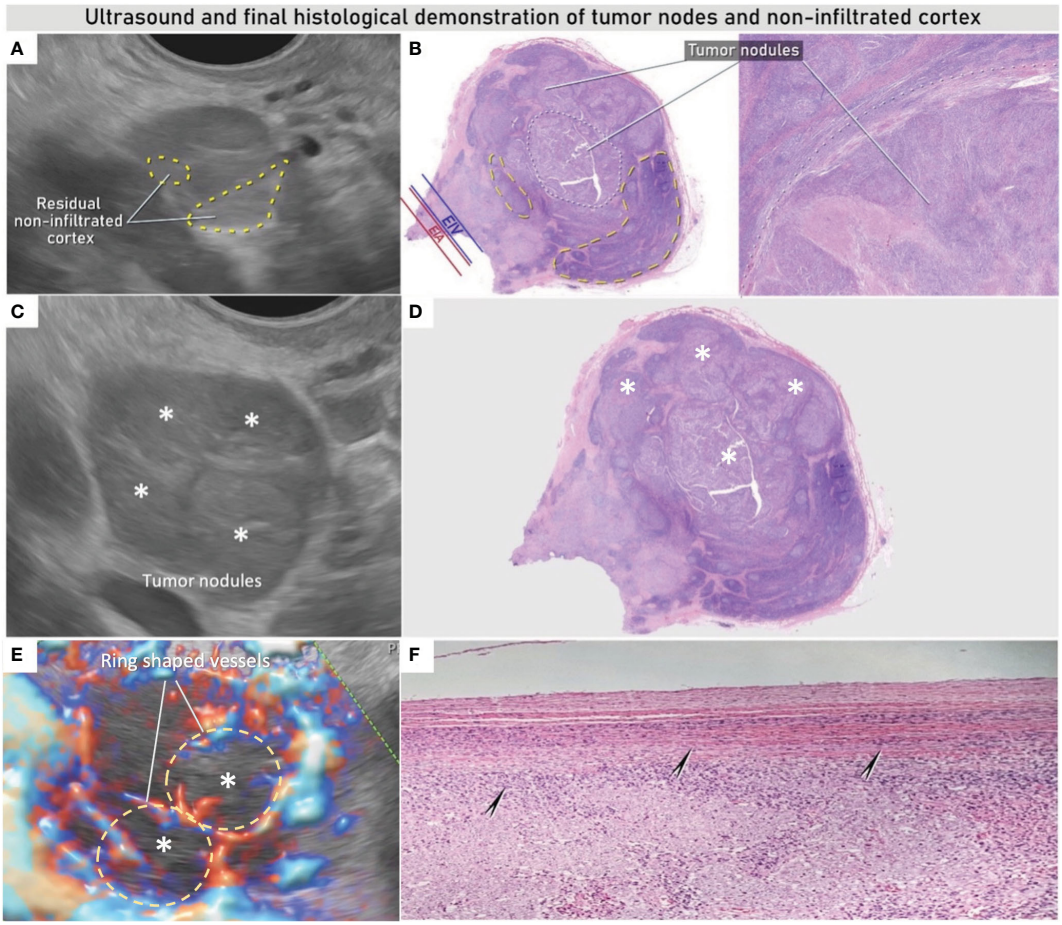

FIGURE 4
Ultrasound and final histological demonstration of infiltrated lymph node. Non-infiltrated residual cortex on the ultrasound and histological imaging of lymph node marked with yellow circles **(A, B)**, with intranodal involvement due to solid sheets of poorly differentiated extensively necrotic carcinoma marked with white circles on specimen **(B)** and white asterisks on ultrasound images **(C, E)** and on the specimen **(D)**; on Power Doppler imaging infiltrated nodules reveal a ring-shaped vascularization (yellow circles) in **(E)**; arrows indicate intact lymph node capsule **(F)**. See also Videoclip 4.

Our case is also unique compared with the published literature in regard to the patient's young age, absence of uterine abnormality, and the absence of a suspicious family history. We can hypothesize that the most likely origin was a primary infiltration from ectopic epithelial Müllerian tissue, which underwent malignant transformation. This could have happened by a possible spillage of endometrial tissue during the previous C-section or by the spread of occult endometriosis/endosalpingiosis reaching the hilum of the lymph nodes and/or the afferent lymphatic vessels. In this presented case, immunosuppression, due to inferferon-β therapy combined with genetic genotype, may have also amplified the cancerogenic cascade.

4 Conclusions

This is a rare case of a primary nodal poorly differentiated endometrioid carcinoma associated with Lynch syndrome. Ultrasound guided tru-cut biopsy of the suspected lymph node is essential for planning appropriate management. Immunohistochemical evaluation of MMR protein expression may help to detect Lynch syndrome-associated endometrioid carcinoma, allowing regular surveillance and immune checkpoint-based treatment options.

Data availability statement

The original contributions presented in the study are included in the article/Supplementary Material. Further inquiries can be directed to the corresponding author.

Ethics statement

Written informed consent was obtained from the individual(s) for the publication of any potentially identifiable images or data included in this article.

Author contributions

DF: diagnosis and monitoring of the case, preparation of images and videos, writing and finalizing of the article. US: preparation of videos, graphics, writing and finalizing the article. NS: preparation of videos, graphics, writing and finalizing the article. TH: drafting the manuscript. AB: preparation of the article, especially the part focused on cross-section imaging, preparation of MRI images, PET-CT. RB: pathological evaluation of tru-cut biopsy, preparation of images. PD: pathological 2nd expert review of all specimens, writing the article. KN: pathological evaluation of definitive specimen and writing the article. MV: oncological geneticist performing Lynch syndrome examination and writing the article. FF: gynecological oncologist performing the tru-cut biopsy under ultrasound control. RK: gynecological oncologist performing radical surgery. DC: gynecological oncologist performing radical surgery. TI-K: writing of the article, proofreading in English. All authors contributed to the article and approved the submitted version.

Funding

This work was supported by the Ministry of Health of the Czech Republic (NU21-03-00461).

Acknowledgments

Thanks to Ladislav Tejml for providing microscopic photo documentation (Institute of Pathology, First Faculty of Medicine, Charles University Prague, Czech Republic), Adam Preisler for providing the illustrations (Polygoniq studio) and to Tomas Herrmann for video editing (the Institute of Scientific Information, First Faculty of Medicine, Charles University Prague, Czech Republic).

Conflict of interest

The authors declare that the research was conducted in the absence of any commercial or financial relationships that could be construed as a potential conflict of interest.

Publisher's note

Supplementary material

The Supplementary Material for this article can be found online at: https://www.frontiersin.org/articles/10.3389/fonc.2023.1092044/full#supplementary-material

SUPPLEMENTARY FIGURE 1
Hepatic focal lesions. Ultrasound imaging demonstrates two inhomogeneous mostly hyperechoic lesions of 25 mm in the S4b segment of liver **(A)**; CECT shows hyperdense formation up to 25 mm in the S4b (arrow) without increased accumulation of 18F-FDG **(B)**; on MRI T2 weighted images with fat saturation, the lesions showed slightly hypointense deposits (arrow) **(C)**; and on the dynamic contrast sequence T1 weighted images with fat saturation, the lesions showed dynamic contrast enhancement in early and late phases (arrows) **(D)**. CECT (contrast enhanced computed tomography), 18F-FDG (18F-fluorodeoxyglucose), and MRI (magnetic resonance imaging). Ultrasound findings are also presented in Videoclip 2.

SUPPLEMENTARY FIGURE 2
Transvaginal tru-cut biopsy technique. In this case the needle penetration depth on the automated biopsy gun was chosen to be 15 mm due to the proximity of the large vessels **(A)**, the biopsy needle is inserted into a needle guide placed on the transvaginal probe; the guide fixes and determines the possible movement of the needle **(B)**; the stylet and cannula move automatically during the biopsy to avoid fragmentation of the sample; the end of the stylet penetrates the tissue, immediately behind it, there is a notch for biopsy sample collection, which is cut through the cannula **(C)**; the tip of the biopsy needle penetrating the target lesion is monitored on an ultrasound monitor during the biopsy **(D)**; and an 18G needle with a length of 30 cm was chosen for the transvaginal approach **(E)**. See also Videoclip 3.

SUPPLEMENTARY FIGURE 3
Morphological assessment of tru-cut biopsy sample. Non-fragmented core obtained from tru-cut biopsy (length 15 mm, width after fixation 1.2 mm) **(A)**, solid sheets of polygonal eosinophilic cells **(B)**.

SUPPLEMENTARY FIGURE 4
Immunoprofile of the tru-cut biopsy sample showed immunohistochemical positivity of cytokeratin 7 (CK7) **(A)** and of hepatocyte nuclear factor 1-beta (HNF1β) **(B)**.

SUPPLEMENTARY FIGURE 5
Timeline reporting the patient's journey from diagnosis to final diagnosis, treatment, and follow-up.

SUPPLEMENTARY VIDEO 1
Three bulky infiltrated lymph nodes can be identified in the right obturator fossa. In the first lymph node, a transcapsular flow and ring-shaped vessels can be seen with color Doppler imaging.

SUPPLEMENTARY VIDEO 2
Ultrasound imaging showing hepatic focal lesions: Two inhomogeneous mostly hyperechoic lesions of 25 mm can be identified in the S4b segment of liver.

SUPPLEMENTARY VIDEO 3
With real-time ultrasound monitoring, the needle tip can be seen to penetrate the target lesion and collect the biopsy as a hyperechogenic line. A total of three samples were taken.

SUPPLEMENTARY VIDEO 4
Ultrasound imaging and histopathology showing residual non-infiltrated lymph node cortex (dashed yellow circles). The yellow filled circles on the ultrasound image and the arrows on the histopathology image show nodular tumor changes within the lymph node; in addition, the white dashed circle in the middle of specimen indicates necrotic changes within the tumor nodule.

References

1. Pavlidis N, Pentheroudakis G. Cancer of unknown primary site. *Lancet (London England)* (2012) 379(9824):1428–35. doi: 10.1016/s0140-6736(11)61178-1

2. Justiz Vaillant AA, Stang CM. *Lymphoproliferative disorders*. StatPearls. Treasure Island (FL: StatPearls Publishing LLC (2021).

3. Tchernev G, Chokoeva A, Popova LV. Primary solitary melanoma of the lymphatic nodes or a single metastasis of unknown melanoma: Do we need a new staging system? *Open Access Maced J Med Sci* (2017) 5(7):970–3. doi: 10.3889/oamjms.2017.222

4. Cormier JN, Xing Y, Feng L, Huang X, Davidson L, Gershenwald JE, et al. Metastatic melanoma to lymph nodes in patients with unknown primary sites. *Cancer* (2006) 106 (9):2012–20. doi: 10.1002/cncr.21835

5. Sah S, Fulmali R, McCluggage WG. Low-grade serous carcinoma arising in inguinal nodal endosalpingiosis: Report of 2 cases and literature review. *Int J Gynecol Pathol* (2020) 39(3):273–8. doi: 10.1097/PGP.0000000000000613

6. Hillen HF. Unknown primary tumours. *Postgraduate Med J* (2000) 76(901):690–3. doi: 10.1136/pmj.76.901.690

7. Zikan M, Fischerova D, Pinkavova I, Dundr P, Cibula D. Ultrasound-guided tru-cut biopsy of abdominal and pelvic tumors in gynecology. *Ultrasound Obstet Gynecol.* (2010) 36(6):767–72. doi: 10.1002/uog.8803

8. National Institute for Health and Care Excellence: Guidelines. *Diagnosis and management of metastatic malignant disease of unknown primary origin*. Cardiff (UK: National Collaborating Centre for Cancer (UK) Copyright © 2010, National Collaborating Centre for Cancer (2010).

9. Fizazi K, Greco FA, Pavlidis N, Daugaard G, Oien K, Pentheroudakis G. Cancers of unknown primary site: ESMO clinical practice guidelines for diagnosis, treatment and follow-up. *Ann Oncol* (2015) 26(Suppl 5):v133–8. doi: 10.1093/annonc/mdv305

10. Fischerova D, Cibula D, Dundr P, Zikan M, Calda P, Freitag P, et al. Ultrasound-guided tru-cut biopsy in the management of advanced abdomino-pelvic tumors. *Int J Gynecol Cancer.* (2008) 18(4):833–7. doi: 10.1111/j.1525-1438.2007.01015.x

11. Epstein E, Van Calster B, Timmerman D, Nikman S. Subjective ultrasound assessment, the ADNEX model and ultrasound-guided tru-cut biopsy to differentiate disseminated primary ovarian cancer from metastatic non-ovarian cancer. *Ultrasound Obstet Gynecol.* (2016) 47(1):110–6. doi: 10.1002/uog.14892

12. Mascilini F, Quagliozzi L, Moro F, Moruzzi MC, De Blasis I, Paris V, et al. Role of transvaginal ultrasound-guided biopsy in gynecology. *Int J Gynecol Cancer.* (2020) 30 (1):128–32. doi: 10.1136/ijgc-2019-000734

13. Verschuere H, Froyman W, Van den Bosch T, Van Hoefs M, Kaijser J, Van Schoubroeck D, et al. Safety and efficiency of performing transvaginal ultrasound-guided tru-cut biopsy for pelvic masses. *Gynecol Oncol* (2021) 161(3):845–51. doi: 10.1016/j.ygyno.2021.03.026

14. Arezzo F, Loizzi V, La Forgia D, Abdulwakil Kawosha A, Silvestris E, Cataldo V, et al. The role of ultrasound guided sampling procedures in the diagnosis of pelvic masses: A narrative review of the literature. *Diagnostics* (2021) (Basel Switzerland) 11(12):2204. doi: 10.3390/diagnostics11122204

15. Rades D, Kuhnel G, Wildfang I, Borner AR, Schmoll HJ, Knapp W. Localised disease in cancer of unknown primary (CUP): The value of positron emission tomography (PET) for individual therapeutic management. *Ann Oncol* (2001) 12 (11):1605–9. doi: 10.1023/a:1013107732572

16. Timmerman D, Planchamp F, Bourne T, Landolfo C, du Bois A, Chiva L, et al. ESGO/ISUOG/IOTA/ESGE consensus statements on the pre-operative diagnosis of ovarian tumours. *Ultrasound Obstet Gynecol* (2021) 58:148–68. doi: 10.1002/uog.23635

17. Carrabin N, Treilleux I, Meeus P, Tredan O, Ray-Coquard I. Primary ovarian borderline tumor in the inguinal lymph node. *Int J Gynecol Pathol* (2013) 32(2):167–70. doi: 10.1097/PGP.0b013e318257def6

18. Restaino S, Mauro J, Zermano S, Pellecchia G, Mariuzzi L, Orsaria M, et al. CUP-syndrome: Inguinal high grade serous ovarian carcinoma lymph node metastases with unknown primary origin - a case report and literature review. *Front Oncol* (2022) 12:987169. doi: 10.3389/fonc.2022.987169

19. Sessa C, Balmana J, Bober SL, Cardoso MJ, Colombo N, Curigliano G, et al. Risk reduction and screening of cancer in hereditary breast-ovarian cancer syndromes: ESMO Clinical Practice Guideline. *Ann Oncol.* (2023) 34(1):33–47.

20. Shu CA, Pike MC, Jotwani AR, Friebel TM, Soslow RA, Levine DA, et al. Uterine cancer after risk-reducing salpingo-oophorectomy without hysterectomy in women with BRCA mutations. *JAMA Oncol* (2016) 2(11):1434–40. doi: 10.1001/jamaoncol.2016.1820

21. de Jonge MM, de Kroon CD, Jenner DJ, Oosting J, de Hullu JA, Mourits MJE, et al. Endometrial cancer risk in women with germline BRCA1 or BRCA2 mutations: Multicenter cohort study. *J Natl Cancer Inst* (2021) 113(9):1203–11. doi: 10.1093/jnci/djab036

22. Moreira L, Balaguer F, Lindor N, de la Chapelle A, Hampel H, Aaltonen LA, et al. Identification of lynch syndrome among patients with colorectal cancer. *Jama* (2012) 308 (15):1555–65. doi: 10.1001/jama.2012.13088

23. Downes MR, Allo G, McCluggage WG, Sy K, Ferguson SE, Aronson M, et al. Review of findings in prophylactic gynaecological specimens in lynch syndrome with literature review and recommendations for grossing. *Histopathology* (2014) 65(2):228–39. doi: 10.1111/his.12386

24. Helder-Woolderink JM, Blok EA, Vasen HF, Hollema H, Mourits MJ, De Bock GH. Ovarian cancer in lynch syndrome: A systematic review. *Eur J Cancer.* (2016) 55:65–73. doi: 10.1016/j.ejca.2015.12.005

25. Bonadona V, Bonaïti B, Olschwang S, Grandjouan S, Huiart L, Longy M, et al. Cancer risks associated with germline mutations in MLH1, MSH2, and MSH6 genes in lynch syndrome. *Jama* (2011) 305(22):2304–10. doi: 10.1001/jama.2011.743

26. Jones NC, Adashek JJ, Ayoub B. Carcinoma of unknown primary in a patient with lynch syndrome. *Cureus* (2021) 13(6):e15690. doi: 10.7759/cureus.15690

27. Ghezzi F, Uccella S, Cromi A, Bogani G, Donadello N, Riva C. Primary peritoneal cancer in lynch syndrome: A clinical-pathologic report of a case and analysis of the literature. *Int J Gynecol Pathol* (2013) 32(2):163–6. doi: 10.1097/PGP.0b013e31825ac5c9

28. Koual M, Benoit L, Pacelli J, Lefrère Belda MA, Azaïs H, Bats AS. Discovery of an endometrioid cancer lymph node metastasis without primary tumor in a context of lynch syndrome. *J Gynecol Obstet Hum Reprod* (2021) 50(3):102060. doi: 10.1016/j.jogoh.2021.102060

29. Murali R, Davidson B, Fadare O, Carlson JA, Crum CP, Gilks CB, et al. High-grade endometrial carcinomas: Morphologic and immunohistochemical features, diagnostic challenges and recommendations. *Int J Gynecol Pathol* (2019) 38 Suppl 1(Iss 1 Suppl 1): S40–s63. doi: 10.1097/pgp.0000000000000491

30. Kobel M, Duggan MA. Napsin a: Another milestone in the subclassification of ovarian carcinoma. *Am J Clin Pathol* (2014) 142(6):735–7. doi: 10.1309/AJCPAVGZKA1A1HVC

31. Richman S. Deficient mismatch repair: Read all about it (Review). *Int J Oncol* (2015) 47(4):1189–202. doi: 10.3892/ijo.2015.3119

32. Stjepanovic N, Moreira L, Carneiro F, Balaguer F, Cervantes A, Balmaña J, et al. Hereditary gastrointestinal cancers: ESMO clinical practice guidelines for diagnosis, treatment and follow-up†. *Ann Oncol* (2019) 30(10):1558–71. doi: 10.1093/annonc/mdz233

33. Gaddey HL, Riegel AM. Unexplained lymphadenopathy: Evaluation and differential diagnosis. *Am Fam Physician.* (2016) 94(11):896–903.

34. Fischerova D, Garganese G, Reina H, Fragomeni SM, Cibula D, Nanka O, et al. Terms, definitions and measurements to describe sonographic features of lymph nodes: consensus opinion from the vulvar international tumor analysis (VITA) group. *Ultrasound Obstet Gynecol.* (2021) 57(6):861–79. doi: 10.1002/uog.23617

frontiers | Frontiers in Oncology

TYPE Case Report
PUBLISHED 05 May 2023
DOI 10.3389/fonc.2023.1027238

OPEN ACCESS

EDITED BY
Consolato M. Sergi,
Children's Hospital of Eastern Ontario (CHEO), Canada

REVIEWED BY
Tudor Lucian Pop,
University of Medicine and Pharmacy Iuliu Hatieganu, Romania
Xuefeng Luo,
Sichuan University, China

*CORRESPONDENCE
Gaoyi Yang
yanggaoyi8@163.com

RECEIVED 27 September 2022
ACCEPTED 20 April 2023
PUBLISHED 05 May 2023

CITATION
Zhang Y, Yu T, Mi Y, Zhang W and Yang G (2023) Case Report: Early detection and intervention of congenital portosystemic shunts in children. *Front. Oncol.* 13:1027238. doi: 10.3389/fonc.2023.1027238

Case Report: Early detection and intervention of congenital portosystemic shunts in children

Ying Zhang[1], Tianzhuo Yu[1], Yanhong Mi[2], Wenzhi Zhang[1] and Gaoyi Yang[1]*

[1]Department of Ultrasound, Hangzhou Red Cross Hospital and Affiliated Hangzhou Chest Hospital, Zhejiang University School of Medicine, Hangzhou, China, [2]Department of Radiology, The Children's Hospital, Zhejiang University School of Medicine, National Clinical Research Center for Child Health, Hangzhou, China

Congenital portosystemic shunts (CPSS) are rare vascular anomalies that cause abnormal communications between the portal and systemic venous systems and may be incidentally detected on imaging or *via* abnormal laboratory parameters due to the lack of specificity in the condition's clinical presentation. Ultrasound (US) is a common tool for examining abdominal solid organs and vessels and is the initial imaging modality for diagnosing CPSS. Here we report the case of an 8-year-old Chinese boy with CPSS diagnosed using color Doppler US. Doppler US first found intrahepatic tumor, then revealed that the left portal vein was directly communicating with the inferior vena cava, and the boy was finally diagnosed with intrahepatic portosystemic shunts. Interventional therapy was employed to occlude the shunt. During the follow-up, the intrahepatic tumor disappeared and no complications. Hence, to be able to differentiate such vascular anomalies, clinicians should be fairly acquainted with the normal ultrasonographic anatomical features in daily clinical work. Furthermore, increased disease awareness and advances in imaging equipment and technology are essential for CPSS diagnosis.

KEYWORDS

child, congenital portosystemic shunts, color Doppler ultrasound, diagnosis, hepatic tumor

1 Introduction

Congenital portosystemic shunts (CPSS) are an abnormal connection between portal veins (PV) and systemic veins, resulting in varying degrees of portal blood flow diversion directed away from the liver to the systemic circulation. It may occur due to incomplete vascular remodeling between the embryonic and fetal hepatic and perihepatic circulations during fetal development (1, 2). The prevalence in neonates is approximately 1 in 30,000–50,000 (3). CPSS may present with various symptoms, including hepatic multiple tumors,

galactosemia, neonatal cholestasis, abnormal liver function, hepatic encephalopathy (HE), among others (3, 4).

Color Doppler ultrasound (US) is the first imaging modality of choice for detecting CPSS and can demonstrate PV waveform, vascular shunts, thrombosis as well as intrahepatic nodules and other related complications (2, 5). Early diagnosis using Doppler US allows the prompt management of potentially life-threatening manifestations, ultimately improving the outcome in these patients (3). This report aimed to describe the case of a patient with CPSS with multiple hepatic tumors diagnosed using color Doppler US in Hangzhou Red Cross Hospital as well as the clinical progress from initial diagnosis to treatment improvement.

2 Case description

An 8-year-old Chinese boy visited our hospital and presented with emaciation without symptoms. He was previously healthy without known medical conditions.

Abdominal US examination revealed multiple hepatic nodules with a maximum size of 4.0 × 3.1 cm (Figure 1A), clear boundary, and non-uniform internal echo, leading to local inferior vena cava (IVC) compression. The following notable findings were reported: the left PV (LPV) directly communicated with IVC (1.2 cm in diameter); color Doppler US confirmed the PV flow toward IVC (Figure 1B), the flow velocity in the shunt was 98 cm/s (Figure 1C), the right PV (RPV) was not shown, and no abnormal echo was observed in IVC; and splenomegaly (2 cm below the ribs). The rest of the abdominal organs showed no abnormal findings, and the abdominal cavity had no effusion. The patient was believed to have ectopic PV drainage (PV communicating with IVC), with unknown nature of multiple nodules. We recommended that the patient should undergo an additional abdominal contrast-enhanced computed tomography (CT) and digital subtraction angiography (DSA) to better understand this anatomic anomaly and clarify the nature of the nodule.

Laboratory tests showed the total bilirubin (TB; 40.6 μmol/L; reference range: 1.7–25.0 μmol/L), direct bilirubin (DB; 13.2 μmol/L; reference range: 0.0–7.1 μmol/L), indirect bilirubin (27.4 μmol/L; reference range: 1.7–19.0 μmol/L), alanine aminotransferase (ALT) (68 U/L; reference range: 3–50 U/L), aspartate aminotransferase (59 U/L; reference range 8–40 U/L), alkaline phosphatase (296 U/L; reference

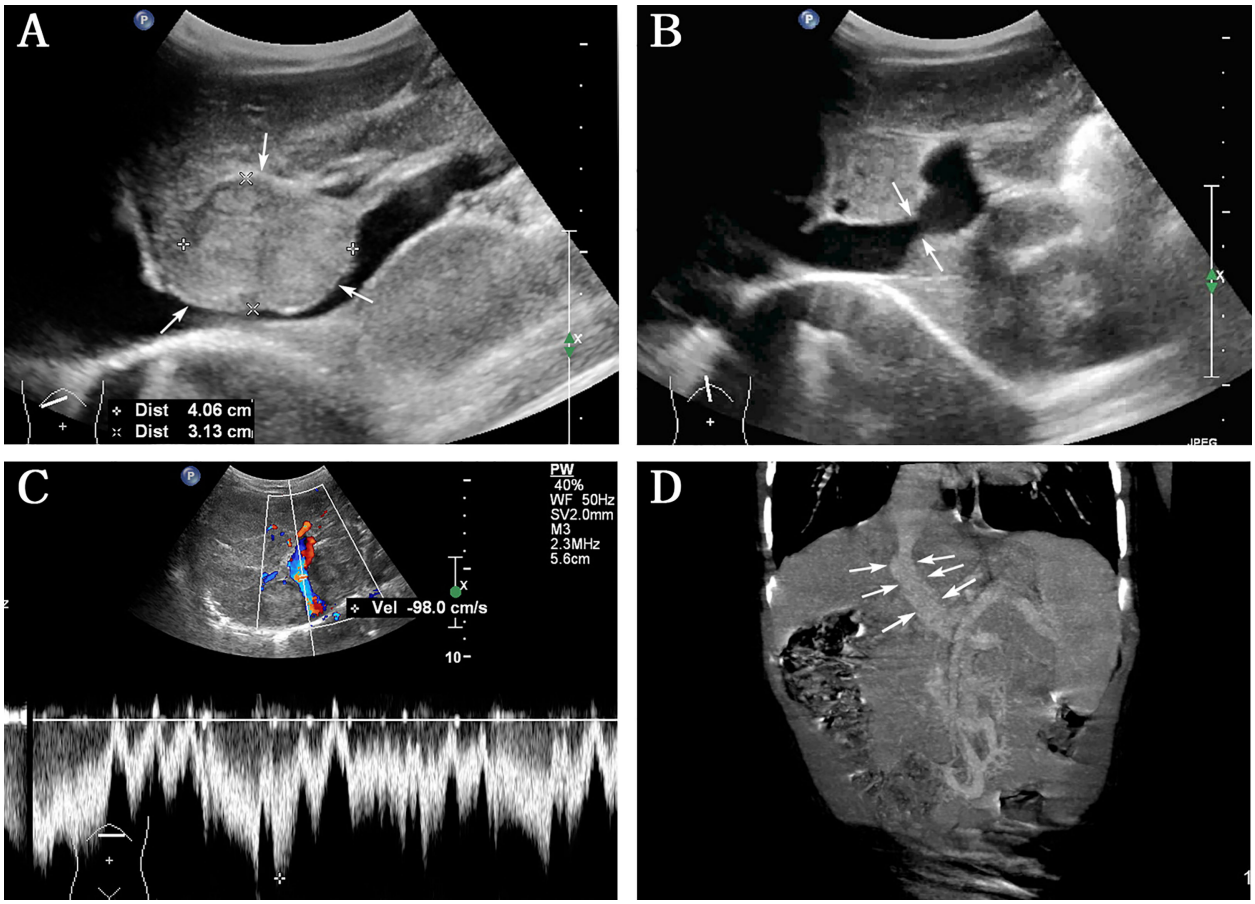

FIGURE 1
Abdominal ultrasound and contrast-enhanced computed tomography (CT) were performed before interventional therapy. **(A)** Grayscale indicates the largest hepatic nodule (arrows) with clear boundary and inferior vena cava (IVC) compression; **(B)** left portal vein directly communicated with IVC (arrows); **(C)** color Doppler ultrasound image confirmed PV flow toward IVC, with a flow velocity of 98 cm/s in the shunt; **(D)** contrast-enhanced CT showed the presence of direct communication between PV and IVC (arrows).

range: 20–145 U/L), and glutamyl transpeptidase (233 U/L; reference range: 3–40 U/L) levels. Prothrombin time (PT) extended to 28.5 s (reference range: 12.0–14.8 s) and the prothrombin activity (PTA) was 28.0% (reference range: 80.0–120.0%). Furthermore, the blood ammonia level increased to 80 μmol/L (reference range: 10.0–47.0 μmol/L) without any evidence of HE.

Based on the abovementioned findings and personal preference, he was admitted to Children's Hospital, Zhejiang University School of Medicine to perform contrast-enhanced CT, which confirmed the presence of direct communication between PV and IVC (Figure 1D). Contrast-enhanced CT revealed the presence of hepatic nodules, which were misinterpreted as hemangiomas.

Subsequently, he was hospitalized in several hospitals in Shanghai, where lung CT, electrocardiogram, tumor marker (alpha fetoprotein, carcinoembryonic antigen, and carbohydrate antigen 199) levels, hepatitis B antigen–antibody, and cranial magnetic resonance imaging (MRI) showed normal results. Hepatic nodule puncture was performed (three puncture tissues at the center and edge of hepatic nodules were collected), with a pathological diagnosis of focal nodular hyperplasia (FNH) or nodular regenerative hyperplasia (NRH). DSA revealed hepatic vascular malformation, LPV was closely associated with IVC, and RPV was not clearly visualized. He was finally diagnosed with intrahepatic portosystemic shunts (IPSS), and interventional therapy was used to occlude the shunt.

The patient visited our hospital 6 months after the shunt closure. Abdominal US revealed the complete disappearance of multiple FNH/NRH (Figure 2A), and the diameter of LPV was 1.3 cm, with a hyperechoic area of 2.1 × 1.3 cm between LPV and IVC (Figure 2B). Subsequent CT examination confirmed that this hyperechoic area was a metal occluder placed after the interventional therapy. Color Doppler US showed bidirectional venous waves in the intraportal spectrum (Figure 2C). Blood tests were repeated several times after the operation, which showed normal blood ammonia level and liver function gradually. No complication occurred during the 3-year follow-up after the shunt occlusion. Abdominal contrast-enhanced CT revealed normal liver size and shape, without local density abnormality and with annular metal density shadows in the hilum of the liver 3 years after the interventional therapy (Figure 2D). The process of disease discovery to patient diagnosis and treatment is shown in Figure 3 as a flowchart.

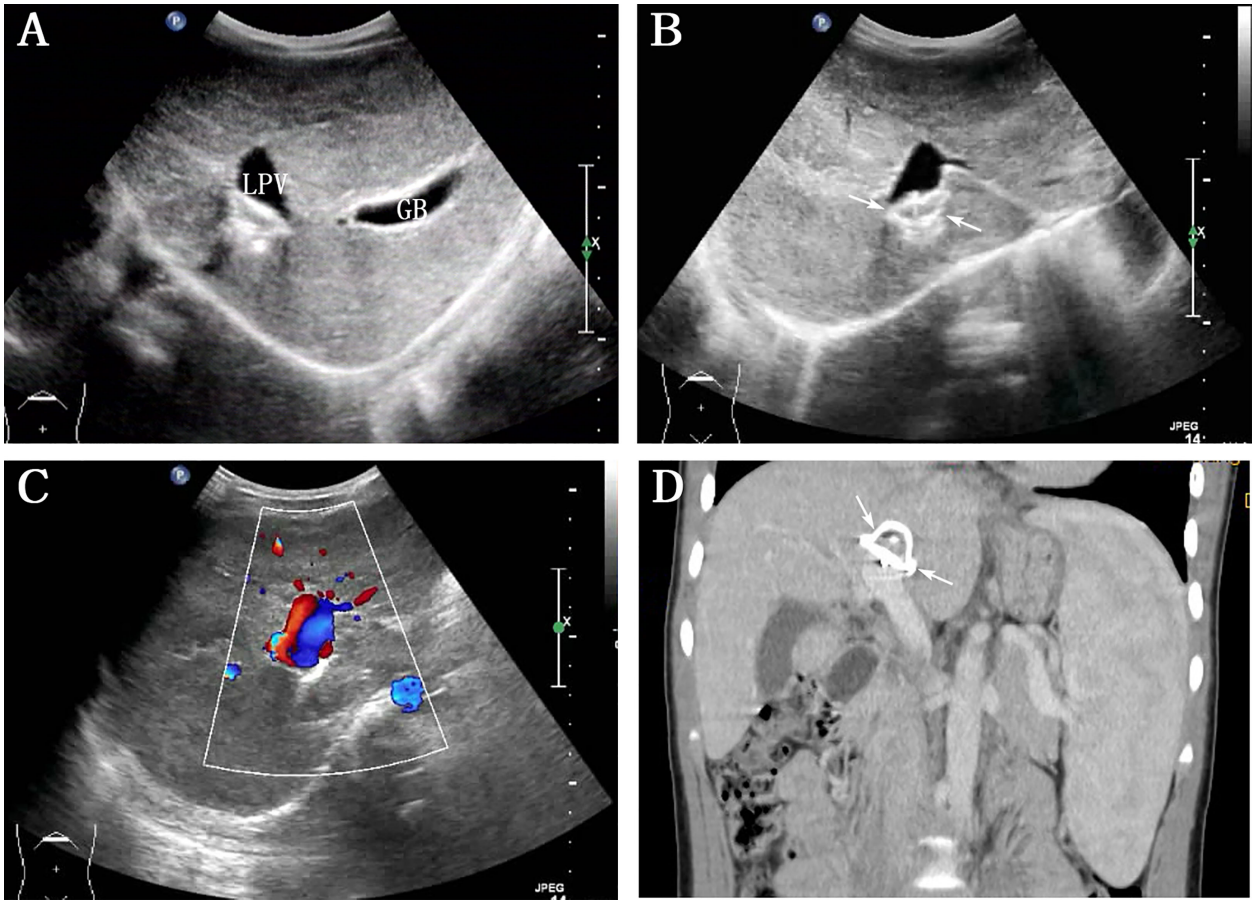

FIGURE 2
Abdominal ultrasound and contrast-enhanced computed tomography (CT) reexamination were performed 3 years after the interventional therapy. **(A)** Grayscale indicates the complete disappearance of multiple intrahepatic nodulars (LPV: left portal vein, GB: gall bladder); **(B)** hyperechogenicity between LPV and inferior vena cava (arrows); **(C)** color Doppler ultrasound image showed bidirectional venous waves in the intraportal spectrum; **(D)** contrast-enhanced CT on this reconstructed coronal view showed annular metal density shadows in the hilum of the liver (arrows).

3 Discussion

CPSS is a malformation wherein the splanchnic vein is directly shunted into the systemic circulation *via* abnormal vascular connections, and is categorized into extrahepatic portosystemic shunts (EPSS, also known as "Abernethy malformations") and IPSS (between PV branches and the hepatic veins or IVC) (4, 6). IPSS can be further classified into five types: type 1 is a connection between the main PV branch and IVC; type 2 is a peripheral vascular connection confined to a single hepatic segment; type 3 is a connection through a PV varix; type 4 is diffuse small connections; and type 5 involves the ductus venosus (2, 7). The current case was type 1 IPSS (LPV–IVC). Prematurity may be a risk factor for IPSS; however, its characteristics and natural history are unclear (8).

In 1956, IPSS was first reported by Doehner et al. (9). In 2000, the reported number of IPSS cases was fewer than 50 (10). Recently, however, the number of reported cases has been increasing with improvements in imaging techniques and enhanced IPSS recognition. Cytter-Kuint et al. (8) reported that IPSS without other hepatic abnormalities was a benign, self-limiting condition and in 15 infant cases, all shunts closed spontaneously without major sequelae. IPSS has a smaller size and reduced blood flow compared with EPSS; hence, it is expected to have fewer complications and a better chance of spontaneous closure. Studies have shown a spontaneous closure ratio of approximately 47% in IPSS compared with 4% in EPSS (3). However, the spontaneous closure had no established predictors. In our patient, IPSS did not exhibit spontaneous closure, which may be related to the presence of hepatic nodules and the size of the shunt. It has been reported that small intrahepatic shunts may spontaneously disappear by the age of 1–2 years, but the large shunts may persist throughout life and carry the risks of complications (4, 11). Sokollik et al. (12) recommended shunt closure in cases where severe complications occurred or IPSS did not disappear even at around 2 years of age.

The methods of closing the shunt include interventional therapy (endovascular), surgical approach and liver transplantation. Interventional therapy is the treatment of choice for most IPSS (1–3). This case was treated with interventional therapy, Multiple hepatic tumors disappeared following 6 months, which is consistent with case C reported by Albers. A 5-year-old boy's hepatic nodules were also misinterpreted as hemangiomas by MRI. Finally, repeat US and re-review of previous imaging confirmed the presence of CPSS between the main PV and the IVC. Hepatic nodule histology was NRH/FNH. In addition, pulmonary hypertension. The difference was that he used surgical approach to close the shunt, and later on the disappearance of hepatic nodules, the pulmonary hypertension disappeared after 2 years after closure (2). The indication for another case to choose surgical shunt closure was that the FNH increased from 2 cm to 8 cm in 8 years follow-up: a failed attempt at interventional closure. Almost complete regression of the FNH after the surger (13). The evolution of liver tumor is consistent with the results reported by previously, stating that benign nodules (even for large nodules) resulting from IPSS show a good prognosis (4, 5). Tyraskis et al. (14) tracked the tumor evolution of 11 benign tumors after shunt closure. Of these, partial (4 patients) or complete (3 patients) tumor regression was observed in 7/11 (64%) patients at shunt closure, 3 patients had no change, and 1 patient presented with malignant transformation 6 months after shunt closure. In our case, the liver tumor completely disappeared after the shunt was closed, which may be related to the cause of tumor formation.

CPSS could develop various clinical features due to different pathophysiologies (15) associated with multisystem complications, with the most common being liver tumors and being present in a wide range of benign (NRH, FNH, adenomas, and hemangiomas) and malignant (hepatoblastomas, hepatocellular carcinomas, and sarcomas) hepatic nodules (14). Of these, the most common are FNH and NRH (6). It is well known that approximately 70% of the liver transfuses blood from the portal venous system during the postnatal period; however, the presence of IPSS reduces portal flow.

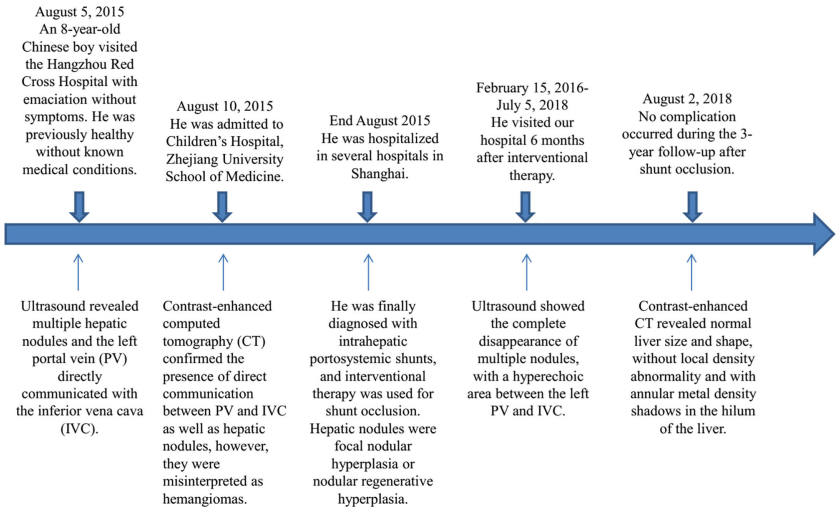

FIGURE 3
The flowchart from disease discovery to patient diagnosis and treatment.

It has been reported that the absence of intrahepatic portal flow has been known to lead to a significantly higher rate of hepatic tumor formation (16). Thus, in our case, IPSS may alter the growth factor and sex hormone metabolism owing to reduced portal venous flow and compensatory increases in hepatic arterial flow, which could drive FNH formation (14). FNH is a non-neoplastic lesion characterized by benign appearing hepatocytes with vascular anomalies and ductal proliferation (13). As reported in a previous study, the main cause of FNH is abnormal blood perfusion, which could involve either PV or arteries (17). In our case was followed-up for 6 months to 3 years, and no new liver tumor was found, indicating that shunt is closed, portal flow contributes to liver health and growth. Contrast-enhanced CT revealed FNH with a typical central stellate scar and spoke-like vascular structures (18). However, the characteristic features in our case were not obvious and were misinterpreted as hemangiomas.

CPSS identification and continued surveillance are essential, especially since timely intervention can improve clinical outcomes in the appropriate circumstances (6). The diagnosis of CPSS relies on imaging and is mostly diagnosed using DSA, which can identify the presence, location, type of CPSS, as well as PV circulation patency (10, 15). Furthermore, the development of prenatal imaging has enabled prenatal diagnosis, which has led up to 42% of CPSS cases, particularly IPSS cases, to be currently diagnosed prenatally (19). Color Doppler US can detect CPSS *via* direct shunt visualization or indirect signs, such as the diameter of the involved vessels (PV and hepatic veins), diameter of PV at the afferent side of the fistula, and size of the liver and spleen (8, 19); however, prenatal CPSS diagnosis requires US reexamination after birth due to changes in circulation. Moreover, color Doppler US is extremely useful in the follow-up of CPSS after treatment (5). In our case, no complications were found during the US follow-up for 3 years following shunt closure; therefore, it is recommended as a screening and monitoring tool (3). However, US has a few limitations: first, the surveillance and imaging protocols were not uniform. Second, the detection of the shunt may not be accurate due to several factors, such as gastrointestinal gas interference, atrophic liver, and limited imaging characteristics. Third, it is often not possible to clearly distinguish EPSS from IPSS. Fourth, EPSS away from the liver may be difficult to detect by US. Xu et al. (15) reported that two IPSSs cases and one EPSS case were missed by abdominal US and later detected by contrast-enhanced CT or MRI. Therefore, contrast-enhanced CT or MRI should be performed to further evaluate the shunt and observe other accompanying abnormalities when clinicians suspect CPSS in patients with negative US results. In summary, each type of examination could provide and supplement the relevant CPSS information.

Studies showed hyperammonemia in 79% (123/156) of children with CPSS and abnormal liver function in 78% (42/54) (4, 13), possibly because venous blood from the intestines and spleen bypasses the liver and directly diverts into the systemic circulation through the abnormal vessels (14). These values decrease after the portal flow restoration and return to normal after several days. Both are useful markers for monitoring the effectiveness of shunt closure (4, 19). Further, the presence of shunts can impair hepatic synthesis, resulting in coagulation disorders (14). PT was prolonged in 40% (31/77) of children involved in a study by Bernard et al. (4). Our patient showed increased blood ammonia levels, abnormal liver function, and prolonged PT at the hospital visit, which did not reach the degree of cholestasis and HE, and the laboratory parameters gradually returned to normal over time following shunt closure, suggesting that interventional therapy was effective for the boy.

In summary, CPSS may be asymptomatic or present with multisystem diseases of varying severity, mimicking common or rare pediatric conditions. Although CPSS is less common, it has gradually been acknowledged by clinicians, which is important for early diagnosis considering the potentially serious clinical consequences. Color Doppler US imaging is free of ionizing radiation and well tolerated, and hence, has become the first choice for assessing the pediatric abdomen. Therefore, color Doppler US is recommended as a noninvasive imaging technique to identify CPSS, monitor the therapeutic response, and conduct follow-up to guide the management of this disease and improve its outcomes.

Data availability statement

The raw data supporting the conclusions of this article will be made available by the authors, without undue reservation.

Ethics statement

The studies involving human participants were reviewed and approved by Hangzhou Red Cross Hospital. Written informed consent to participate in this study was provided by the participants' legal guardian/next of kin. Written informed consent was obtained from the minor(s)' legal guardian/next of kin for the publication of any potentially identifiable images or data included in this article.

Author contributions

YZ: manuscript writing. TY: data collection. YM: data collection. WZ: data collection. YZ: data collection. GY: supervision and data collection. All authorscontributed to the article and approved the submitted version.

Acknowledgments

We thank all authors of this study for their valuable input and full cooperation.

Conflict of interest

The authors declare that the research was conducted in the absence of any commercial or financial relationships that could be construed as a potential conflict of interest.

Publisher's note

References

1. McLin VA, Franchi Abella S, Debray D, Guérin F, Beghetti M, Savale L, et al. Congenital portosystemic shunts: current diagnosis and management. *J Pediatr Gastroenterol Nutr* (2019) 68:615–22. doi: 10.1097/MPG.0000000000002263

2. Albers BK, Khanna G. Vascular anomalies of the pediatric liver. *Radiographics* (2019) 39:842–56. doi: 10.1148/rg.2019180146

3. Bahadori A, Kuhlmann B, Debray D, Franchi-Abella S, Wacker J, Beghetti M, et al. Presentation of congenital portosystemic shunts in children. *Children (Basel)* (2022) 9:243. doi: 10.3390/children9020243

4. Bernard O, Franchi-Abella S, Branchereau S, Pariente D, Gauthier F, Jacquemin E. Congenital portosystemic shunts in children: recognition, evaluation, and management. *Semin Liver Dis* (2012) 32:273–87. doi: 10.1055/s-0032-1329896

5. Franchi-Abella S, Gonzales E, Ackermann O, Branchereau S, Pariente D, Guérin F. International registry of congenital portosystemic shunt members. Congenital portosystemic shunts: diagnosis and treatment. *Abdom Radiol (NY)* (2018) 43:2023–36. doi: 10.1007/s00261-018-1619-8

6. DiPaola F, Trout AT, Walther AE, Gupta A, Sheridan R, Campbell KM, et al. Congenital portosystemic shunts in children: associations, complications, and outcomes. *Dig Dis Sci* (2020) 65:1239–51. doi: 10.1007/s10620-019-05834-w

7. Park JH, Cha SH, Han JK, Shteyer E. Intrahepatic portosystemic venous shunt. *AJR Am J Roentgenol* (1990) 155:527–8. doi: 10.1007/s00431-021-03949-9

8. Cytter-Kuint R, Slae M, Kvyat K, Shteyer E. Characterization and natural history of congenital intrahepatic portosystemic shunts. *Eur J Pediatr* (2021) 180:1733–37. doi: 10.1007/s00431-021-03949-9

9. Doehner GA, Ruzicka FFJr, Rousselot LM, Hoffman G. The portal venous system: on its pathological roentgen anatomy. *Radiology* (1956) 66:206–17. doi: 10.1148/66.2.206

10. Golli M, Kriaa S, Said M, Belguith M, Zbidi M, Saad J, et al. Intrahepatic spontaneous portosystemic venous shunt: value of color and power Doppler sonography. *J Clin Ultrasound* (2000) 28:47–50. doi: 10.1002/(sici)1097-0096(200001)28:1<47::aid-jcu8>3.0.co;2-v

11. Franchi-Abella S, Branchereau S, Lambert V, Fabre M, Steimberg C, Losay J, et al. Complications of congenital portosystemic shunts in children: therapeutic options and outcomes. *J Pediatr Gastroenterol Nutr* (2010) 51:322–30. doi: 10.1097/MPG.0b013e3181d9cb92

12. Sokollik C, Bandsma RH, Gana JC, van den Heuvel M, Ling SC. Congenital portosystemic shunt: characterization of a multisystem disease. *J Pediatr Gastroenterol Nutr* (2013) 56:675–81. doi: 10.1097/MPG.0b013e31828b3750

13. Zarfati A, Chambers G, Pio L, Guerin F, Fouquet V, Franchi-Abella S, et al. Management of focal nodular hyperplasia of the liver: experience of 50 pediatric patients in a tertiary center. *J Pediatr Surg* (2020) 55:1885–91. doi: 10.1016/j.jpedsurg.2020.01.009

14. Tyraskis A, Davenport M, Deganello A, Sellars M, De Vito C, Kane P, et al. Complications of congenital portosystemic shunts: liver tumors are affected by shunt severity, but pulmonary and neurocognitive associations are not. *Hepatol Int* (2022) 16:918–25. doi: 10.1007/s12072-022-10328-5

15. Xu S, Zhang P, Hu L, Zhou W , Cheng G. Case report: clinical features of congenital portosystemic shunts in the neonatal period. *Front Pediatr* (2021) 9:778791. doi: 10.3389/fped.2021

16. Tyraskis A, Deganello A, Sellars M, De Vito C, Thompson R, Quaglia A, et al. Portal venous deprivation in patients with portosystemic shunts and its effect on liver tumors. *J Pediatr Surg* (2020) 55:651–4. doi: 10.1016/j.jpedsurg.2019.05.027

17. Franchi-Abella S, Branchereau S. Benign hepatocellular tumors in children: focal nodular hyperplasia and hepatocellular adenoma. *Int J Hepatol* (2013) 2013:215064. doi: 10.1155/2013/215064

18. Yao Z, Zeng Q, Yu X, Lin S, Jiang S, Ma D, et al. Case report: ultrasound-guided percutaneous microwave ablation of focal nodular hyperplasia in a 9-Year-Old girl. *Front Pediatr* (2021) 9:710779. doi: 10.3389/fped.2021.710779

19. Guérin F, Franchi Abella S, McLin V, Ackermann O, Girard M, Cervoni JP, et al. Congenital portosystemic shunts: vascular liver diseases: position papers from the francophone network for vascular liver diseases, the French association for the study of the liver (AFEF), and ERN-rare liver. *Clin Res Hepatol Gastroenterol* (2020) 44:452–59. doi: 10.1016/j.clinre.2020.03.004

Frontiers in Oncology

Advances knowledge of carcinogenesis and tumor progression for better treatment and management

The third most-cited oncology journal, which highlights research in carcinogenesis and tumor progression, bridging the gap between basic research and applications to imrpove diagnosis, therapeutics and management strategies.

Discover the latest Research Topics

See more →

Frontiers

Avenue du Tribunal-Fédéral 34
1005 Lausanne, Switzerland
frontiersin.org

Contact us

+41 (0)21 510 17 00
frontiersin.org/about/contact